FLUIDIZED-BED COMBUSTION

OF COAL

-by-

DONALD P. NAUDÉ

Thesis submitted to the University of Cape Town in fulfilment of the requirements of the degree of Master of Science in Engineering.

September 1977

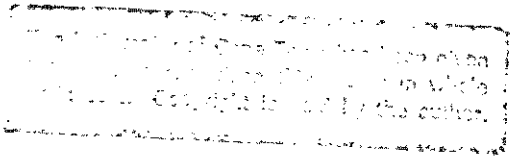

ABSTRACT

A general review of the literature pertaining to the combustion of coal in an atmospheric fluidized bed of inert particles is presented. In particular, the phenomena of fluidization and combustion have been investigated and the status of research and development in various parts of the world is considered.

A 300 mm diameter refractory lined open top atmospheric fluidized bed combustor has been built to study the combustion efficiencies and entrainment rates of the fluidized-bed combustion process in shallow fluidized beds, with static bed heights ranging from about 150 mm to 230 mm. A low pressure drop type of distributor was used for all of the tests so as to test a system compatible with most industrial requirements. As the combustor vessel is refractory lined, cooling is provided by supplying air to the rig well in excess of that required for stoichiometric combustion. As a result, no oxygen deficient regions occur within the fluidized bed, ensuring complete combustion of both the fixed carbon component of the coal to carbon dioxide and the volatile component within the bed section.

Experimental results have been obtained from the combustion of a coal with a high fines content of which there is at present a supply which exceeds the demand. The coal has been burned in an inert bed comprising a closely graded silica sand. It has been found possible to correlate the combustion efficiencies in terms of the bed temperature, superficial gas velocity and the static bed height within the following ranges of these parameters:

Bed Temperature	700 to 1000°C
Gas Velocity	0,9 to 1,5 m/s
Static Bed Height	150 to 230 mm

By using a bed material substantially different from the coal feed, it has been found possible to separate the

entrainment rate into two components, the first due to elutriation and the second as a result of splashing. However only qualitative conclusions have been drawn from the splashing phenomenon. The increased splashing rates associated with the deeper beds may be attributed in part to the possible transition from a bubbling to a slugging flow regime taking place in the fluidized bed.

A semi-quantitative model has been derived based on the work of a few authors to describe the combustion and entrainment phenomena. Although the model predicts trends satisfactorily, much work is required to determine attrition rate constants and the nature of the resulting ash on combustion of the coal particle as these parameters are artificially supplied as input to the computer model.

ACKNOWLEDGEMENTS

The author wishes to express his thanks and appreciation to Professor R.K. Dutkiewicz for his active interest and valued advice. Further, he would like to acknowledge the help and support of the following:

Mr. R.M. Stegan for his willingness to assist and for his advice in the construction and commissioning of the experimental equipment. To the staff of the workshop of the University of Cape Town, and in particular Mr. W.K. Bettesworth and Mr. L.R. Watkins for whom no request was too difficult and who built the rig in a quick and efficient manner.

The author's thanks are extended to Mr. N. Magasiner of John Thompson (Africa) (Pty.) Ltd., for his advice and to Mr. Grant of Athlone Power Station for performing some of the coal and ash analyses.

A word of thanks is also extended to Mrs. M. Stewart who so willingly typed this thesis in its entirety.

Finally, the author wishes to acknowledge the contribution of his mother and father who impressed on him the importance of education at an early age, and to his wife for her patience and encouragement.

TABLE OF CONTENTS

LIST OF TABLES

Page

A Detailed Tabulation of Results is Contained in Appendix H.

LIST OF FIGURES

NOMENCLATURE

Lower Case Symbols

$\breve{a}$ – fraction of ash in coal (-); constant defined by equation (17) (mm); constant defined by equation (28) (m^{-1});

b – constant defined by equation (17) (mm)

b_i – coefficients of the multiple regression equation (-)

c_c – fraction of carbon contained in the ash (-)

c_p – specific heat (kJ/kg ^oC)

Δd – change in diameter (m)

d – diameter (m)

d_B – bubble diameter at height h above the distributor (m)

d_{BM} – maximum bubble diameter as a result of coalescence (m)

d_{BO} – initial bubble diameter at the distributor (m)

d_p – mean particle diameter (m)

d_t – diameter of fluidized bed reactor vessel (m)

d_x – particle diameter for mass fraction x (m)

f – fraction of bubbles in the bed (-)

f_d – fraction of particles in the bed of size smaller than d (-)

g – gravitational constant (m/s^2)

g_{ij} - element of the inverted bivariate correlation coefficient matrix (-)

h - bed height (m)

h_c - unburnt carbon loss (-)

k - first order particulate phase velocity constant, equation (33) (sec^{-1})

k^* - dimensionless velocity constant (-)

k_g - mass transfer coefficient (m/s)

m - number of independent variables in the regression analysis

$m(d)$ - mass of particles of size d (kg)

m_c - coal feed rate from equation (12) (kg/h)

n - exponent of equation (8); molar flow of oxygen to a coal particle (mol/s); feeder speed (rpm); number of points used in the regression analysis

Δp_d - pressure drop across the distributor plate (mm Wg)

$\Delta p_{d,r}$ - pressure drop across both the distributor plate and refractory layer (mm Wg)

Δp_{mf} - pressure drop through a bed of particulate material at a velocity U_{mf} (N/m^2)

Δp_r - pressure drop through the refractory stone layer above the distributor (mm Wg)

$p_c(d)$ - size distribution of the combustible particles within a fluidized bed (m^{-1})

$p_0(d)$ - size distribution of the feed material (m^{-1})

$p_1(d)$ - size distribution of the bed overflow material (m^{-1})

r - particle radius, equation (34) (m)

r_{ij} - bivariate correlation coefficient between X_i and X_j (-)

s_{Xi} - sample variance of X_i

s_{XiXj} - covariance between X_i and X_j

Δt - time interval (s)

t - time (s); percentile of Student t-distribution

u - velocity (m/s)

u_B - natural velocity of rise of a bubble (m/s)

u_{BS} - absolute velocity of rise of a bubble (m/s)

u_f - superficial gas velocity (m/s)

u_{mf} - minimum fluidizing velocity (m/s)

x - mass fraction of particles in a particular size interval

Upper Case Symbols

A - abrasion rate constant (m^{-1}); constant (-)

A^* - modified abrasion rate constant (m^{-1})

A_t - cross sectional area of the fluidized bed reactor vessel (m^2)

B - constant (-)

B_i - standard normal correlation coefficient (-)

B_i' - interval estimate of the standard normal correlation coefficient (-)

C - concentration of a particular component (-)

C_b - molar oxygen concentration in the bubble phase (mol/m^3)

C_o - molar oxygen concentration of the inlet air (mol/m^3)

C_p - molar oxygen concentration of the particulate phase (mol/m^3)

D_t - diameter of reactor vessel (m)

F - constant defined by equation (28); percentile of F-distribution

F_a - rate of production of fines per unit area (kg/m^2s)

F_0 - mass flow rate of the feed material (kg/s)

F_1 - mass flow rate of the overflow material (kg/s)

F_2 - mass flow rate of the entrained material (kg/s)

G - gas diffusion coefficient (m^2/s)

H_{dyn} - dynamic bed height (mm)

H_f , H_{mf} - bed height at U_f and U_{mf} (m)

$I(d,d_{max})$ - function defined by equation (56) (-)

K - elutriation rate constant (kg/m^2s)

K^* - elutriation rate constant (sec^{-1})

K_{bp} - gas interchange coefficient between the bubble and particulate phases (sec^{-1})

M - bed mass (kg)

M_a , M_g - air flow rate and gas flow rate (kg/s)

M_b - total bed mass (kg)

M_c - mass of combustible matter contained in the bed (kg)

M_d - mass of particles of diameter d (kg)

M_f , M_{fo} - rate of coal burnt and coal feed rate (kg/s)

N - number of holes per unit area of a perforated plate distributor (m^{-2})

NCV - net calorific value of the fuel (kJ/kg)

O - overflow rate (kg/s)

Q_B - effective volumetric interchange between bubble and bed (m^3/s)

Q_w - heat loss through the combustor walls (kW)

R - multiple correlation coefficient (-); bed expansion ratio (-)

S - splashing rate constant (sec^{-1})

ΔT - temperature difference (^oC)

T - bed temperature (^oC)

U - overall heat transfer coefficient ($W/m^2\ ^oC$)

V_B - bubble volume (m^3)

W - weight of bed material (kg)

X - transfer factor denoting the number of times a bubble interchanges its volume as it moves through a bed of height H

X_i - independent variables of multiple regression analysis

Y - dependent variable of multiple regression analysis

Z - mean removal rate constant defined by equation (62) (s^{-1})

Dimensionless Numbers

Fr_{mf} - Froude Number at minimum fluidizing velocity $(\frac{u^2}{g \cdot d})$

Ga - Galileo Number $(\frac{\rho_s - \rho_g}{\mu^2} \cdot g \cdot \rho_g \cdot d^3)$

Re, Re_{mf}, $Re_{p,mf}$ - Reynolds Number in general, at minimum fluidizing velocity and particle Reynolds Number at minimum fluidizing velocity $(\frac{\rho \cdot u \cdot d}{\mu})$

Sh - Sherwood Number $(k_g \cdot d / G)$

Greek Symbols

ε, ε_{mf} - voidage fraction (-)

η, η_c - combustion efficiency (-,%)

μ - dynamic viscosity (kg/ms)

ρ_c, ρ_g, ρ_s - density of coal, gas and bed material (kg/m^3)

ϕ_s - particle shape factor (-)

$\Gamma(d)$ - rate expression for particle shrinkage (m/s)

$\Gamma_a(d)$ - rate expression for particle shrinkage due to abrasion (m/s)

$\Gamma_c(d)$ - rate expression for particle shrinkage due to combustion (m/s)

ABBREVIATIONS

AIChE	–	American Institute of Chemical Engineers
ASME	–	American Society of Mechanical Engineers
BCURA	–	British Coal Utilization Research Association
CEGB	–	Central Electricity Generating Board
CRE	–	Coal Research Establishment
CSIRO	–	Commonwealth Scientific and Industrial Research Organization
EPA	–	Environmental Protection Agency
EPRI	–	Electric Power Research Institute
ERDA	–	Energy Research and Development Authority
FRI	–	Fuel Research Institute of South Africa
NCB	–	National Coal Board
NRDC	–	National Research Development Corporation
TVA	–	Tennessee Valley Authority

CHAPTER 1

INTRODUCTION

The combustion of coal is a complicated process, involving both heterogeneous and homogeneous chemical reactions as well as being dependent on such complex parameters as particle shape, ash distribution within the particle, air distribution, volatile content etc. The approach to explaining the combustion phenomenon has been largely empirical concerned mainly with improving the combustion efficiency. Traditional methods of coal combustion have been developed to such an extent that any further improvements in these processes will only result in marginal if any increase in the efficiency of combustion. These traditional coal burning techniques, in particular when applied to the generation of steam, impose limitations on the coal which can be fired. In particular, plants have to be specifically designed for burning high ash or low volatile coals resulting in a certain amount of inflexibility especially should the fuel properties change over the life of the installation.

Fluidized-bed combustion represents the only outstanding development in coal combustion technology since the introduction of pulverised fuel firing during the late 1920's. Fluidized-bed combustion provides a simple method of burning any fuel, solid, liquid or gas with reduced atmospheric pollution. It further provides a means of burning high ash coals, (it is possible to burn coal with an ash content of over 85% in a fluidized-bed combustor,) which have hitherto not been considered as a source of energy. A typical fluidized-bed combustor could be used to burn a complete range of coals, as well as liquid or gaseous fuels, as the process is almost independent of the nature of the fuel. The energy 'crisis', propagated by the dramatic increase in the price of oil in the latter half of 1973, resulted in a renewed interest in coal as a source of energy. Fluidized-bed combustion represents a positive step forward towards the successful burning of low grade coals, and the

implementation of this technique will result in an increase in the useful coal reserves of South Africa in particular, as well as the rest of the world.

1.1 THE PRINCIPLE OF FLUIDIZED-BED COMBUSTION

Fluidized-bed combustion in its broadest sense consists of the burning of a fuel in a bed of inert particles which are fluidized by means of a gas transporting the oxidizing agent required for the combustion process. Fluidization is not a new technique, but has been used extensively in the chemical industry, becoming "after 1940, one of the chemical engineers' and extractive metallurgists' most important tools" (1). Since then a vast quantity of information, both theoretical and empirical, has been accumulated on the subject. The burning of a fuel within a fluidized bed of inert particles has however only been investigated in depth over the last fifteen years. In a fluidized-bed combustion process the bed of inert particles is fluidized and the fuel introduced into this bubbling mass of particles. In the case of coal combustion, the bed of particles must be heated to a temperature above the ignition temperature of the coal for the process to be self propagating. The burning coal particles transfer the heat of combustion to the gas and inert particles, which in turn transfer the heat to any heat exchange surfaces immersed in the bed. The remainder of the heat is removed from the system in the exhaust gases at the bed temperature. The vigorous bubbling action of the fluidized bed ensures that the bed temperature remains uniform, although the burning coal particles may be several degrees higher than the temperature of the bed. An important feature of a fluidized bed combustor using coal as a fuel, is that the proportion of coal contained within the bed represents only about a 0,5% to 2% of the total bed weight. This would imply that the process is almost independent of the quality of the coal feed, it is dependent only on the ash handling facilities and the requirement that the heating value of the coal is sufficient to heat the inert content and combustion air to the bed temperature.

1.1.1 Gas Fluidization

The process of gas fluidization can be described by considering a bed of particles resting on a perforated or porous plate or any similar device which would serve as an air distributor. At low flow rates, the air passes upwards through the bed between the particles which behave as a fixed bed. As the flow rate is increased, a point will be reached at which the pressure drop across the bed becomes equal to the weight per unit area of the bed and the bed is then at the point of becoming fluidized. The velocity, measured in terms of the empty vessel and designated as the superficial gas velocity, at which this occurs is called the minimum fluidizing velocity. If the flow rate is increased above this value, one of two things will occur; either the bed will continue to expand so that the average distance between the particles will become greater, or the excess fluid will pass through the bed in the form of bubbles giving rise essentially to a two phase system. These two types of fluidization are referred to as being respectively "particulate" and "aggragative" (2, pg 26). In general, aggragative fluidization is associated with most gas-solid systems and particulate fluidization with most liquid-solid systems. Harrison et al (3) have suggested that the type of fluidization could be related to maximum stable bubble size which can exist in the bed. They also have found that this can be related to the mean diameter of the particles. Kunii and Levenspiel (4, pg 80) attribute the difference between particulate and aggragative fluidization to the difference of densities of the two fluids. They recommend the use of four dimensionless groups as given in equation (1) for establishing the mode of fluidization.

$$\left.\begin{array}{ll} Fr_{mf} \cdot Re_{p,mf} \cdot \left(\dfrac{\rho_s - \rho_g}{\rho_g}\right) \cdot \dfrac{H_{mf}}{d_t} < 100 & particulate \\ Fr_{mf} \cdot Re_{p,mf} \cdot \left(\dfrac{\rho_s - \rho_g}{\rho_g}\right) \cdot \dfrac{H_{mf}}{d_t} > 100 & aggragative \end{array}\right\} \quad (1)$$

The work described in this thesis makes exclusive use of aggragative fluidized beds, and only this system is considered in the discussion below. As the gas flow is

increased through the bed, the fluidization becomes steadily more vigorous, taking on the appearance of a violently boiling liquid. Further increases in the gas velocity may result in a transition from this bubbling regime, to a slug flow regime which is also dependent on the geometrical configuration of the system. A limiting condition will eventually be reached at which the gas velocity becomes equal to the free fall velocity of the particles, or in other words the particle terminal velocity. At this point the particles are carried out of the vessel or entrained in the fluidizing gas. The fluidizing vessel then behaves as pneumatic conveying tube. The qualitative differences between the different fluidization regimes have been illustrated by Zenz and Othmer (5, pg 231) and is reproduced in Figure 1.

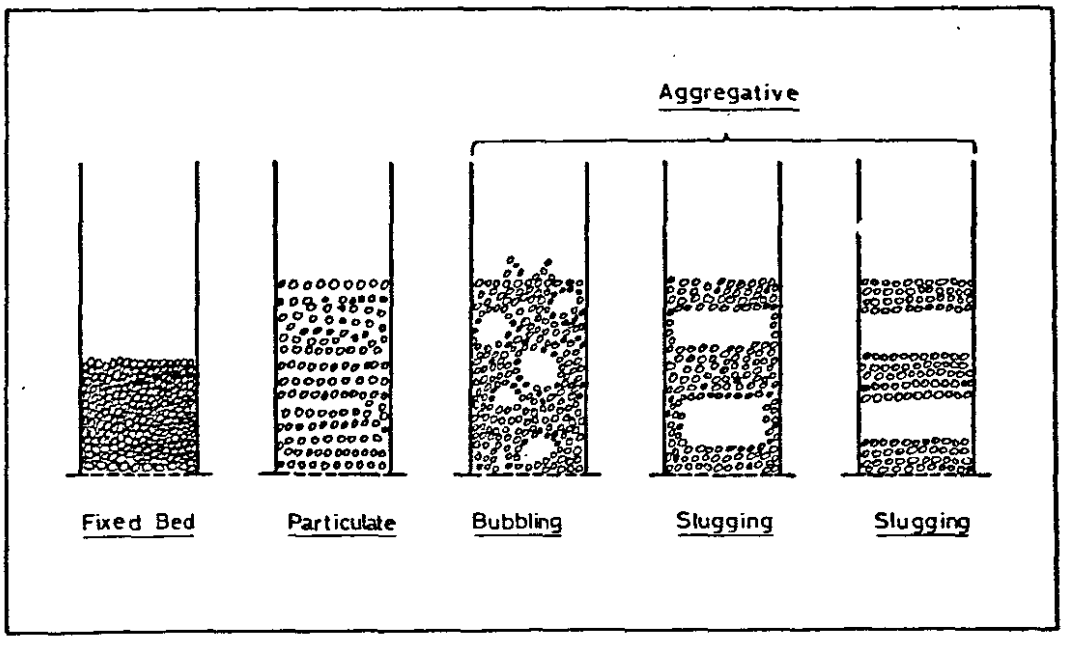

Figure 1 : Qualitative Representation of the Different Regimes of Fluidization

1.1.2 The Combustion Phenomenon

"When coal is heated to a sufficiently high temperature it begins to decompose producing tars and gases termed volatile matter or just volatiles. The volatiles consist of a mixture of combustible gases, carbon dioxide and water vapour. Apart from the carbon dioxide and hydrogen the combustible gases are mainly hydrocarbons, although there are small quantities of phenolic and other compounds" (6, pg 155). The combustion of coal thus comprises two reactions, a homogeneous gas phase combustion reaction, and the heterogeneous reaction that takes place at the surface of the char that remains after the evolution of the volatiles.

The rate at which the volatiles are evolved, or the rate at which the coal particle decomposes depends on the time/temperature history of its heating. Two classes of decomposition reactions are distinguished (6, Ch 4), rapid decomposition involving a particle heating rate of the order of 10^4 $^{o}C/s$ or more with a decomposition period of less than one second, and slow decomposition in which the particle is heated at a rate of 10 $^{o}C/min$. Rapid decomposition rates can only be attained with very small coal particles, less than 100 micron, as a finite time is required for a large particle to be uniformly heated, as well as to allow for the diffusion of the volatile matter away from the surface of the remaining char particle.

Pitt (7) has studied the rate of evolution of volatile matter from coal particles by mixing coal with preheated sand in a preheated reaction vessel. The sand and coal particles were then fluidized with nitrogen and the rate of decomposition measured. The minimum time scale of decomposition was limited to 10 seconds whilst temperatures of 300^{o} to $650^{o}C$ were used. The results indicated that a major portion of the volatile matter was evolved within the first 10 seconds even at the lower temperatures. Skinner (8, pg 104) states that the volatiles are evolved within the first two to three seconds after the coal enters the fluidized bed. The volatiles would be emitted in close proximity to the coal feed point, and should

the oxygen supply be limited in the region of this point, poor combustion efficiency may result. Bishop et al (9) have reported the existence of areas of unburnt hydrocarbons close to the coal feed point situated to the side of an 1800 mm by 450 mm bed. Complete combustion of the volatiles in the bed section was achieved by increasing the static bed height to 300 mm (750 mm expanded). They (9) report further that at low bed temperatures, and with an excess air level limited to 5%, the hydrocarbon concentrations were found to be relatively high, at between 800 to 1000 ppm. At higher bed temperatures, the hydrocarbon concentration was reduced to near zero with an increase in the excess air to 17%.

Little work has been done in assessing the combustion of the volatiles in a coal fired fluidized bed combustion chamber. Although the time taken for the combustion of the volatiles would appear to be of the order of two seconds in comparison to a residence time of between 60 to 350 seconds for coal particles between 0,2 and 2 mm in a fluidized bed (10), work in this field may be of value particularly in assessing combustion mechanisms and combustor efficiencies. Basu et al (11) point out that on evolution of the volatile matter, swelling of the remaining char particle may take place which would alter the surface structure. This may explain differences in the combustion of different coals in fluidized beds, and in particular differences in the combustion of the volatile component of the different coal types.

After the liberation of the volatiles, the second step in the combustion process can be considered, i.e. the combustion of the remaining char. An evaluation of the mechanism and the burning rates of individual particles is of importance in the prediction of the oxygen throughput, the bed carbon loading and the combustion efficiency of the fluidized bed combustor. Field et al (6, Ch 6) consider the overall reaction process to involve a number of steps in sequence,

viz. the transport of oxygen to the particle surface, reaction at the surface and the transfer of the products away from the surface. Basu et al (11) consider two different mechanisms for the combustion of the carbon particle with oxygen. In the first, designated as Model 1, oxygen comes in contact with the carbon surface to form carbon monoxide and carbon dioxide. The excape of the carbon monoxide into the surroundings is dependent on the prevailing velocity and temperature conditions. If the temperature is above the ignition temperature of carbon monoxide (about 650°C) then this gas burns in a reaction zone surrounding the carbon particle (11). The reactions pertinent to Model 1 are illustrated in Figure 2.

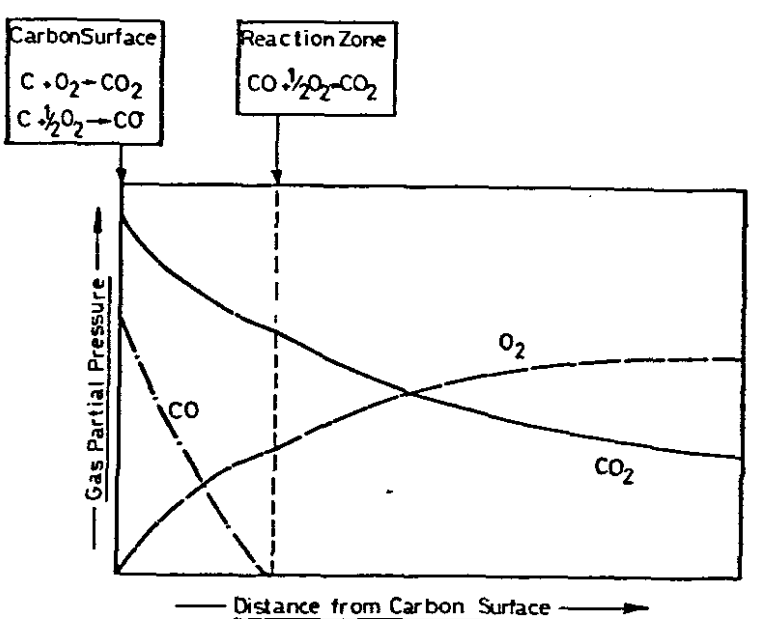

Figure 2 : Partial Pressure Profiles in the Gas Surrounding a Particle Burning according to Model 1.

The second mechanism, Model 2, has also been proposed by a number of authors who have shown (6, Ch 6) that if the reactions of carbon dioxide with carbon and of carbon monoxide with oxygen were fast enough then the mechanism of combustion would be completely different from the direct oxidation of carbon. This model has been called the two film theory and is diagramatically represented by Figure 3. According to this model, carbon dioxide reacts with the carbon surface to produce carbon monoxide, which in turn diffuses outwards to meet oxygen diffusing inwards. Two moles of carbon monoxide burn in a thin film surrounding the particle with a single mole of oxygen to form two moles of carbon dioxide. Half of the carbon dioxide diffuses back towards the char particle whilst the remainder diffuses into the free stream. The reactions taking place in Model 2 are illustrated by the partial pressure profiles of Figure 4.

Basu et al (11) have attempted to determine the actual combustion mechanism under the temperature and velocity conditions prevailing in fluidized beds. They propose that a change-over from Model 1 to Model 2 takes place, though further experiments would be required to mark this change-over in terms of temperature and particle size. Although they (11) indicate, in contrast to most other authors, that Model 1 represents the type of reaction taking place within fluidized beds, the basis of the theoretical approach in this thesis will be modelled on Model 2 due to the lack of any substantial supporting evidence for Model 1.

Avedesian and Davidson (10) have studied the mechanism of combustion of batch charges of carbon in fluidized beds with a view to establishing whether the combustion of the fixed carbon component of coal is controlled by chemical kinetics, mass transfer or a combination of both. They applied the combustion mechanism described by Model 2 to relate the theoretical work with their experimental results. They have further assumed the two phase theory of fluidization (12) and consider the bubble phase to be completely devoid

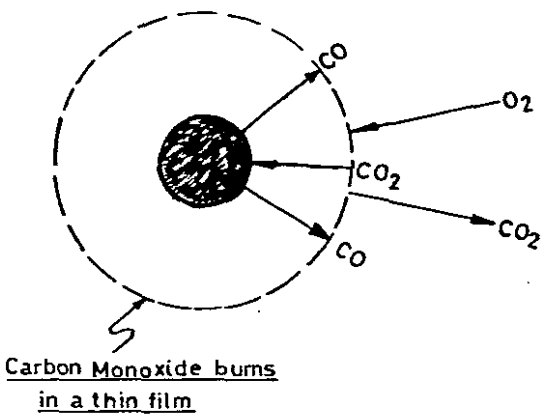

Figure 3 : Diagramatic Representation of the Combustion Mechanism of Model 2, Field et al (6, pg 205)

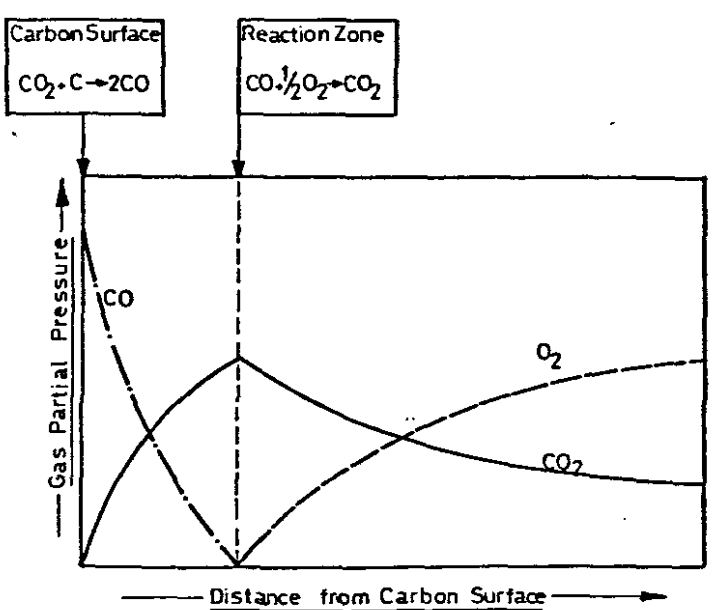

Figure 4 : Partial Pressure Profiles in the Gas Surrounding a Particle Burning according to Model 2.

of particles. Combustion thus takes place in the particulate phase of the fluidized bed, with each coal particle completely surrounded by inert material. Avedesian and Davidson (10) cite the findings of various authors who have shown that the burning rate of pulverised particles, i.e. having diameters less than 50 microns is controlled by chemical kinetics, whilst the combustion of particles greater than 100 microns is diffusion controlled. The transition from kinetic to diffusion control takes place over the particle size range from 50 micron to 100 micron. They (10) established from both theory and experiment that the combustion of coal in a fluidized bed of inert particles could be assumed to be controlled by two diffusional resistances, viz. the interphase transfer of oxygen from the bubbles of air to the surrounding ash particles, and the diffusion of oxygen through the ash phase of each burning carbon particle.

Campbell and Davidson (13) have extended the work of Avedesian and Davidson (10) to allow for a finite concentration of carbon dioxide in the particulate phase and have applied the model to allow for the continuous feeding of the coal. Basu et al (11) have further refined the model by determining a varying voidage function in the particulate phase which alters the Sherwood number. The accuracy of this work is questioned by Pyle (14) who further considers that the refinement to allow for varying voidage is unnecessary when much of the process is still not fully understood.

It is evident that the combustion of coal is a complex phenomenon. When applied to fluidized bed combustion further unknowns are introduced, and in summary the combustion process could best be described as follows:

Once a coal particle has been introduced into a bubbling fluidized-bed of inert particles at a temperature of the order of 800°C, the volatile fraction will be liberated within the first two or three seconds, to burn either completely or partially within the bed, dependent on the prevailing conditions. The remaining char particle burns within the particulate phase, at a rate determined by the rate of diffusion of oxygen from the bubble to this particulate phase, and by the rate of diffusion through the ash phase of the burning carbon particle. The carbon particle steadily reduces in size through the combined action of attrition and combustion until it is small enough to be entrained in the fluidizing gas as a result of splashing or elutriation.

1.2 THE BASIC PARAMETERS AFFECTING THE COMBUSTION PROCESS

For efficient combustion, the reactants - viz. the fuel and the oxidizing agent - must be in contact with each other for a sufficient length of time, at a sufficiently high temperature whilst a high degree of turbulence must be maintained to ensure a rapid and effective transfer of the products of combustion away from the source of the reaction and a transfer of fresh reactants to a zone where the reaction may be sustained. These criteria apply equally to the fluidized bed combustion process. The main parameters affecting this process are described below to illustrate the potential advantages as well as indicate possible disadvantages of the fluidized-bed combustion process.

1.2.1 Mean Particle Diameter

The bed material will be made up of particles having a range of diameters. It is therefore of value to define a mean particle diameter. A large number of different

means or averages may be defined (5, Ch 3), the significance of which are largely dependent upon the use to which the material is being applied. Botterill (15, pg 68) quotes a number of sources as finding the characteristic dimensions most appropriate for use as the mean particle diameter as being the volume to surface ratio of the particle. For spherical particles, equation (2) should be applied.

$$d_p = \frac{1}{\Sigma\, x/d_x} \qquad (2)$$

The above equation can be used for non-spherical particles if the diameter of the sphere with the same specific surface as the particles is used. A shape factor, or particle sphericity, is defined by equation (3) to allow the equations derived for spherical particles to be used for particles of different shapes.

$$\phi_s = \frac{\textit{surface area of equivalent volume sphere}}{\textit{surface area of the particle}} \qquad (3)$$

The diameter, d_x, of equation (2) is thus replaced by $\phi_s \cdot d_x$ for the equation to apply to a different shaped particle.

1.2.2 Minimum Fluidizing Velocity

The determination of the minimum fluidizing velocity is of the utmost importance in the design of fluidized beds as it sets a lower limit for the fluid throughput and is a basic variable of those mathematical models based on the two phase theory of fluidization. The definition of the minimum fluidizing velocity may be simply stated as the superficial gas velocity at which the bed of particles becomes fluidized. In practice the point of fluidization is not as clearly defined as the preceding definition may imply, and the definition is best described by considering Figure 5. Point A represents the pressure drop through

the bed of particles when a gas is passed through the bed for the first time. As the velocity is increased, the pressure increases in accordance with a fixed-bed pressure drop to velocity relationship. Because of the tendency of the particles to interlock with one another, partial bridging can occur, and pressure drops in excess of the theoretical value will be obtained (3, Ch 3). The curve passes through a maximum pressure drop, exhibiting a small characteristic "hump" as shown in Figure 5. On increasing the velocity still further, the pressure drop across the bed remains constant until the velocity attains a value equal to the particle terminal velocity, U_t. At this point, the fluidized-bed reactor vessel behaves as a pneumatic conveying tube. On decreasing the velocity from point E to B the pressure drop through the bed remains constant once again. Point B represents a deviation from the ideal de-fluidizing curve which is shown by the dashed lines. This deviation is a result of non-uniformity in

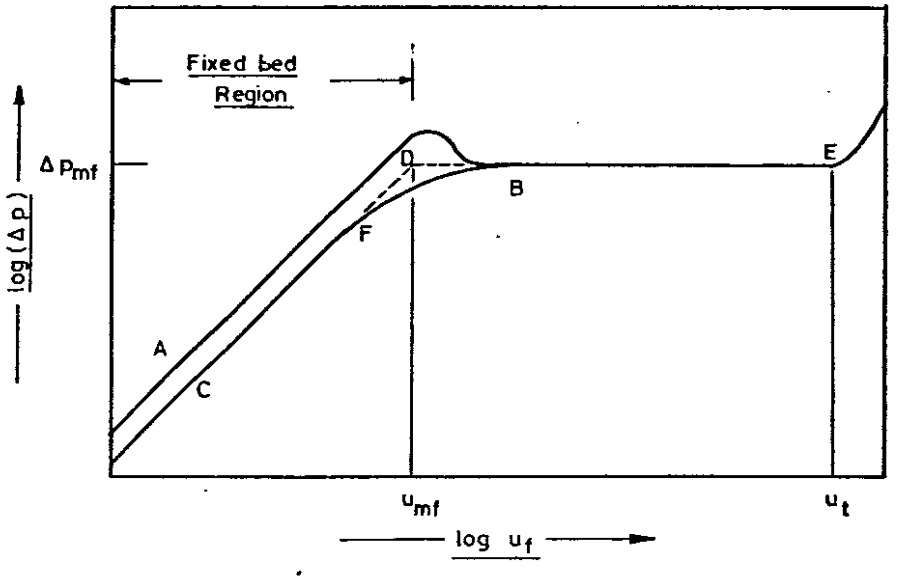

Figure 5 : Fluidization Curve to Illustrate some Deviations from Ideal Behaviour.

the bed structure resulting in fixed and fluidized regions co-existing within the bed. Although the bed may appear to be well fluidized, part of the bed may be supported by the distributor resulting in the pressure drop being less than expected. Further decreases in velocity result in a pressure drop characteristic displaced to the right of the original line. This is as a result of the particles becoming re-arranged so that the resistance to flow is minimized, and in general the voidage of the bed will have increased to the value existing at the point of incipient fluidization. Further increasing and decreasing of the gas velocity will be represented by the line CFBE. The minimum fluidizing velocity can therefore be obtained in practice by determining the intersection of the constant pressure line and the straight section of the line CF obtained on slowly decreasing the velocity. The intersection of these two lines is indicated by the point D in Figure 5.

It is often useful to be able to calculate the minimum fluidizing velocity. Three different methods of approaching this calculation can be distinguished. The first involves the determination of the drag coefficient for a single particle which is found to be related to the drag force of the multiparticle system by the voidage fraction raised to a power (16,17). This power has been found by Lewis et al (18) to have a value of 4,65. Although Reh (16) uses this form of correlation to determine different fluidization conditions in gas-fluidized beds, Wen and Yu (17) suggest that the equation they determined by this approach may be applicable to particulate fluidization.

A more recent paper (19) proposes that incipient fluidization conditions be characterized by a generalized fluidization and sedimentation correlation. The third approach and most common method is based upon a fixed bed pressure drop correlation where the pressure drop is set

equal to the effective solid weight of the bed. The voidage fraction at minimum fluidization conditions is then used in this correlation. The bed pressure drop under these conditions is in fact the constant value for the pressure as indicated in Figure 5 and can be obtained from equation (4).

$$\Delta p_{mf} = H_{mf} \cdot (1 - \varepsilon_{mf}) \cdot (\rho_s - \rho_g) \cdot g \qquad (4)$$

For small particles, where the flow can be assumed to be laminar, a Kozeny-Carman type relation is generally used to relate fixed bed pressure drops to velocity. As the Reynolds number increases from about 20 to 500, the flow would be in the transitional flow regime, and Leva (20, Ch3) recommends that pressure drop is proportional to velocity raised to a power, the value of the exponent being dependent on the Reynolds number and ranging from unity to two. Hence for larger particles a more general equation such as the Ergun pressure drop relation for fixed beds would probably yield the best results (2, pg 35). Equation (5) represents this relationship at minimum fluidizing conditions from which the minimum fluidizing velocity can be calculated after the Reynolds number has been evaluated.

Ergun pressure drop relation for fixed beds

$$Ga = \frac{150 \cdot (1 - \varepsilon_{mf})}{\phi_s^2 \cdot \varepsilon_{mf}^3} \cdot Re_{mf} + \frac{1{,}75}{\phi_s \cdot \varepsilon_{mf}^3} \cdot Re_{mf}^2 \qquad (5)$$

The first term on the right hand side of equation (5) is proportional to the losses as a result of viscous forces whilst the second is proportional to the kinetic energy losses. It is of interest to note that the Galileo number Ga, is dependent only on temperature of the fluid and the particle diameter raised to the third power.

In most cases the voidage fraction at incipient fluidization and the particle shape factor will not be known.

Wen and Yu (17) have overcome this by correlating the data of numerous workers into an equation in which these two parameters have been eliminated. This correlation is represented by equation (6) and has a standard deviation of 34% from the data used in its derivation.

$$Ga = 1650 \cdot Re_{mf} + 24{,}5 \cdot Re_{mf}^2 \qquad (6)$$

Broughton (21) recommends the use of only the first term on the right hand side of equation (6) for Reynolds numbers less than 20 and further claims that for Reynolds numbers less than 10, the minimum fluidizing velocity can be predicted to within 15% by the following equation.

$$Ga = 1440 \cdot Re_{mf} \qquad (7)$$

However, Avedesian and Davidson (10) have used an expression similar to equation (7), but with the constant term having a value of 1650, to relate their findings at elevated temperatures to a minimum fluidizing velocity to an acceptable degree of accuracy. In this thesis, the minimum fluidizing velocity at ambient temperature has been used to evaluate this limiting velocity at the higher temperatures. The method of correlation is discussed in Section 3.2.1.

1.2.3 Entrainment and Elutriation

Kunii and Levenspiel (4, Ch 10) make a distinction between entrainment and elutriation. They state that "In general, entrainment refers to the removal of solids from the bed by fluidizing gas ..." and that "Elutriation refers to the separation or removal of the fines ...". From this it is evident that the elutriation rate approaches the entrainment rate as the freeboard height becomes very large. Thus elutriation refers only to the removal of those particles of

size less than the particle size d_t, whose terminal velocity is the same as the superficial gas velocity. Merrick and Highley (22) have found existing correlations of elutriation rate constants to be inadequate particularly for the finest particles and the coarser particles. Most of the correlations predict that particles of diameter greater than the particle of size d_t, are not elutriated whereas it has been found (22) that even with freeboards of about 4 metres this is incorrect. Merrick and Highley (22) conclude that the existing empirical and semi-empirical correlations which have generally been obtained from small slugging beds are not applicable to their data. They derive a new form of correlation based on dimensionless groups incorporating the particle terminal velocity, the minimum fluidizing gas velocity, the fluidizing velocity, the gas mass flow rate and the particle entrainment rate.

Although this approach does offer a solution to the entrainment problem which allows for the explanation of the removal of larger particles from the bed, the general application of the method is doubtful. Gibbs (23), in his development of a combustion model, introduces a splashing rate constant to account for the entrainment of those particles of a size larger than would be elutriated. This second approach considers entrainment as being made up of two mechanisms, splashing and elutriation. The elutriation rate constant can be obtained from a correlation such as that given by Wen and Hashinger (24) whilst the splashing rate constant could be obtained empirically. This latter constant would clearly be dependent on the freeboard height and corrections for this value would have to be made when comparing tests on different rigs.

From the above, it is apparent that although the terminal velocity of the particle plays an important part in determining the entrainment rate, other factors have to be considered to allow for the loss of material from the bed in systems having a finite freeboard section.

1.2.4 Superficial Gas Velocity

The fluidizing air may be regarded as the key reactant, for it supplies the oxygen for combustion as well as being the fluidizing medium. The superficial gas velocity is defined as that velocity which would exist in the empty reactor vessel. The limiting fluidizing velocity sets the absolute lower limit, as below this value the bed would defluidize. In practice, a value somewhat above the minimum fluidizing velocity is specified to ensure that localized defluidization of the bed does not take place. The upper limit is also restricted by the particle terminal velocity, above which the fluidized bed reactor vessel would behave as a pneumatic conveying tube. In the fluidized bed combustion of coal, this upper limit is particularly important, as the higher the superficial gas velocity, the larger the entrained particles will be and hence the greater the unburnt carbon loss from the system. Should the entrained carbon loss be of such a value, collection of this carbon for re-introduction into the fluidized bed may be necessary to improve the combustion efficiency. McLaren and Williams (25) have demonstrated that improvements in combustion efficiency could be obtained in this way, although Bishop et al (9) reported only a slight improvement in the combustion efficiency by recycling of fines. These latter workers advocate the use of a carbon burn-up cell (26), in which the entrained carbon is collected and burnt in a separate bed at a lower velocity and higher temperature.

The two extreme limits for fluidized bed operation are shown in Figure 6 which illustrates the effect of mean particle diameter. The lower line is that for the minimum fluidizing velocity as determined from equation (6) whilst the upper limit is given by the particle terminal velocity. This latter curve is evaluated from Stokes' law for low Reynolds numbers, the Schiller and Naumann equation for intermediate values and Newton's law for high values of the Reynolds number (2, pg 51).

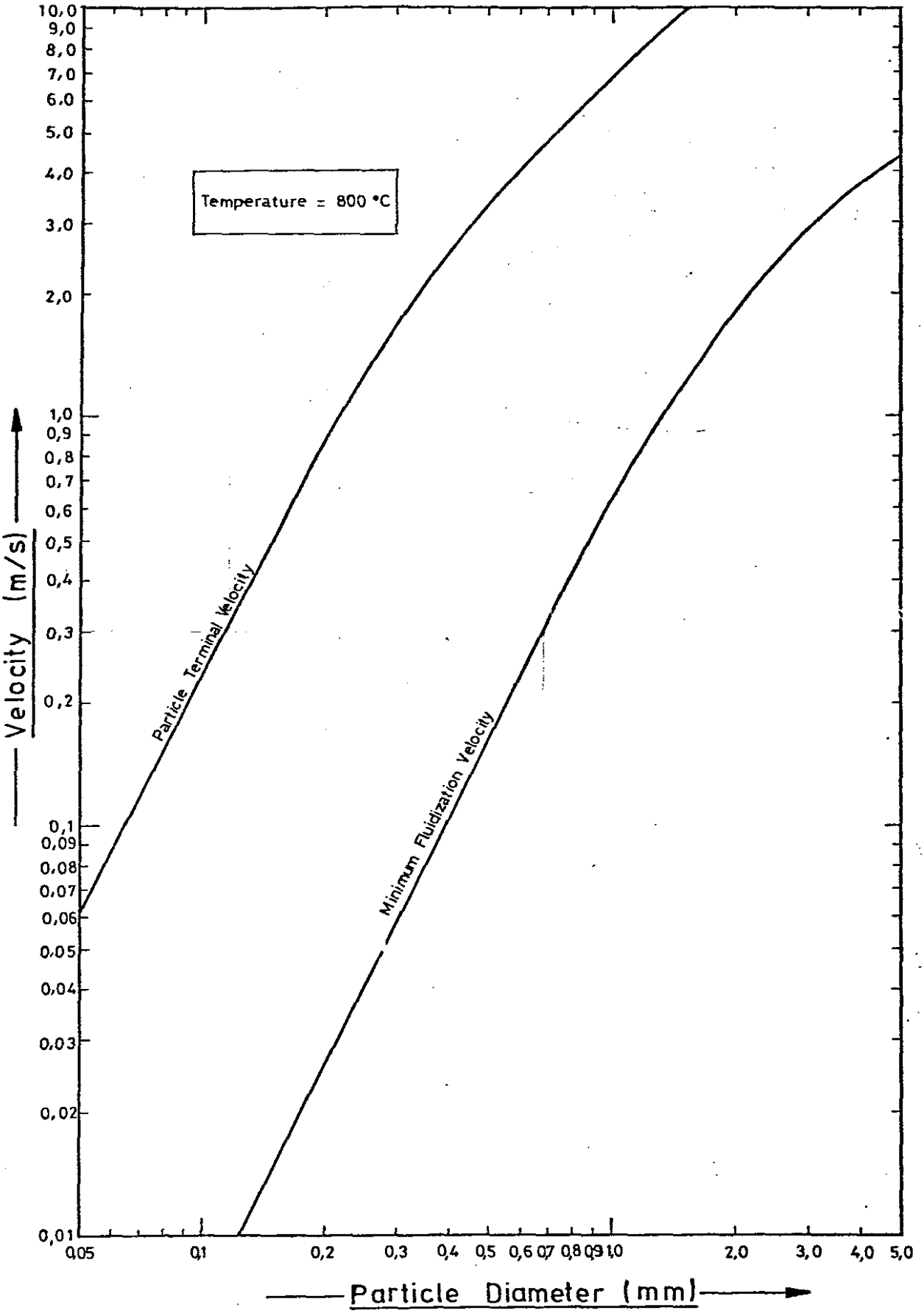

Figure 6 : Representation of the Variation of both the Minimum Fluidizing Velocity and the Particle Terminal Velocity at Different Particle Diameters when Fluidized by Air at 800°C.

1.2.5 The Bed Temperature

Further limitations are imposed on the fluidized-bed combustion process by the bed temperature. The lower limit is set by the coal ignition temperature, for below this value combustion will not be sustained. The maximum bed temperature is restricted by the initial ash deformation temperature as this would lead to sintering and fusing of the bed material. Bishop et al (9) have recommended that the bed operating temperature be maintained at least 100°C below the initial ash deformation temperature, whilst in some instances a value of 250°C to 300°C below this temperature is suggested (27).

As expected, empirical correlations by Ehrlich (26) and Vogel et al (29) indicate a strong influence of bed temperature on the combustion efficiency, with the higher bed temperatures yielding higher efficiencies of combustion. Carbon monoxide formation will be clearly evident at temperatures below 750°C when the combustion air is about 20% in excess of that required for stoichiometric combustion. Whilst at temperatures above 800°C combustion would appear to be complete, i.e. with regard to the formation of carbon monoxide. Campbell and Davidson (13) could not detect the presence of carbon monoxide in the off gases at bed temperatures above 820°C.

1.2.6 The Particle Residence Time

The combustion efficiency for any coal burning process will be greatly enhanced by increasing the time during which the coal particle remains in the combustion zone. Skinner (8, pg 91) reporting on the effect of bed height on combustion efficiency quotes the findings of BCURA when operating with bed heights ranging from 300 mm to 450 mm as indicating that efficiency increases with deeper beds. However, the work of the CRE with bed heights ranging from 300 mm to 700 mm showed no significant variation of combustion efficiency with bed height. Ehrlich (28) in a more recent study found combustion

efficiency to be influenced by bed height such that an improvement in efficiency resulted from increasing the bed depth. It would appear therefore, that deeper beds will result in improved combustion efficiencies. It is evident that, as only a small percentage of combustibles are present in the bed at any one time, the major loss of combustibles is due to entrainment from the bed before combustion is completed. Waters (30) has found that well over 80% of the combustibles loss is as a result of carbon being entrained in the off-gases. By increasing the residence time in the bed, this loss could be reduced. Deeper beds imply an increased bed weight which results in a decrease in the elutriation velocity constant (2, pg 642). This decrease in elutriation constant results in a decrease in the quantity of material elutriated and thus an increase in the residence time in the bed. However, entrainment can be considered as the sum of both elutriation and splashing, cf. Section 1.2.3, and this latter phenomenon is expected to increase with increasing bubble diameters resulting from bubble coalescence as the bed depth is increased. Harrison et al (3) indicate that a maximum stable diameter exists which would imply that the increased loss due to splashing would probably reach a maximum for a particular bed depth. The loss of combustible material as a result of splashing will be less than that lost through elutriation as the amount of combustibles in the splashed product represents only a fraction of this product. The resulting entrainment rate, as a result of the combined effect of decreased elutriation and increased splashing loss as the bed height is increased would also increase when the particle shrinkage rate is assumed to be the result of the combustion phenomenon alone.

However, particle size reduction is also effected by attrition, the attrition rate being directly proportional to the bed weight (22). Thus increasing the bed depth would increase the production of fines by attrition and hence result in a reduced residence time in the bed through increased elutriation. Although some workers have found

increased combustion efficiencies in deeper beds, this may not always be the case when the combined action of elutriation, splashing and attrition of the combustible matter is considered.

Another method of increasing the particle residence time is by re-introducing the entrained material into the combustion zone. Improvements in combustion efficiency have been reported by recycling of fines (25) although Bishop et al (11) report only marginal improvements in efficiency from recycling. In order to obtain a significant improvement in the combustion efficiency by employing these means, high recycle rates would be necessary (28) in which the dust flow exceeded the coal flow by a factor of five or more. Wright (31) reports that experiments conducted at BCURA indicated that the combustion of the recycled fines was not very efficient and suggested that fresh coal may take up oxygen preferentially because of its higher reactivity as a result of the recycled fines being deficient in volatiles.

1.2.7 The Quality of Fluidization

Uniform fluidization is a necessary requirement for the combustion of coal in a fluidized bed so that the heat liberated can be efficiently transferred throughout the bed thus eliminating locallized 'hot spots'. A quantitative assessment of the quality of fluidization is not readily available, and though a bed may appear to be well fluidized, part of its weight may still be borne by the distributor. Vreedenberg (32) defines the degree of fluidization as the ratio of the product of the gas mass velocity and kinematic viscosity at the prevailing conditions, to this product at conditions of incipient fluidization. Merrick and Highley (22) introduced the velocity ratio:

$$(u_f - u_{mf}) / u_{mf}$$

to represent the vigorousness of bubbling within the bed.

However neither of the above two criteria adequately define the quality of fluidization. The major cause of poor fluidization is due to poor distribution which may result in channelling. Siegel (33) reports that the tendency to channel depends on stability considerations. The stability depends on the combined pressure drop characteristics of the particle bed and the distributor. Should a channel form in a fluidized bed, it will offer a low resistance path for the flow of gas. As the velocity is increased, there will be a tendency for the channel to become larger. In order to prevent this tendency, "the decrease in pressure drop with flow rate across the channel should be at least compensated by the increase in pressure drop across the section of distributor" (2, pg 31). This implies that the pressure drop across the distributor should be of the same order as that across the bed. Siegel (33) has developed some relationships for determining the tendency towards channelling in terms of dimensionless parameters characterising fluidized bed behaviour. Using this approach, he found that in order to maintain uniform fluidization with particles having a diameter of 0,50 mm, the pressure drop across the distributor should be greater than approximately 25% of the pressure drop across the bed.

From experimental results, Wright (34) reports that a distributor pressure drop of 50 to 75 mm W.g. resulted in no evidence of maldistribution of the flow where the pressure drop through a 600 mm deep bed was 450 mm W.g. Skinner (8, pg 83) reporting on work done by CRE and BCURA up to 1969 indicates that though higher pressure drop distributors had been used by CRE, workers at BCURA had achieved uniform fluidization with a distributor pressure drop of 125 mm W.g. with the respective bed pressure drop being 625 mm W.g.

It is evident that though high pressure drop distributors will invariably result in uniform fluidization, they are associated with a higher fan power consumption. There is therefore, a

strong economic incentive for the use of low pressure drop distributor types.

1.3 THE ADVANTAGES AND LIMITATIONS OF FLUIDIZED-BED COMBUSTION

The major potential application for the fluidized-bed combustion of coal is in steam generation for industrial use or electricity generation. Both these industries rely on tried and proven methods of steam raising which are both efficient and result in high plant availabilities. It is therefore essential and prudent to consider the potential advantages as well as the limitations of any new technique which may replace either in part or as a whole, the existing methods.

1.3.1 Advantages

a) Poor Quality Coals

Since the fluidized bed only contains a very small amount of combustible matter within it, typically from 0,5% to 2% of the total bed weight, the process is insensitive to the amount of ash contained in the fuel. Experiments conducted with high ash fuels in both Australia (30) and India (35) have indicated that it would be possible to burn coals with ash contents as high as 85%. Thurlow (36) has pointed out that the less reactive a fuel was, the harder it would be to burn, even in a fluidized bed at 800°C, and although anthracite had been burned in a fluidized bed, the combustion of coke breeze may not be possible. However, fluidized-bed combustion offers a potential means of burning this latter fuel.

b) Heat Transfer

The extremely large area of contact between the solids and the gas permits the achievement of high overall rates of

heat and mass transfer between the solid and gas. The heat transferred to surfaces immersed within the fluidized bed is far higher than to surfaces in conventional systems due to the high convective heat transfer coefficient (15, Ch 5). The improved heat transfer results in reduced surface area requirements, this is of particular interest when considering the large radiant combustion chamber evident in all conventional pulverised coal fired steam generators. The use of immersed heat exchange surfaces can lead to substantial savings in the capital cost of the plant concerned. Thurlow (37) has dramatically illustrated the reduction in size of a conventional 660 MW_e pulverized fuel fired boiler when compared firstly with an atmospheric fluidized-bed boiler and the further size reduction when a pressurized fluidized-bed boiler is considered.

c) Pollution Control

By introducing an absorbent such as limestone or dolomite, the sulphur dioxide formed during the combustion of the coal can be captured. Thus high sulphur coals could be burned without having to adopt expensive and as yet unreliable exhaust gas scrubbers and yet remain within stringent emission requirements. The fluidized-bed combustion process provides a clean method of burning high sulphur coals and further eliminates the added expense of sulphur dioxide extraction plants necessary to meet pollution standards in the United States. In Britain, where the emphasis is on the ground level concentration of the pollutant a "high stack policy" has been adopted to allow for the dispersing of the pollutant. The advantages from a pollution consideration in the United Kingdom may not, therefore, be as great as would be obtained in the United States.

The temperature in the fluidized-bed combustion zone is much less than the temperature prevalent in conventional systems. Thus the formation of NO_x will be suppressed resulting in lower NO_x emissions.

d) Low Temperature Combustion

In order to prevent sintering or fusing of the ash particles within the bed, the bed temperature is maintained well below the ash fusion point. Thus slagging or fouling of heat transfer surfaces is reduced or possibly eliminated. The resulting ash which has been formed at the low temperatures is much softer and friable than the ash formed in conventional furnaces. Cooke and Rogers (38) have indicated that the expected fireside corrosion would be less for fluidized-bed boilers than for conventional plant, however, increased rates of corrosion were found in several tests (38) using a high chlorine coal when operating difficulties such as loss of fluidization occurred.

e) Coal Preparation

In comparison with pulverised coal systems, the coal preparation required for fluidized bed combustion is minimal as the excessive power required for grinding the coal is eliminated. However some crushing of the coal will be required as a maximum coal particle size of approximately 6 mm will have to be specified for a fluidized-bed combustor.

f) Elevated Pressure Operation

Pressurized combustion is being developed primarily for power generation. Operation at elevated pressure increases the air supply rate at constant fluidizing velocity and thus allows the combustion rate to be increased in proportion to the operating pressure. The hot high pressure combustion gases can be expanded through a gas turbine which drives the air compressor and an electrical generator. By employing pressurized fluidized-bed combustion, steam can be generated in the fluidized-bed combustion chamber, whilst the high pressure gas is used to drive a gas turbine as described above. By integrating the gas and steam cycles

into a single combined cycle unit, the gas cycle can be used to extract energy at a high temperature, whilst the steam cycle rejects heat at a low temperature resulting in substantial gains in overall plant efficiencies.

1.3.2 Limitations

a) Fan Power Requirement

The pressure drop through bed and distributor is far in excess of any pressures existing in conventional plant. This increased pressure results in higher fan power requirements with a corresponding increase in the power input to the fan. In order to reduce this, work is being carried out into the use of shallow fluidized beds (39, 40, 41).

b) Flexibility of the System to Changes in Load

The gas velocity in the bed section is limited by the minimum fluidizing velocity and an upper velocity limit is reached at which the entrained carbon loss becomes excessive. A further complication exists when useful heat transfer surfaces are installed within the bed. With these surfaces, the rate of heat exchange and bed temperature become inter-dependent. However, the fireside heat transfer coefficient is almost independent of the superficial gas velocity. The behaviour of the fluidized bed in response to changes in heat input and thus to changes in load are best illustrated by considering a steam generating system, which would be the most likely application of the technology. "If the rating is changed by altering the coal consumption rate without significantly altering the fluidization characteristics of the bed and the water-side conditions are nucleate boiling, then the substantially constant bed-side heat transfer coefficient will be controlling and the value of the overall heat transfer will remain constant. This means that as the rating is reduced, the bed heat release is reduced, whilst

the heat extraction rate remains constant so that the bed temperature will fall until some new equilibrium is established. Thus at some rating and bed temperature, fixed by fuel reactivity, the fire will be extinguished. If, however, the bed heat transfer surface is being used as a steam superheater, then the steam side coefficient will be controlling and the heat transferred will fall with falling rating, and although it will be proportional to some power less than unity of the rating, the result will be that a wider turndown ratio could be used without extinguishing the fire" (42).

The velocity and temperature limitations impose restrictions on the flexibility of the system resulting in it having a far smaller turndown capability than conventional systems. However various ingenious systems have been proposed and are being developed to overcome this difficulty eg, by recirculating of the bed material, changing the bed height or defluidizing sections of the bed (43).

1.4 REVIEW OF THE DEVELOPMENT OF FLUIDIZED-BED COMBUSTION

The Winkler gasification process developed in the early 1920's represents the first application of fluidized-bed combustion. By 1929 five Winkler gasifiers were operating at Leuna, East Germany, producing power gas to fuel gas engines driving ammonia synthesis compressors (44). A total shaft power of 130 MW was developed. In the Winkler process, fine coal particles are gasified in a fluidized bed with steam and air to form hydrogen and carbon monoxide. It is suggested (1) that the Winkler generator inspired the development of the fluid cat-cracker which incorporated a fluid bed combustor in the regenerator.

In the United States, pioneering work into fluidized-bed combustion was propagated by Odell, who filed a patent for fluidized-bed cat cracking in 1929. This patent was eventually granted in 1930. Subsequent to these initial processes, the development of fluidized-bed combustion has passed through three phases, and represents fluidized-bed combustion in the generally accepted sense. The first phase was initiated in the early 1950's and is characterized by processes in which the main aim was the use of fluidized-bed combustion as a means of burning low grade coals without incurring coal preparation costs associated with pulverised fuel firing. A further characteristic of this initial phase, was that no attempt was made to extract heat directly from the bed. This was followed by investigations into the extraction of heat from surfaces immersed within the bed. The final stage of development has seen the use of the fluidized bed as a means of reducing atmospheric pollution.

1.4.1 Fluidized-Bed Combustion without Direct Heat Extraction

A number of these processes have been described by Teague and Wright (42) who compared them with ratings and efficiencies achieved by conventional pulverised fuel fired and chain grate type systems. Four fluidized bed processes were assessed. The first of these is the Stouff process which was used to burn untreated coal fines in a refractory lined cone (included angle of 30^{o}) with air being blown up through the base in the bottom. Carry over was high whilst agglomerates were removed through the bottom. In the second system, the Ignifluid process, coal is fluidized and burnt on a sloping chain grate. At the combustion temperatures used the ash agglomerates and falls onto the chain grate which removes it from the bed. This system is presently in use, and the current status of the process is described in more detail below. The Yokoyama system is a cross

between pulverised fuel firing and dilute-phase fluidized combustion requiring both crushing and drying of the coal. The fourth system considered was a pilot plant in Rumània used for the combustion of lignites. The furnace section is refractory lined with two inclined walls to produce a reduced cross-section at the distributor plate. Coal is introduced about 1,5 metres above the distributor. Teague and Wright (42) report that all but the Stouff process achieved reasonable success, although only the Yokoyama process achieved combustion efficiencies in the range of true pulverised fuel firing.

The Ignifluid Boiler

The Ignifluid boiler, developed in France in the early 1950's for the burning of low grade anthracite fines (45), represents a fluidized-bed combustion system which has been fully developed as a commercial process for raising of 3 000 - 50 000 kg/hr (8, pg 12) of steam in water tube boilers. The bed is operated at a temperature high enough to fuse the ash which falls onto a sloping chain grate by means of which it is removed from the bed. Secondary air is introduced above the bed to complete the combustion process. The first Ignifluid-fired industrial boiler was commissioned in the French Alps in 1955, having an evaporation of 3 500 kg/h. Boilers based on the Ignifluid principle are currently in operation in France and Morocco (46) whilst Teague and Wright (42) report the installation of an Ignifluid combustion system in the three boilers associated with the Westfield plant in Scotland. Cosar and Godel (47) report on the construction of a 100 000 kg/h Ignifluid boiler unit with future projections aimed at 400 000 kg/hr systems. Processes basically similar to the Ignifluid have been devised in Rumania, Czechoslovakia and Belgium (8, pg 12).

1.4.2 Early Processes with Direct Extraction of Heat

A major incentive for the application of fluidized-bed combustion is the high rate of heat transfer which can be achieved by immersing surfaces in a fluidized bed. In conventional steam raising processes, about half of the heat is transferred by radiation, the remainder being transferred by a relatively poor convective process. The large area of contact between the solids and the gas results in a rapid transfer of the heat of combustion to the inert solid particles which then transfer heat to the immersed surfaces. Healey and Stockwell (48) quote heat fluxes of the order of 300 kW/m^2 to boiling water tubes immersed within a fluidized bed. This is compared with a radiant heat flux of 500 kW/m^2 from a pulverised fuel flame at 1400^oC, but as this latter flux is only received by part of the tube facing the flame the effective level is less than 200 kW/m^2. The heat fluxes in the convective passes of conventional steam generating plant are of the order of 40 kW/m^2 whilst figures of 120 kW/m^2 are quoted for tubes immersed in a fluidized bed (48). These figures illustrate the potential advantages which can be obtained by immersing heating surface into the fluidized bed.

Processes which utilized the direct extraction of heat from fluidized combustion systems were only patented during the 1950's, of which it would appear that only two (8, pg 13) resulted in the establishment of plants.

Skinner (8, pg 13) reports that a process patented by Standard Oil in 1952 was the earliest instance where the extraction of heat from a fluidized bed was proposed for the raising of steam. The patent described a fluidized process "for controlling the temperature of exothermic reactions such as the gasification of carbonaceous solids" notably coal. A second process, patented in 1954 in Germany by the Badische Analin-und-Soda Fabrik AG, similar to the processes evolved in the United Kingdom in the 1960's,

described a process in which finely divided coal of high ash content was burned in a fluidized bed of non-combustible particles preferably ash derived from the fuel itself. Heat was withdrawn from the bed by means of heat absorbing members within or surrounding it. Another process, developed by Lurgi, for the utilisation of low-grade fuels had a number of cooling tubes located in the bed to prevent agglomeration when richer fuels were burnt, as well as allowing for the production of a carbon-free ash suitable for cement manufacture. This system was installed in three West German power stations which were however closed down towards the end of the 1950's when the incentive to use low-grade fuels was greatly reduced

Combustion Engineering filed a number of patents in the mid-1950's relating to fluidized-bed combustion in steam generation. Besides extracting heat from the bed, the processes patented incorporated the use of an inert bed made up of a highly active oxidizing catalyst to enable combustion to be carried out at wider temperature ranges. Skinner (8, pg 18) finally reports on a number of elaborate schemes patented by the Union Carbide Corp. which made use of the generation of steam in a steam coil which was subsequently mixed with the resulting off gases from the fluidized-bed combustor and finally used for driving gas turbines for electricity generation.

1.4.3 Investigations Leading up to Current Developments

Once it had been established that combustion could be maintained satisfactorily in a bed where the carbon concentration was very low, thus ensuring a minimal formation of carbon monoxide, research was conducted into the means of reducing the entrained carbon loss, and by so doing improve the combustion efficiency. Pioneering work into the reduction of atmospheric pollutants was conducted in the United Kingdom towards the end of the 1960's followed

by extensive research programmes in the United States in the mid-seventies. Work in the United States has been initiated as a result of stringent pollution requirements combined with the abundance of high sulphur coals. A substantial effort is also being utilized in the United States towards the development of pressurised fluidized-bed combustion for application in the power generation field. The major contributions in the field of fluidized-bed combustion until the end of 1975 have been made in the United Kingdom. The renewed interest into fluidized-bed combustion in the United States will probably lead to this country taking the lead in the technology towards the end of the 1970's.

Work into fluidized-bed combustion is being conducted in various other parts of the world. However the scale of this research is small when compared to that in either the United Kingdom or the United States. It is clear, that any major developments or break-throughs are likely to come from these two countries. The developments over the last fifteen to twenty years and the probable course of the technology are discussed below.

1.4.3.1 The United Kingdom

The initial work in the U.K. was undertaken in the late fifties and early sixties by the CEGB and BCURA. The objectives were to study new methods of using coal in power raising. Preliminary tests were carried out at the CEGB's Marchwood Engineering Laboratories. The first tests demonstrated that coal could be burnt successfully in a fluidized bed operating below the ash fusion temperature. In 1964, the development of fluidized-bed combustion was taken over by the NCB and BCURA because of the CEGB's involvement in development programmes for pulverised fuel firing, and nuclear power at the time (49). By 1969 several small experimental rigs were in operation at the NCB's coal research establishment.

It was recognised that although prospects were not favourable for the exploitation of fluidized-bed combustion in the U.K. opportunities existed in other countries. In 1971, the exploitation of the NCB's expertise in fluidized-bed combustion became the responsibility of the National Research and Development Corporation (49). In 1972 a joint company, Combustion Systems Ltd. was formed by the NCB, NRDC and British Petroleum to develop and commercialize the work of its parent companies in the field of fluidized-bed combustion and to continue with the commercial development of the wide range of processes that the technology makes possible (43).

Boiler manufacturers have become involved both independently and in collaboration with the NCB in the development of commercial applications of fluidized-bed combustion. A number of universities have become actively engaged in this new technology, particularly in the study of the fundamental concepts to obtain a better insight into the fluidization, heat transfer and combustion phenomena.

a) The Coal Research Establishment

Up to the beginning of 1969, researchers at the Coal Research Establishment of the NCB accumulated information from combustion experiments on two small rigs. The first was made up of a 150 mm diameter stainless steel vessel with a cooling coil immersed in the bed section for the removal of the heat liberated within the bed. The main series of experiments were devoted to the study of combustion efficiencies. Investigations were also made into an assessment into the reaction taking place above the bed, the control of bed temperature, start-up procedures as well as a series of tests into sulphur and chlorine retention in the bed. The second rig comprises a combustor body made up of a stainless steel plate having a cross-section 300 mm square. The combustor is completely lagged with the heat being removed by immersed cooling coils. The off gases pass through a

cyclone before being exhausted to atmosphere.

Although a number of other rigs have been built at the CRE, current research into fluidized-bed combustion still makes use of these original two combustors. Preliminary investigations are performed in the 300 mm square rig (50, 51) in order to assess from short and fairly simple tests, the form that the ash of a particular feedstock will yield as well as to determine the qualitative characteristics of combustion and to yield information on probable feeding problems. The 150 mm diameter rig is very highly instrumented to enable full heat and mass balances to be carried out and is therefore used extensively in the evaluation of carry-over rates, on the effect of grit refiring and of the addition of limestone for the suppression of sulphur dioxide emission. This 150 mm diameter rig is the standard unit with which a fuel is assessed (50).

In 1971 an application for fluidized combustion in the incineration of colliery waste slurries was recognized (52), and a development programme was started, the object being to produce a dry product for disposal instead of the slurry. Tests were first carried out in the 300 mm square rig mentioned above (53). Having established the technical feasibility of treating colliery thickened tailings, using the fluidized combustion technique, a 900 mm square rig which had originally been commissioned in 1969 to carry out development into the fluidized-bed combustion of coal, was converted to examine any scale-up problems. The successful operation of this rig led to the construction of a 1500 mm diameter demonstration pilot plant. The 900 mm square rig was dismantled to allow the same ancillaries, control equipment and instrumentation to be used for the 1500 mm diameter rig which was commissioned in February 1976. A replica of this plant has been built at Carnarvon for the burning of sewerage (54).

In 1973 a new programme was sponsored by the NCB's marketing department to develop fluidized combustion for industrial boilers and furnaces (52). In order to overcome the difficulties of operating with a limited freeboard height and the resulting high entrainment rate, a new approach was developed in which uncrushed coal sized between 25 mm and 50 mm was burnt by "floating" these particles in a shallow fluidized bed of dense particles such as alumina (39). Initial tests proved that coal could be burnt in 150 mm deep beds at combustion efficiencies of about 96 to 97 percent. In order to demonstrate the concept on a larger scale, fluidized bed burners have been operated in a 600 kW hot water boiler and a 1,2 MW horizontal shell type steam raising boiler.

An additional application for the shallow fluidized-bed combustion of large coal is in the production of hot gas. Following the development work using a 2 MW furnace during 1974, the first commercially operating unit of 5 MW is now in operation (52).

Work into corrosion and erosion in fluidized beds is carried out in a 300 mm square rig. Initially this rig was used to study fouling on boiler tubes immersed within a fluidized bed, however this rig has recently been modified (52) to study corrosion and erosion of turbine blade materials in the gases from a fluidized-bed combustor. This latter work is being done under contract to the EPRI. A small 150 mm diameter open top type rig has recently been commissioned (54) for the testing of different types of limestones in order to assess their ability to absorb sulphur dioxide.

b) <u>The British Coal Utilization Research Association</u>

In the mid-sixties, BCURA constructed and operated two experimental fluidized-bed combustion rigs with a view to obtaining design and operating data for a prototype fluidized-bed industrial boiler (8, pg 28). The first of these rigs

was an open top design with a water jacketed combustor vessel. The objective of this rig was to provide data for a larger closed unit. This original open top design was made up of a conical combustor vessel, the diameter at the distributor being 300 mm with an exit diameter of 400 mm. The included angle of the cone was about 14^{o}. Because of its size the results from this rig were limited, covering only a narrow range of fluidization conditions. However data from this rig were used in the design of a closed pilot scale combustor having an internal diameter of 685 mm. The main functions of this rig were to establish operational conditions, to obtain information on heat release rates and heat transfer and further to study combustion efficiency with and without fines recycle and obtain information on turn-down ratios.

By 1968 it was considered that sufficient data had been obtained and the design of a 3 500 kg/h fluidized-bed shell boiler commenced. It is reported (43) that this boiler has been operating on an experimental and routine basis since about 1970. Hoy (55) reports that the boiler was converted to firing oil in a fluidized bed quite early in its history as there was less support at that time for coal firing. It is presently being used as a service boiler for the BCURA establishment.

The major contribution of BCURA to fluidized-bed combustion lies in their pioneering work into pressurized fluidized combustion. Indeed the only research of any significance into this aspect of fluidized-bed combustion has been conducted at BCURA, whilst the rig represents the largest operating pressurized fluidized-bed combustor in the world at present (early 1977). The combustor has an output of 2 MW and can be operated at pressures up to 6 bar.

The latest development in pressurized fluidized-bed technology in Britain is the placing of contracts in February 1977 by the International Energy Agency for the construction of a

research facility to permit fundamental research into pressurized fluidized-bed combustion at Grimethorpe, Yorkshire (56). The plant has been sized to take an 1800 mm square bed for operation at pressures up to 25 atmospheres allowing thermal inputs ranging from 3,5 MW to 80 MW. The staff at BCURA have been acting as technical consultants for the project.

c) The Commitment of Private Enterprise

"Despite the commercial potential, practically no active encouragement has been given to British companies in development work. The NCB, through the various research organizations which it controls, has a virtual monopoly on the development of the system in Britain" (56). However, Energy Equipment have converted a 4 500 kg/h shell boiler for firing with oil or coal in a fluidized bed (57, 58). An essential feature of the system is a complete absence of cooling tubes within the bed itself. Combustion is only partially completed within the bed, with carbon monoxide and volatiles being burned in the remaining flue of the furnace.

In a joint venture funded by Combustion Systems Ltd. and Babcock and Wilcox, and using CSL technology the Babcock and Wilcox works boiler at Renfrew has been converted to an atmospheric fluidized-bed combustion unit by replacing the chain grate with a fluidized bed. This converted boiler went into operation in June 1975 with the fluidizing velocity limited to 1,2 m/s with an evaporation rate of about 10 000 kg/h (43). McKenzie (59) reports that full boiler rating of about 20 000 kg/h has been attained with a heat input of 17,6 MW. Initial trials have indicated that fluidized-bed combustion is a viable system

1.4.3.2. The United States

Whereas research in Britain into fluidized-bed combustion

was begun for its potential as a coal burning technique, work in the United States has been conducted primarily as a means of reducing air pollutants. The Energy Research and Development Administration (ERDA) heads the efforts in the United States, with the Environmental Pollution Agency (EPA) playing a supporting role in assessing the environmental impact of fluidized-bed combustion (60). The Electric Power Research Institute, a non-profit organization, is backing investigations for its member utility firms who supply the funding to the Institute so that sufficient funds are available to enable work and development on a large enough scale to be meaningful for utility applications.

Work into fluidized-bed combustion was originally conducted by the United States Bureau of Mines at both their Morgantown and Pittsburg Research Centres (8, pg 42). The Morgantown rig consisted of a 600 mm diameter refractory lined combustor which was used for the assessment of heat transfer coefficients, establishing optimum conditions of operation and finally for determining the effectiveness of limestone injection for the control of sulphur dioxide emission. The Pittsburgh Station Rig comprised a 450 mm diameter waterjacketed combustion chamber. It was used for the study of heat transfer coefficients, heat release rates and the effect of increasing feed rate on bed temperature.

In 1965 a contract was awarded to Pope, Evans and Robbins by the Office of Coal Research to undertake research and development into the application of fluidized-bed combustion for steam raising. This work led to the development of a modular unit having a steam capacity of about 3 000 kg/h. This modular approach was incorporated into a design for a 135 000 kg/h boiler required for a 30 MW_e demonstration unit at Rivesville, West Virginia (61). Iammartino (60) reports that a substantial proportion of the capital for this unit was being supplied by ERDA, whilst the boiler was constructed by Foster Wheeler Corporation. Commissioning of the unit

was scheduled for August 1976 (61) with continuous operation to follow after a few months. This unit will rank as the largest by far of the world's growing list of test installations. This 30 MW_e unit incorporates features which will provide information for scale up to a larger 200 MW_e demonstration unit. In March 1977, the Tennessee Valley Authority announced that studies had begun for the preliminary design and support studies for a 200 MW_e demonstration generating plant that will burn coal by atmospheric fluidized-bed combustion (62). The plant is scheduled to be on line by 1984 and by adopting the fluidized-bed combustion process, TVA will be able to utilize their high sulphur coals and remain within environmental pollution standards.

Jonke et al (63a) have reported on the experimental programme at the Argonne National Laboratory. Work on a 150 mm diameter pressurized fluidized-bed combustor and its associated 75 mm diameter regenerator, for the regeneration of limestone or dolomite, is funded by the EPA. The major portion of this work is concerned with the application of fluidized combustion as a means of limiting atmospheric pollutants.

The current status of fluidized-bed combustion in the United States is aptly described by Iammartino (60). He reports that Exxon Research and Engineering in Linden are studying the combustion of coal in a 300 mm diameter pressurized combustor of 0,67 MW capacity. Under an EPA contract, Westinghouse Electric and Foster and Wheeler have completed a preliminary design for a 600 MW_e power plant. Further, ERDA has awarded a contract to Curtiss Wright Corp. for a 4 500 kg/h of coal elevated pressure unit for operation by 1980, and is also planning two 100 MW_t systems. The first will b an atmospheric pressure unit to be installed at Morgantown, and the second a high pressure unit to be installed at Argonne National Laboratory.

1.4.3.3 Research in other Major Centres

Besides Britain and the United States, a number of other nations are becoming actively engaged in research and development into fluidized-bed combustion, in particular those countries with large indigenous fossil fuel reserves. The work being conducted in these countries is briefly described below:

a) West Germany

The original development of fluidized bed combustion took place in Germany during the twenties with the development of the Winkler gasification process. It was only in the fifties, however, that development of the fluidized-bed combustion process took place along the more familiar lines apparent today, with patents for the extraction of heat from fluidized beds of fuel and inert material for the generation of steam. This work was conducted by the Badische Analin und Soda Fabrik AG. More recently, Iammartino (60) has reported that West Germany's coal mining and energy company, Saarbergwerke announced a co-operation with the NCB, covering amongst others, fluidized-bed combustion. Reh (63b) reports on the planning of a pressurized fluidized-bed combustor and associated gas turbine by the Bergbau-Forschung GmbH, with funding from the West German government.

However the major portion of work in Germany has been in the field of special types of equipment incorporating fluidized-bed combustion. In particular, Reh (63b) reports on the Lurgi fluidized-bed roasting process, for the roasting of sulphide ores, with the following combustion reaction:

$$Me \cdot S + \frac{3}{2} \cdot O_2 \rightarrow Me \cdot O + S O_2$$

in which the ore has a heating value of 3,5 to 8,5 MJ/kg. A fluidized-bed roaster of 12,5 m diameter with a maximum

steam generation capacity of 40 000 kg/h (10 kg/s) has been built by Lurgi.

Finally, through the International Energy Agency a seven-year agreement has been reached between the United Kingdom, Germany and the USA to share equally a project, of constructing and programming the rig to be built at Grimethorpe Colliery, Yorkshire, cf Section 1.4.3.1b.

b) Australia

Bowling and Waters (64) have reported on original work being conducted by the Commonwealth Scientific and Industrial Research Organization until the beginning of 1969 on a small 230 mm diameter combustor. Investigations were made into the combustion efficiency, heat release rates and heat transfer. They found that combustion was almost complete in shallow beds, about 150 mm deep, and that deep beds were unnecessary except for purposes of heat transfer. Further work at the CSIRO found that fouling and corrosion of heat exchange surfaces in fluidized beds is less than that normally associated with conventional furnaces (65). A mathematical model of the heat transfer mechanism was studied.

More recently, Waters (66) has investigated the combustion of low grade fuels in a 400 mm diameter combustor, and in particular the combustion of washery rejects resulting from the process of producing coking coal for export. Data obtained from the tests were used for assessing the relative importance of physical and chemical factors in the fluidized combustion of low grade fuels.

c) New Zealand

Research is being carried out on a small scale with a combustor being designed and built at the University of Canterbury in 1970 (67). The combustor consists of a refractory lined furnace with a 280 mm square distributor.

The rig was designed to obtain operating experience and to establish data for the eventual design of a prototype boiler. Much effort has been directed at trying to find an effective method of start-up, seeking a suitable bed material and matching the size range to the air and coal rate. Heat release rates are much less than those found elsewhere in the literature.

d) India

Rama Prasad (35) has reported on tests conducted on a 590 mm square refractory lined combustor as well as more detailed investigations using an octagonal bench scale combustion apparatus. Substantial deposits of low grade coal are available in India, and it is hoped that fluidized-bed combustion could provide a means for utilizing these reserves. A further advantage of this technology is the reduction in coal preparation costs, as Indian coals are extremely abrasive causing frequent breakdowns of coal pulverisers and associated equipment. The tests (35) have indicated that the high ash Indian coals are amenable to combustion in fluidized beds. It was found that screened coal could be burnt without further preparatory steps.

e) South Africa

The Fuel Research Institute commenced work into the fluidized-bed combustion of large coal in December 1975. A crude 210 mm diameter test rig was tested (68) with a view to obtaining experience for the design of a pilot scale combustor. Information obtained from the rig was mainly of a qualitative nature and indications are that a wide range of South African fuels are amenable to combustion in a fluidized bed. It was found that except in the case of unwashed coal, all the ash was elutriated. The Fuel Research Institute are interested in applying the fluidized-bed combustion technique to shallow beds for firing coal of sizes larger

than 12,5 mm by floating the coal on the bed as proposed by Highley et al (39). The Institute are also interested in applying this shallow bed technique to the drying of crops. Work on the 210 mm diameter rig has ceased, and the design and construction of a pilot plant with a 500 mm square bed is in progress.

Holsteyn (69) reports on the design and construction of a 4 000 kg/h boiler built under a licence agreement negotiated with Combustion Systems Ltd. at the beginning of 1975, this contract has also been mentioned by Thurlow (51) and Hoy (55). The boiler was completed by the middle of August 1975, the main object of this boiler was to use a cheap form of fuel. At that time, it was desirable to use duff, a coal having a top size of 6 mm and containing a large proportion of fines, as this was available at the mere cost of transport. At the present time this remains a cheap form of fuel, and by burning this coal, a fuel for which there is no industrial market can be utilized.

1.5 OBJECTIVES OF THIS THESIS

Research into fluidized-bed combustion in South Africa is at a very early stage of development. This country is therefore in the fortunate position of being able to assess trends in the development process without being committed to a particular line of research whilst at the same time avoiding time-consuming and costly pitfalls. Whereas research at the FRI is towards the development of the burning of large coal particles, and that reported by Holsteyn (69) is intent on 'buying' technology and exploiting it commercially, the objectives of this research are the burning of a locally available coal, preferably one not normally utilised, in an environment acceptable to industry. The work is divided into two phases, an experimental and a theoretical phase.

In the experimental analysis, combustion efficiencies and entrainment rates have been monitored. The results have been statistically analysed and the effect of the main controlling variables assessed. In order for the experiments to be compatible with industrial requirements, only shallow bed depths and a distributor having a low pressure drop will be utilized. Moderate fluidizing velocities will be adopted to retain the efficiency within acceptable limits, whilst as wide a range of bed temperatures as possible will be employed.

The second phase of the work will consist of a theoretical study to model the fluidized-bed combustion and entrainment processes. Empirical factors determined from the experimental work will be used in the theoretical model to correlate both theory and experiment. One of the major objectives of the theoretical work will be to obtain a better understanding of the complex interactions taking place in a fluidized-bed combustion system.

CHAPTER 2

EXPERIMENTAL EQUIPMENT

As the prime objectives of the research are the assessment of the combustion and entrainment phenomena, and in view of the limited resources at the university, no heat transfer surface has been provided in the experimental rig. The heat generated by the combustion process has therefore to be removed by the fluidizing gas. Thus about three times the air which would normally be required for stoichiometric combustion has to be supplied to the rig to maintain the bed temperature within acceptable limits. Such a system is likely to suppress any carbon monoxide formation and ensure complete combustion within the bed section as a result of the abundance of oxygen. Further, the combustion of the volatile component of the coal should also be completed within the bed and very little combustion in the freeboard section can be expected.

2.1 GENERAL ARRANGEMENT

The general arrangement of the major components of the fluidized-bed combustion test rig is illustrated in Figure 7. The rig is housed in the Boiler Room of the Mechanical Engineering Laboratories at Cape Town University. The combustor vessel forms the central piece of equipment (Figure 7) with coal being screw fed into the side of the vessel. Fluidizing air, which also performs the functions of combustion air and the rig cooling medium, is supplied by means of a high pressure fan to a 200 mm deep windbox or plenum chamber situated at the base of the combustor. The gases emitted from the combustor are cooled by mixing with the surrounding air and removed from the Boiler Room through an extraction hood placed centrally above the combustor. The gas/air mixture then passes through a short straight

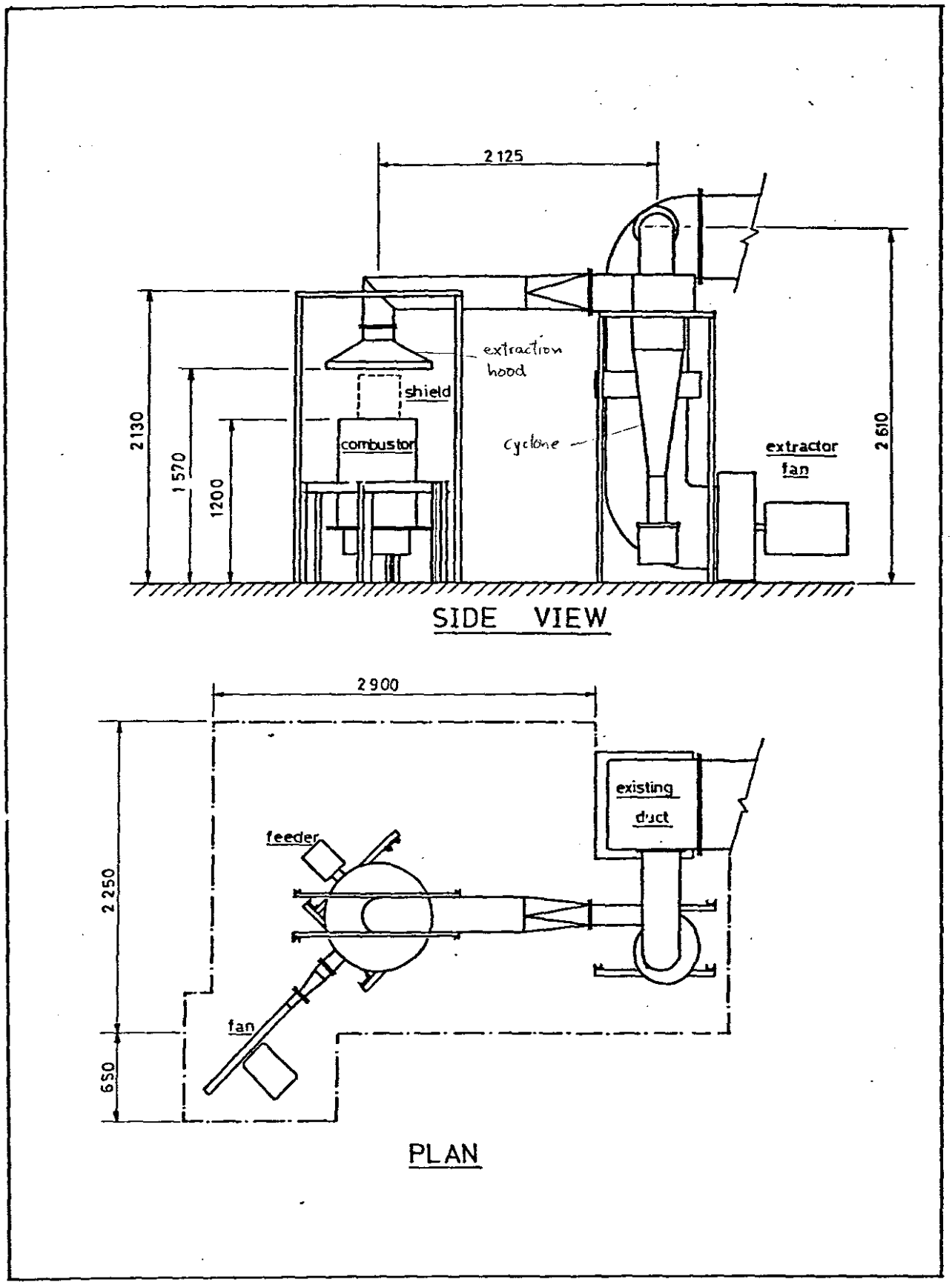

Figure 7 : General Arrangement of the Major Components of the Fluidized-Bed Combustion Test Rig.

section of ducting before entering a medium efficiency cyclone. The major portion of the entrained dust is removed by the cyclone and collected in a small bin for analysis at a later stage. The cleaned gas/air mixture then passes through the exit gas ducting from the cyclone which is connected to the existing boiler exhaust gas ducting. The induced draught fan of the boiler is used as an extractor fan for the fluidized-bed combustion rig, emitting the resulting gas/air mixture via a chimney to the atmosphere.

A flow diagram of the fluidized-bed combustion test rig is represented by Figure 8. This figure includes details of the gas ignition system. It should be noted that this system is only used during start-up, whilst during normal operation the pilot burner will be removed and the gas supply to the plenum chamber shut off.

2.2 INDIVIDUAL COMPONENTS AND SUB-SYSTEMS

As is evident from the preceding section, the fluidized-bed combustion test rig is made up of a number of individual components and sub-systems. These include the air and fuel supply systems, the combustor vessel itself, the gas extraction and dust removal system, and the gas ignition equipment required to raise the bed to a temperature at which the combustion of the coal becomes self-sustaining. A general description of the components making up each of these sub-systems is included below, whilst diagrams and the detailed design of the components are to be found in Appendix A.

2.2.1 The Combustor Vessel

The combustor vessel has been designed so as to limit the quantity of heat lost to the surroundings, and therefore

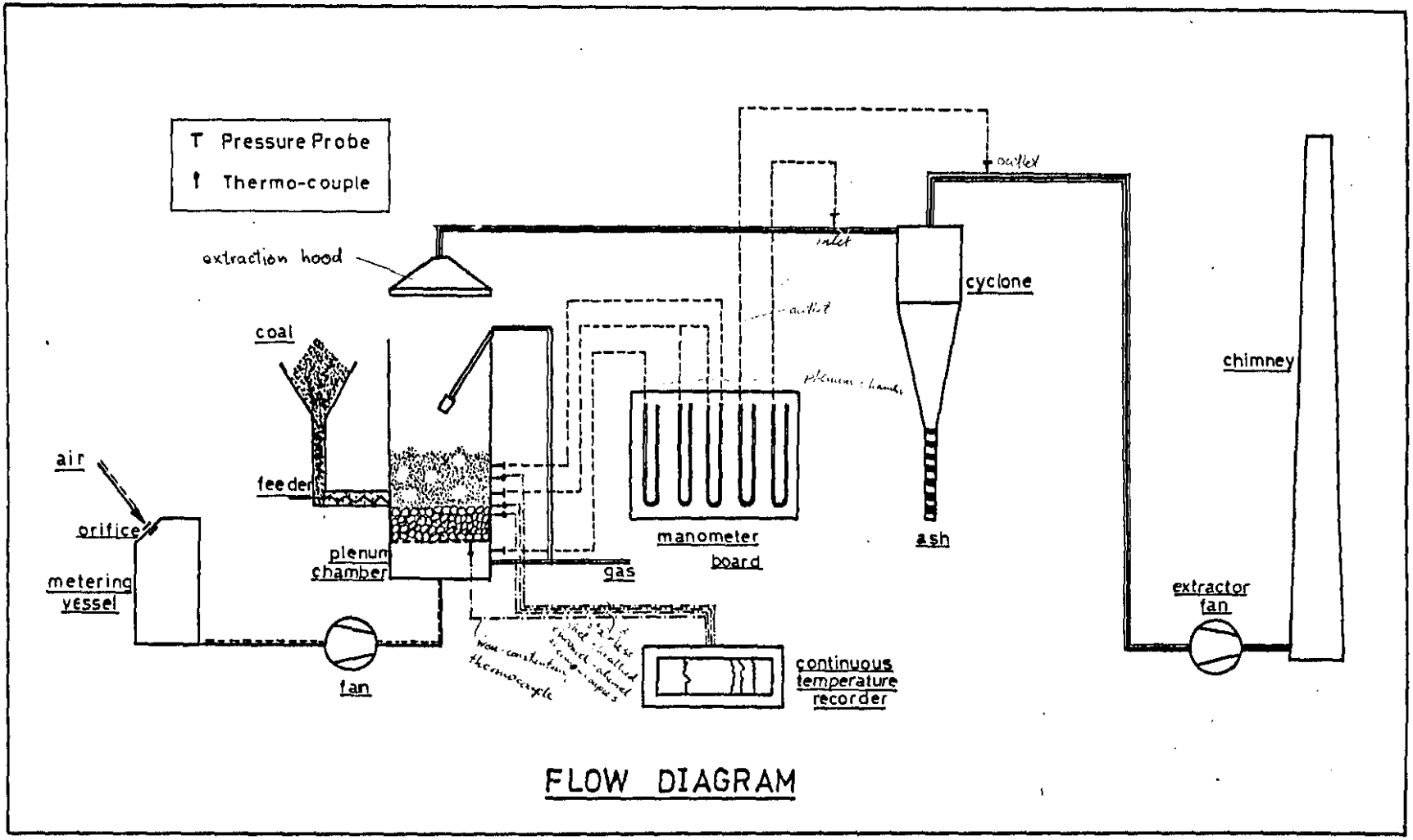

Figure 8 : Flow Diagram of Fluidized-Bed Combustion Test Rig

the combustor walls have been made up of insulating material. A diagram to illustrate the basic combustor details is represented by Figure 9, whilst details of apertures provided for coal feeding, instrumentation etc. are given in Figure A1 of Appendix A.

The distributor is situated at the base of the combustor vessel. The vessel has an internal diameter of 300 mm and is lined with a high temperature refractory on the inside with an insulating material surrounding the refractory. Both layers are 75 mm thick, and are encased in a 5 mm thick rolled plate shell. The castable refractory forming the layer and thus the walls of the combustion chamber, has a maximum service temperature of 1300°C and has been designed to reduce the temperature prevailing in the fluidized bed by about 100°C. The high strength characteristics of this material over the entire temperature range enables it to be used in direct contact with the fluidized bed. This high temperature refractory is enclosed by an annular layer of vermiculite based castable insulating material which reduces the temperature to about 100°C. This layer limits the heat lost through the combustor walls to a very small fraction of the heat liberated by the coal such that this heat loss is about less than 1% of the heat liberated.

2.2.2 The Distributor

"Because the pressure drop of a fluidized bed depends only on the weight of the bed per unit area and is independent of the fluidizing gas flow rate ...., there are no self-regulating properties to help maintain a uniform flow rate across the bed" (15, pg 80). The major function of the distributor is to promote uniform fluidization by stabilizing the effect of gas distribution. The distributor is generally used to support the de-fluidized bed, and must be designed to prevent a back flow of material during normal operation or when the bed is shut down.

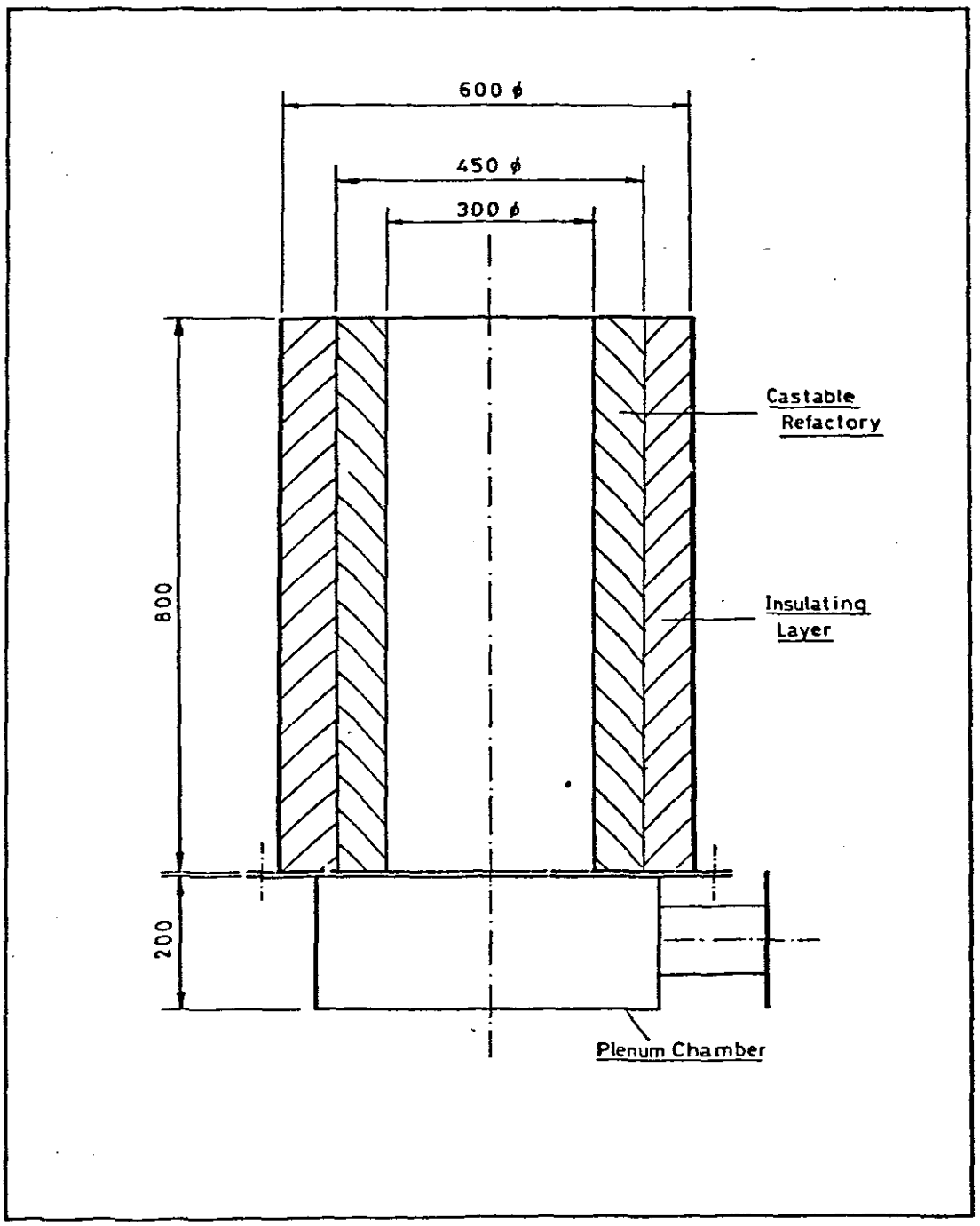

Figure 9 : Diagram to Illustrate the Basic Combustor Details.

Many different types of distributor have been reported for use in fluidized beds, Kunii and Levenspiel (4, Ch 3) and Perry and Chilton (70, pg 20.66). These may be divided into perforated plates, bubble cap types, and sintered metal or porous ceramic types. The use of sparge tubes has been reported by the NCB (71), whilst Rigby et al (72) have developed a double pipe distributor for overcoming back filling in intermittently fluidized beds at elevated temperatures.

In order to maintain the equipment as simple as possible, a perforated plate type was selected. The method of attaching the distributor to the combustor vessel is given in Appendix A and makes allowance for the use of different distributors ranging in thickness from 100 mm and less. In order to produce a design which would provide uniform fluidization of the particles with a low pressure drop across the distributor plate, the designs of perforated plate distributors used by different authors were considered. Blinichev et al (73) recommend that in order to have relatively uniform fluidization and minimum attrition of particles the distributor should have a free cross section of 3 to 4% with the diameter of the openings as small as possible. However, Agarwall et al (74) found that satisfactory fluidization was achieved with a 4,5% free area. Norman (75) used a 20 mm thick disc with 1,5 mm diameter holes whilst another design (76) used a 25 mm thick cast iron plate drilled with 3 mm diameter holes to produce free areas ranging from 3 to 5%.

With this in mind, a perforated plate was designed based on orifice theory as recommended by Richardson (77). The resulting distributor was 12,5 mm thick, having 2,5 mm diameter holes drilled on a 12,5 mm square pitch. This resulted in 437 holes yielding 3,03% free area. On testing the distributor, the pressure drop across it was found to be much lower than that predicted by the method of Richardson

(77). The distributor was tested with a bed of sand about 270 mm deep to determine whether uniform fluidization could be achieved. It was decided to block some of the holes, and after a number of tests and successive steps of reduction in the mean free area, satisfactory fluidization was achieved. The number of open holes was reduced to 268 giving a mean free area of 1,86%.

A layer of refractory stones, approximately sized between 6 and 9 mm in diameter was placed on top of the distributor to prevent back flow of the bed material through the distributor and to act as an insulating layer between the bed and the distributor plate. It is essential to prevent the distributor from overheating to ensure that it does not distort at high temperatures and further to prevent the possibility of damage to the seal between the distributor and combustor vessel. The refractory stone layer was about 90 mm deep, such that the top of the stone layer was flush with the lower point of the coal feed aperture, as illustrated by Figure 10.

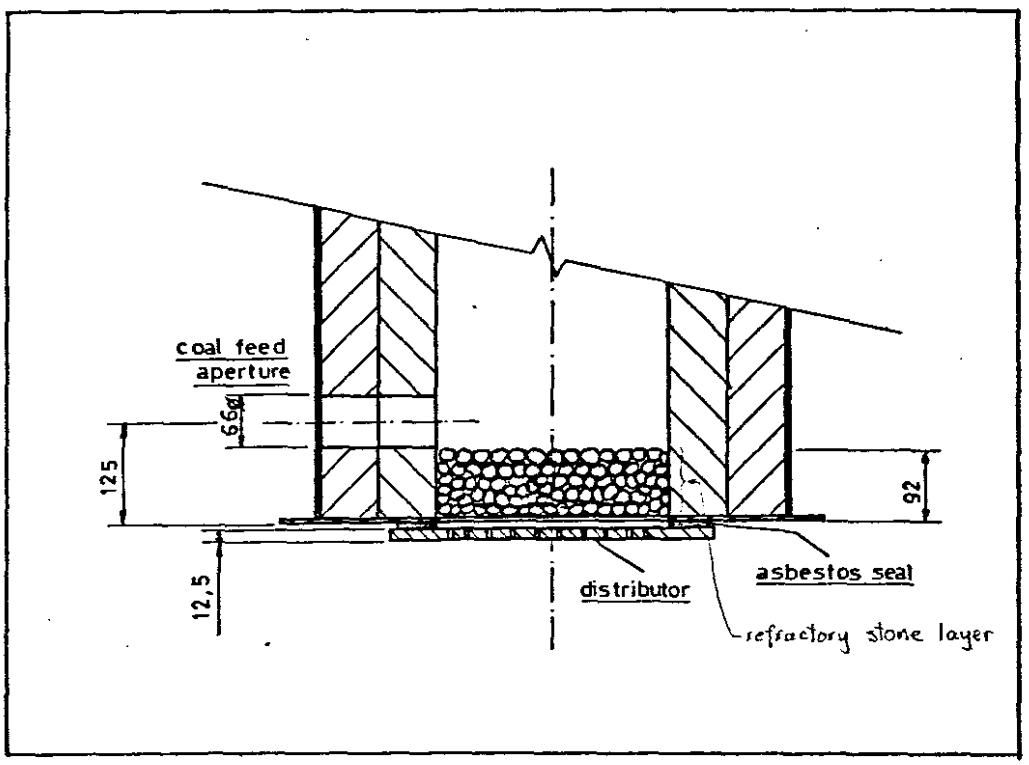

Figure 10 : Diagram to Illustrate the positioning of the Coal Feed Aperture in Relation to the Distributor and Refractory Stone Layer.

Pressure drops through the plate alone and through both the plate and refractory grog layer have been measured and statistically correlated, cf. Section 2.4.1, to give the following equations:

$$\Delta p_d = 231 \cdot u_f^2 \qquad (10)$$

$$\Delta p_{d,r} = 297 \cdot u_f^2 \qquad (11)$$

2.2.3 The Coal Feed System

The coal is fed into the combustor by means of a screw feeder into the base of the fluidized bed as illustrated in Figure 10. Because of the low coal flow rates anticipated with the rig, the feeder could not be bought and had to be specifically designed and manufactured in the University workshops. Details of the design are included in Appendix A.

The feeder is driven by means of a D.C. motor and gearbox unit which has a maximum output speed of 50 rpm. This speed is then reduced by means of a chain and sprocket drive having a reduction of almost 4 to 1, resulting in a feeder speed about a quarter of that from the gearbox output shaft. The motor has a separately excited field winding, thus enabling speed control by varying the armature voltage. The single phase mains voltage is rectified by means of a full wave rectifier to supply a constant D.C. voltage of 220 V to the shunt field winding. In order to be able to vary the voltage supplied to the armature, the constant source single phase mains supply is used as input to a variable voltage transformer. The output from this device can therefore be varied between zero and 220 V. This output is rectified by means of a second full wave rectifier. The output speed from the D.C. motor and gearbox unit is thus easily controlled from zero to 50 rpm in an almost infinite number of steps by varying the input armature voltage from zero to 220 V. A circuit diagram illustrating

the input controls to the D.C. motor is given in Appendix A.

A small coal storage hopper has been constructed about 750 mm above the coal feeder. The hopper is connected by means of a 75 mm diameter pipe to the coal feeder and is capable of storing about 10 kg of coal.

2.2.4 The Air Supply System

Air is supplied to a 200 mm deep windbox or plenum chamber by means of a high pressure fan. The volumetric flow from the fan is regulated by means of both a butterfly valve and an isolating type gate valve, both situated in series on the discharge side of the fan. It has been found convenient to use both valves simultaneously to obtain better control. The butterfly valve is used for the less accurate control, whilst the gate valve is used to obtain a more precise value of the required flow rate.

Because of space restrictions, the flow has been measured by installing the measuring device on the suction side of the fan. This measuring device consists of a large calibrated vessel, about 1600 mm high by 500 mm in diameter, open to atmosphere by means of two orifice plates. By connecting the suction side of the fan to this vessel, the vessel pressure, or rather the amount by which the pressure in the vessel is less than atmospheric is measured. This value in fact corresponds to the pressure drop across the orifice plates, and therefore this pressure drop can be related to an air flow measurement.

2.2.5 The Gas Extraction System

The exhaust gases are removed via an extraction hood and cyclone before being exhausted to atmosphere through the existing chimney by means of the existing boiler induced

draught fan. As the cyclone had to be located on the suction side of the induced draught fan and further as this fan can only deliver a very small pressure head, the pressure drop across the cyclone is limited. This pressure drop has been measured as 39 mm Wg. The cyclone was therefore designed as a medium efficiency device (78, Ch 12, 79, Ch 11). Although this may appear to be a severe limitation, it is of value to note that the greater proportion of particles entrained in the flue gas stream would have a diameter in excess of 60 microns. Reference to Appendix K indicates that the cyclone efficiency for this particle size would exceed 80%.

2.2.6 Gas Ignition System

Before the combustion of coal will be self supporting, the coal particle must be raised to a temperature in excess of the ignition temperature. For coal surrounded by a mass of inert particles as in a fluidized-bed combustion system, the entire mass of coal and inerts must be raised to the temperature at which coal combustion becomes self sustaining. The method adopted on the test rig and indicated in the flow diagram of Figure 8 is that of gas ignition.

Gas is introduced into the plenum chamber where it mixes with the combustion air before passing through the distributor into the combustion vessel. The gas is ignited above the bed section by means of a pilot flame. By careful adjustment of the gas flow rate indicated by means of a rotameter, the gas air mixture can be caused to burn within the bed section. An inherent danger of such a gas ignition system lies in the potentially explosive gas mixture in the plenum chamber. Prevention of the ignition of this mixture before it has left the plenum chamber is ensured by maintaining the distributor plate at a low temperature and by having the velocity through the distributor orifices well in excess of the flame front velocity.

The first requirement is obtained by the refractory stones placed on the distributor plate insulating this component from the fluidized bed. A number of Iron-Constantan thermo-couples have been peened into the lower side of the distributor plate to monitor this temperature and ensure that it remains a few hundred degrees below the spontaneous ignition temperature of the gas and air mixture. The velocity through each of the orifices will always be in excess of 25 m/s to ensure fluidization, as should the bed be slumped, the gas will burn above the static bed section. The maximum velocity of flame propagation of a propane air mixture is 0,86 m/s whilst the ignition temperature is 500°C.

2.2.7 Instrumentation

The condition of the fluidized bed is monitored by a number of pressure and temperature probes. Due to the large quantity of air in excess of that required for combustion supplied to the rig, carbon monoxide formation will be suppressed. Even should some carbon monoxide be formed, this would only represent a small fraction of the total gas flow and be difficult to measure reliably. Thus the off gas composition has not been monitored.

a) Temperature Measurement

The bed temperature is measured by means of three stainless steel sheathed chromel-alumel thermo-couples situated at different points within the bed as illustrated by Figure 11. The lower thermo-couple has been bent upwards so that it measures the temperature at the base of the fluidized-bed. The off-gas temperature is measured by a bare chromel-alumel thermo-couple, whilst iron-constantan thermo- couples in the lower portion of the distributor are used to monitor the temperature of this component.

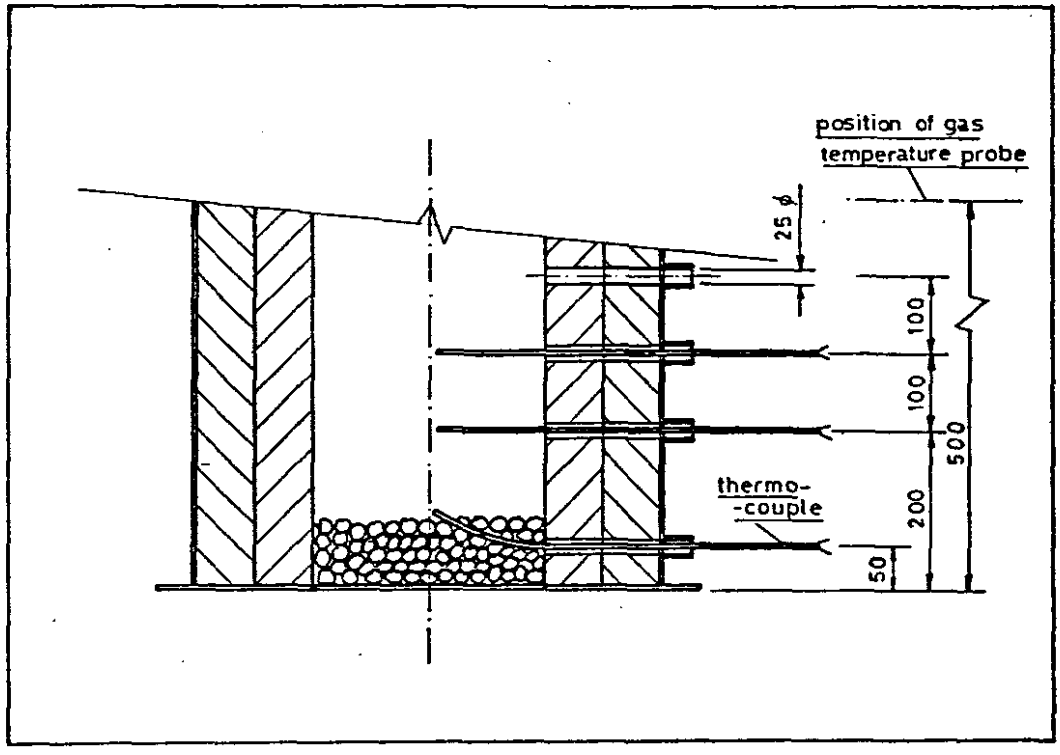

Figure 11 : Diagram to Illustrate the Location of Thermo-couples for the Measurement of Bed Temperatures.

b) Pressure Measurement

Pressures are measured by means of water manometers which have all been built onto a common manometer board.[49] Static pressure tappings have been made to measure these pressures in the plenum chamber, and at inlet to and outlet from the cyclone.[see p 49] These latter two pressure tappings have been located at points at the end of straight lengths of ducting.

The bed pressure probes are worth special note. Up the side of the combustor vessel, a number of instrumentation apertures, each 25 mm in diameter have been provided for the introduction of the relevant instruments. Each of these apertures pass from the inside of the combustor, through both the refractory and insulating layers, with a 25 mm diameter pipe stub welded onto the combustor vessel casing thus completing the cylindrical passage through the

combustor wall. A 25 mm diameter end cap is then screwed onto each stub. The thermo-couples mentioned previously each pass through an end cap which acts as a locating device. Each of these end caps are further drilled and threaded to accommodate the bed pressure measuring probe as indicated in Figure 12.p60 The pressure probe consists of a 6 mm outside diameter steel pipe, Part C, which is located within the rig by means of a brass locating piece, Part B, which is screwed onto the end cap. A knurled brass end cap, Part A, is used to complete the seal on the pressure probe as well as tightly crimping the seal between the locating lug and the pressure probe, so preventing movement of this latter part. The pressure probes are located so as to lie flush with the inner wall of the rig. The positions of the two probes used are indicated in Figure 19.p24

c) Ignition Gas Measurement

The flow of the ignition gas is measured by means of a rotameter, whilst the pressure is determined by a mercury manometer. These quantities are only monitored during start-up as once coal firing has been established the gas ignition equipment is isolated from the remainder of the rig.

d) Other Quantities Monitored

The input voltage to the armature of the feeder motor is measured on a moving coil instrument. This is used to provide an estimate of the coal flow, as the actual value is obtained by determining the rotational speed of the feeder. Finally, the air flow rate is measured by observing the orifice pressure drop as mentioned in Section 2.2.4.

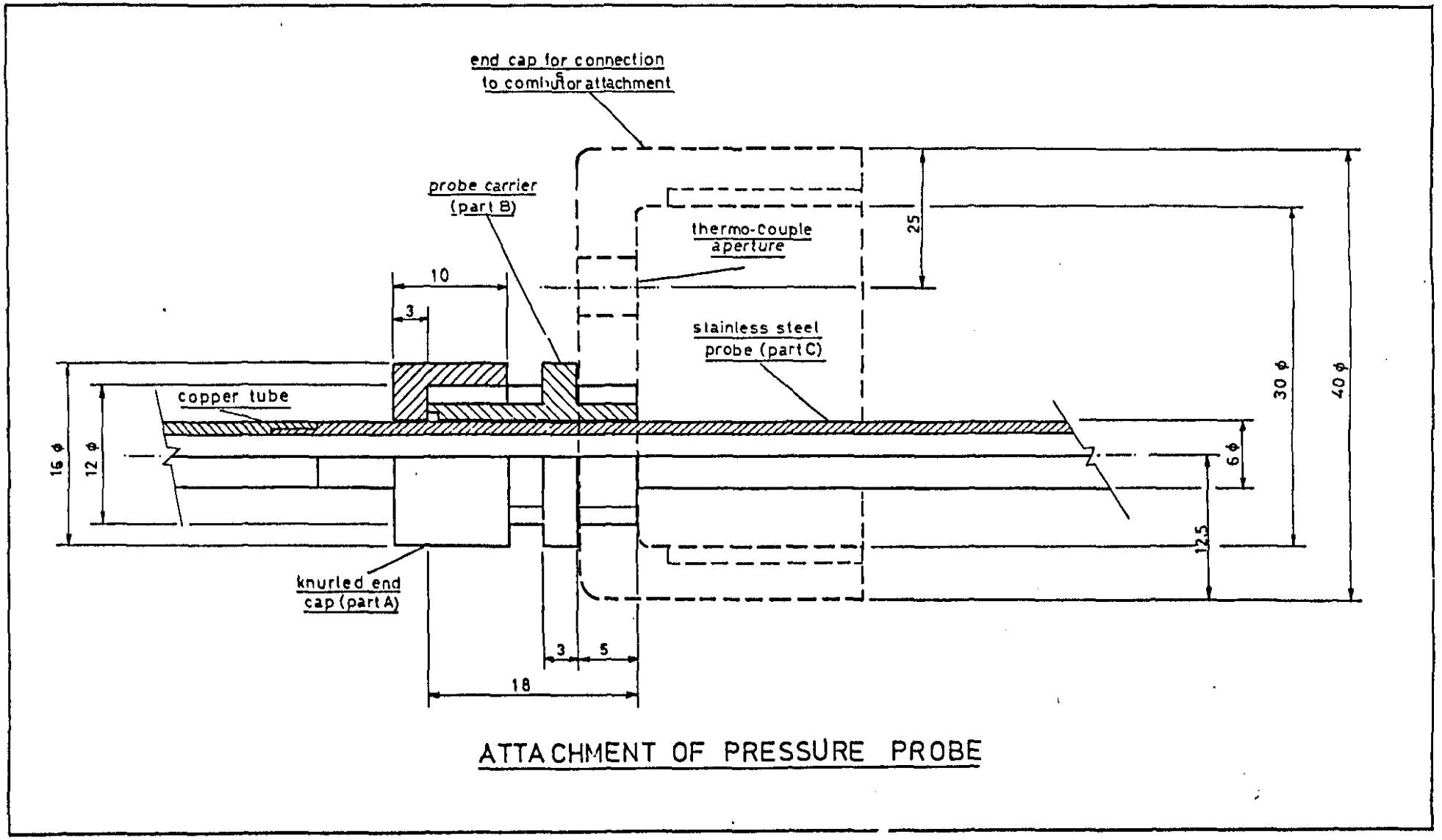

Figure 12 : Attachment of Bed Pressure Probes to the Combustor Vessel

2.3 OPERATING PROCEDURE

2.3.1 Start-up Procedure

a) Original Ignition Procedures

Originally attempts were made to raise the bed temperature without the use of a secondary fuel. A layer of coal was placed on the top surface of the bed and ignited by a thin layer of paraffin soaked coal resting above it. This method was similar to that employed by Gilmour (67). Little success was achieved as only the upper surface became hot. The method was extended by mixing coal and sand in a 40 to 60 mixture, similar to the practice adopted by Rama Prasad (35). This resulted in very localized heating which was difficult to control, causing some of the sand particles to fuse. The major difficulty lies in supplying an adequate amount of air to the bed to provide sufficient fluidization and hence the elimination of localized hot spots, but at the same time preventing an excessive air flow thereby causing high and intense rates of combustion of the coal in the bed. Further tests were made by mixing charcoal and sand together to form the bed material as has been employed by Wright (27). The heat release was not as intense as when coal was used and the susceptibility of the sand to fuse locally was reduced. It was concluded that charcoal sized from 6 mm to 1 mm and mixed with the bed material in a 50 : 50 volumetric proportion represents the best solution for starting the bed from cold without the introduction of a secondary fuel. Although this method did yield a means of raising the bed temperature to a level at which coal combustion becomes self supporting, the method did not yield satisfactory control of the bed temperature and further it was difficult to guarantee a successful ignition all the time. It was decided that much experience would be necessary to perfect this method, and as a result the method of gas ignition was employed.

b) Gas Ignition Procedure

The use of gas as a secondary fuel to raise the bed temperature to the required level for coal combustion represents a simple and easily repeatable start-up technique. After initial attempts at start-up without resorting to a secondary source of fuel, a gas ignition system was designed and constructed. A series of gas start-up trials were performed to commission the system which proved to be highly successful and has been adopted as the means of raising the bed temperature from cold. The start-up procedure is described below.

The sand bed is first fully fluidized with cold air and a pilot gas flame is ignited above the bed. Gas is then introduced into the plenum chamber where it mixes with the air, forming a mixture having approximately 50% excess air. This gas air mixture is then ignited above the bed by means of the pilot flame. By careful adjustment of the gas flow rate, the gas air mixture is forced to burn within the sand bed resulting in a rapid increase in the bed temperature. To minimise the quantity of heat lost from the combustor in the off gases during start-up, gas and air flow rates are decreased continuously as the bed temperature increases, thus maintaining an almost constant superficial gas velocity in the bed section. This results in a reduction of the cooling effect of the excess air, causing the bed temperature to rise more rapidly.

Once a bed temperature of between 500 and 550^{o}C has been obtained, coal is introduced into the bed. Shortly after the temperature exceeds 610^{o}C the gas flow is discontinued and further increases in temperature are accommodated by adjusting the coal or air flow rates. Two experimentally determined start-up curves are illustrated for the rig in Figure 13. The first represents the start-up rate for a bed having a static bed height of 250 mm, whilst the second depicts the start-up rate for a shallower bed having a

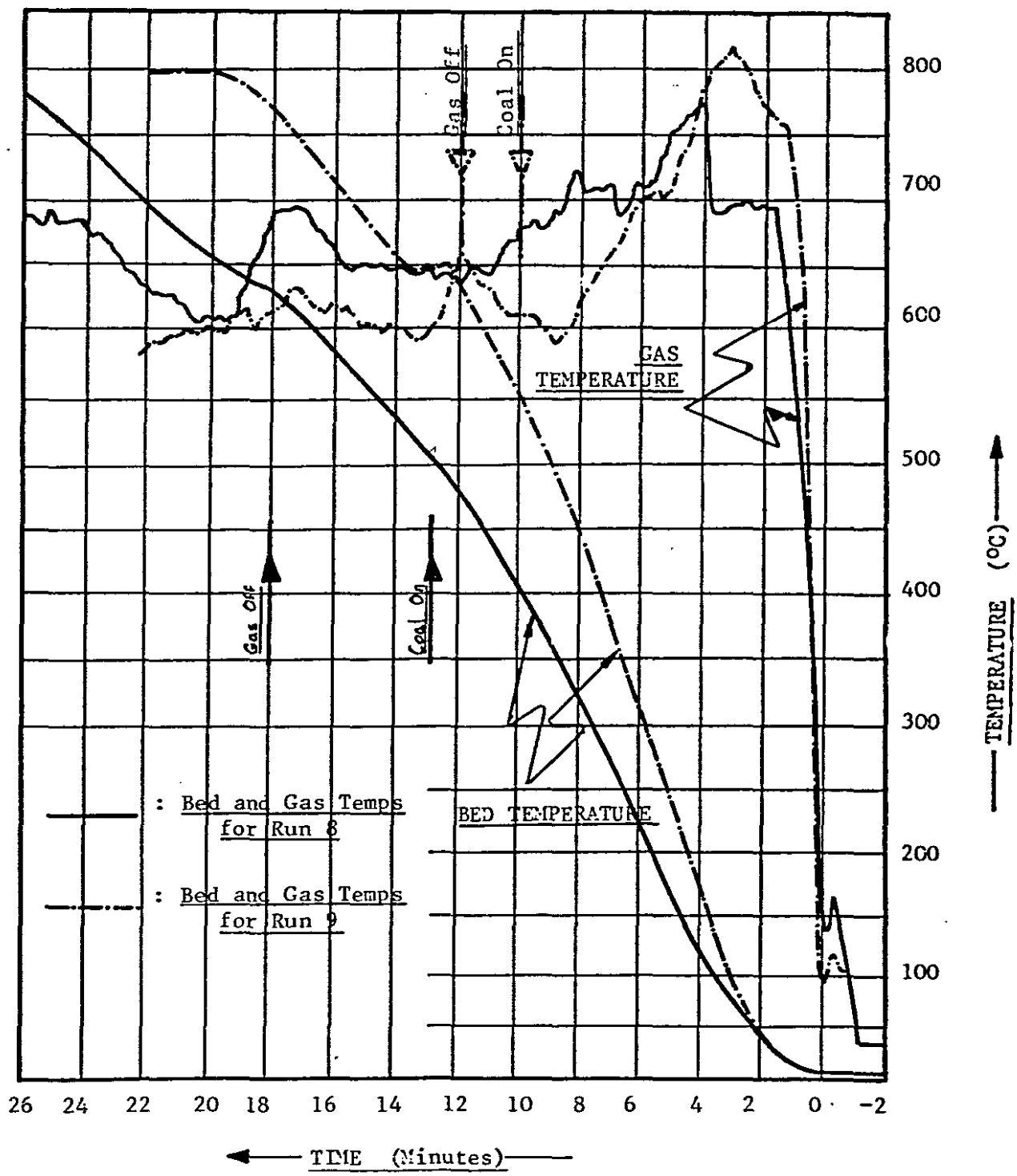

FIGURE 13 : Typical Start-Up Curves for a Deep Bed (Run 8) and a Shallow Bed (Run 9).

static bed height of 170 mm. The measured gas temperature is inaccurate, as the thermo-couple is unshielded and therefore affected by the low temperature of the walls as well as the extraction hood.

2.3.2 General Operation

Once coal combustion has been established, the air flow rate is set to a predetermined value which would result in a particular superficial gas velocity in the rig at a specific temperature. The bed temperature is adjusted to this particular value by varying the coal input. Once steady conditions pertaining to a particular test have been attained for at least fifteen minutes, the test is commenced. The only adjustment made during a test is to the coal flow rate in order to maintain a constant bed temperature.

2.4 EXPERIMENTAL PROCEDURE

2.4.1 Calibration of Equipment

Prior to the performance of any tests, the test equipment must be adequately calibrated. The calibration of various items of plant are discussed below. The air flow measurement was by means of a calibrated orifice plate and pressure vessel and therefore was not calibrated specifically for this thesis. Further, no calibration has been performed for any of the manometers, as these are sufficiently accurate for the purpose of the tests, whilst only a rough check on the calibration of the stainless steel sheathed thermo-couples was made.

a) *Thermo-couples*

The bed temperature measurements have been made using

stainless steel sheathed mineral-insulated chromel-alumel thermo-couples. The gas temperature has been measured by making use of a bare chromel-alumel thermo-couple. This latter thermo-couple is a standard measuring thermo-couple having been calibrated with an associated moving coil instrument, to read temperature directly. The temperature graduations are in steps of 20°C and therefore, the temperature can at best be read to the nearest 5°C. The three stainless steel sheathed chromel-alumel thermo-couples milli-volt outputs were checked against the temperature of standard thermo-couples and found to be within the $\pm$ 5°C measuring tolerance over the range of temperatures anticipated. For the fluidized-bed performance tests, the bare thermo-couple was disconnected from the moving coil instrument and compensating leads, and connected directly to a multi-point recorder together with the three other thermo-couples.

The iron-constantant thermo-couples were not calibrated, as they are not required for accurate measurements but rather for determining whether the distributor is becoming overheated or not.

b) *Distributor*

Prior to each run the combustor vessel was emptied and the pressure drop across the distributor plate determined to ensure that the distributor plate seal had not been damaged and to establish whether any of the holes in the perforated plate had been blocked. A layer of refractory stones was then placed on the plate to a height of about 90 mm, as indicated in Figure 10, and a further series of pressure drop measurements were made to establish what the total pressure drop across the plate and stones was. All these readings were then correlated to form a pressure drop to velocity relationship by means of a least squares technique. A total of 69 points were used for the plate only analysis,

and 71 for the plate and refractory stones analysis. Both analyses were made assuming an equation of the form below.

$$\Delta p = c \cdot u^n \qquad (8)$$

where Δp is in mm W.g. and c and n are constants. The exponent n for the plate alone should theoretically be 2, whilst the value of n for the plate and stones theoretically lies between unity and two and varies as the velocity increases. However the contribution of the plate is well in excess of that by the stones, and further as the stones are of a rather large diameter the kinetic energy component of a familiar fixed bed pressure drop relationship becomes predominant. Such a relationship has been proposed by Ergun and is represented by equation (9) below, cf. Section 1.2.2.

$$\frac{\Delta p_r}{H} = 150 \cdot \frac{1-\varepsilon^2}{\varepsilon^3} \cdot \frac{\mu \cdot u}{(\phi_s \cdot d)^2} + 1{,}75 \cdot \frac{1-\varepsilon}{\varepsilon^3 \cdot \phi_s} \frac{\rho u^2}{d_p} \qquad (9)$$

where Δp_r is the pressure through the layer of stones in N/m^2. The second term on the right hand side represents the kinetic energy losses.

In the regression analysis of equation (8), the exponent n assumed values of 2,102 and 2,088 for the plate alone and for the plate and stones together respectively. The theoretical value of 2 for the exponent n could be shown to be statistically the same as the above two values and therefore the regression analysis was repeated to obtain the constant c of equation (8) when the exponent n of this same equation was set at 2. The resulting equations are given by equations (10) and (11) below.

$$\Delta p_d = 231 \cdot u_f^2 \qquad (10)$$

$$\Delta p_{d,r} = 297 \cdot u_f^2 \qquad (11)$$

These two relations are reproduced in Figure 14 illustrating the range of velocities and pressures used for the regression analysis.

c) Coal Feeder

Two extensive series of calibrations, the second taking place some two months after the first, have been performed. The coal mass flow rate was assumed to bear a linear relationship with the feeder speed. The data was fitted to such a curve by means of a linear regression technique, resulting in the following equation.

$$m_c = 0,364 + 2,191 \cdot n \qquad (12)$$

where M_c and n are the coal mass flow rate (kg/h) and feeder speed (rpm) respectively. From a sample of twenty-one points of the measured coal flow rates for particular feeder speeds, the initial three tests were rejected as the coal flow rates measured from these three points were less than anticipated. The regression analysis has therefore been performed by making use of the remaining eighteen points.

In order to obtain a more meaningful interpretation of equation (12) the confidence interval for each of the regression coefficients was calculated. By applying a 95% confidence interval the intercept with the vertical axis, (a = 0,364 in equation (12)), is found to have a value ranging from

$$0,033 < a < 0,761$$

whilst the slope of the line, (b = 2,191 in equation (12)), is found to lie between

$$2,136 < b < 2,246$$

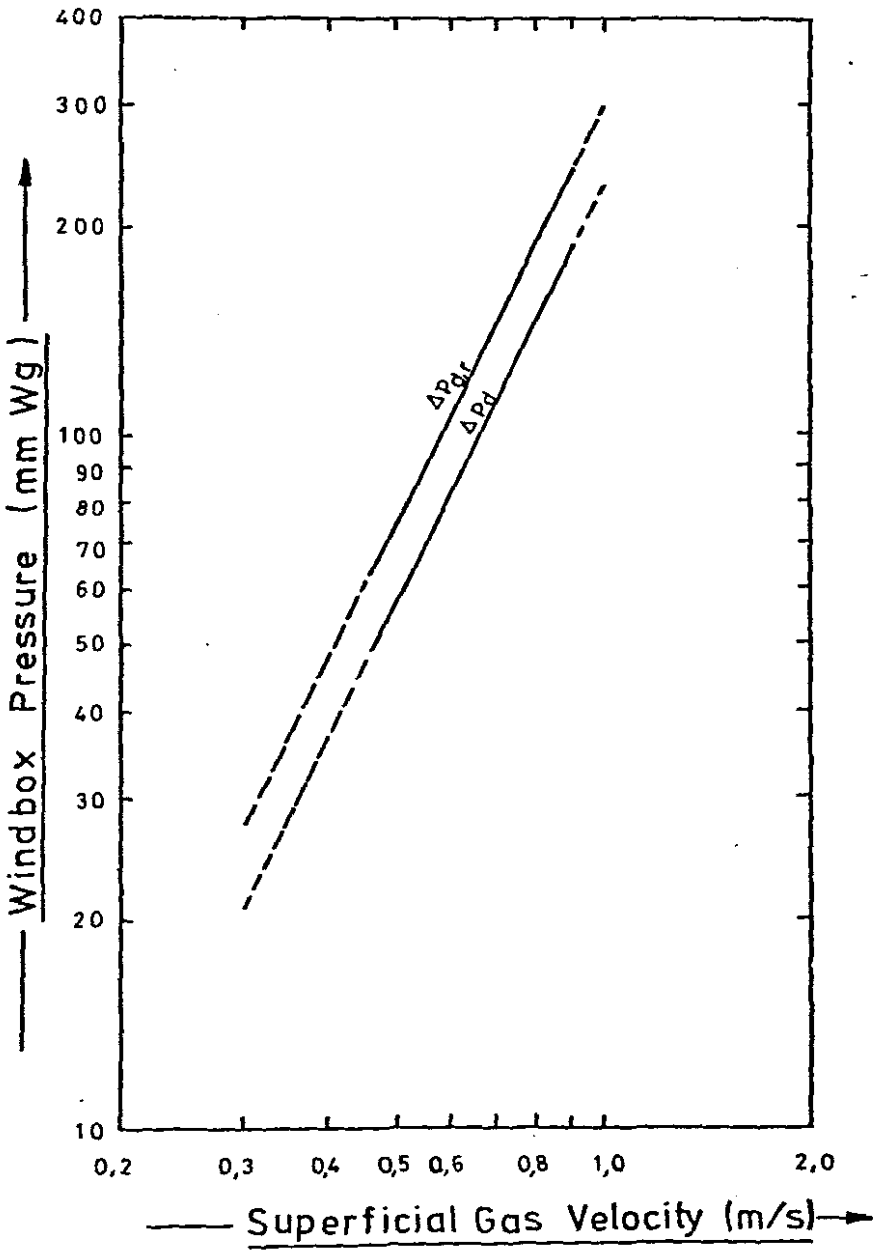

Figure 14 : Correlations for the Distributor Pressure Drop with ($\Delta p_{d,r}$) and without (Δp_d) the Insulating Layer of Refractory Stones as a Function of Velocity.

The regression line of coal flow rate as a function of feeder speed was expected to pass through the origin, and therefore the interval estimate of 'a' should have included zero. Although the lower value for this interval estimate of 'a' is close to zero, it was decided to use equation (12) as the regression line for the coal feed rate.

The feeder speed was varied from about 0,8 to 10,0 rpm. As this speed only exceeds 3 rpm for a single test during the fluidized-bed performance tests the regression curve of equation (12) has been drawn in Figure 15 for this lower speed range of the line. Included in Figure 15 are the 95% confidence bands for the resulting coal flow for a particular feeder speed. The correlation coefficient and the standard error of estimate for the above regression analysis have been determined as 0,9997 and 0,224 respectively.

Finally it should be noted that as the feeder speed should be related to the volumetric flow rate, differences can be expected when using a different coal type and grading.

2.4.2 Outline of Tests Performed

Initial tests were made to commission the rig and the various auxiliary components such as the instrumentation and the gas ignition system. A detailed analysis of the last five test runs which have been designated as Run Numbers 6, 7, 8, 9 and 10 has been made. These test runs each range from $4\frac{1}{2}$ to 10 hours duration and have been divided into twenty-two individual tests performed under steady conditions for a time interval of at least 30 minutes. These tests have been used to evaluate the combustion efficiency (as defined in Appendix B) and entrainment rates.

Run Number 6 is is the only test during which a silica sand graded between 0,6 mm and 1,0 mm was used. The minimum

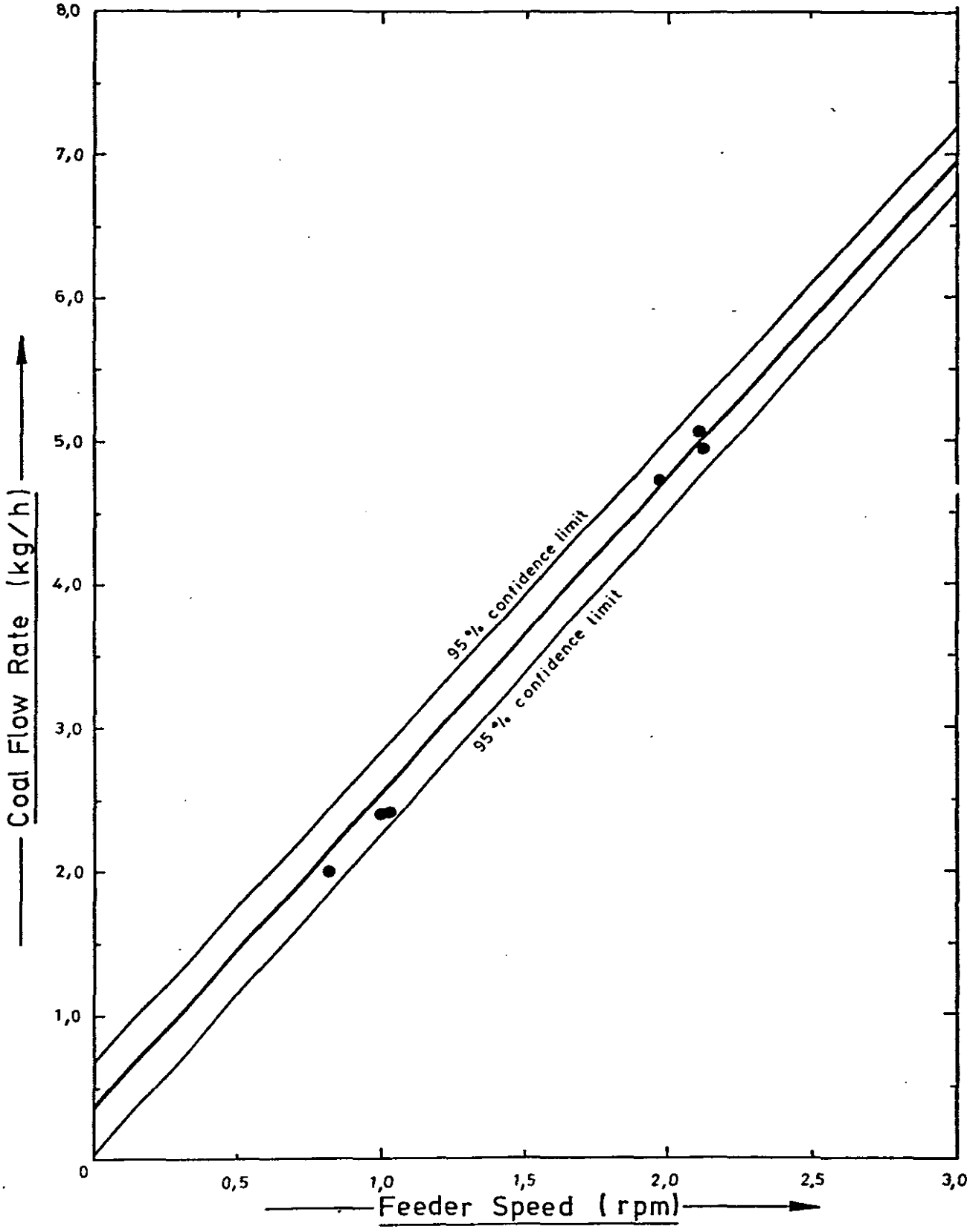

Figure 15 : Coal Feeder Calibration Curve with 95% Confidence Limits for the Portion of the Curve from Zero to 3 rpm Feeder Speed.

fluidizing velocity determined experimentally for this sand was 0,36 m/s at about 40°C and enabled a test to be performed with a superficial gas velocity of 0,9 m/s. The remaining runs were conducted using a commercially available silica sand with a size grading as represented by Figure 16. The bulk density of the sand was determined as 1640 kg/m^3 with a particle density determined by means of the S.G. bottle method of BS 1377 : 1975, of 2640 kg/m^3. The minimum fluidizing velocity at about 40°C when fluidized with air was recorded as 0,53 m/s. When operating with this sand at bed velocities close to 0,9 m/s lumps of clinker formed in the bed. These lumps are relatively soft and easily broken down by increasing the velocity. The superficial gas velocity for tests 7 to 10 was thus varied between 1,1 and 1,5 m/s with no evidence of clinker formation. At higher velocities, and especially with the deeper beds, bubbles bursting at the surface caused splashing of the bed material out of the combustor vessel. A cylindrical shield about 300 mm high and having a diameter of 450 mm was placed on top of the combustor to prevent spillage of bed material onto the floor.

Runs 6, 7 and 8 were conducted with 30 kg of sand as the bed material. This corresponds to a static bed height of about 230 mm whilst Runs 9 and 10 were conducted with beds of sand of 20 kg, resulting in static bed heights of about 150 mm. Tables 2.1 a and 2.1 b summarize the approximate operating parameters of the different tests. More accurate values are produced with the individual test results in the table contained in Appendix H.

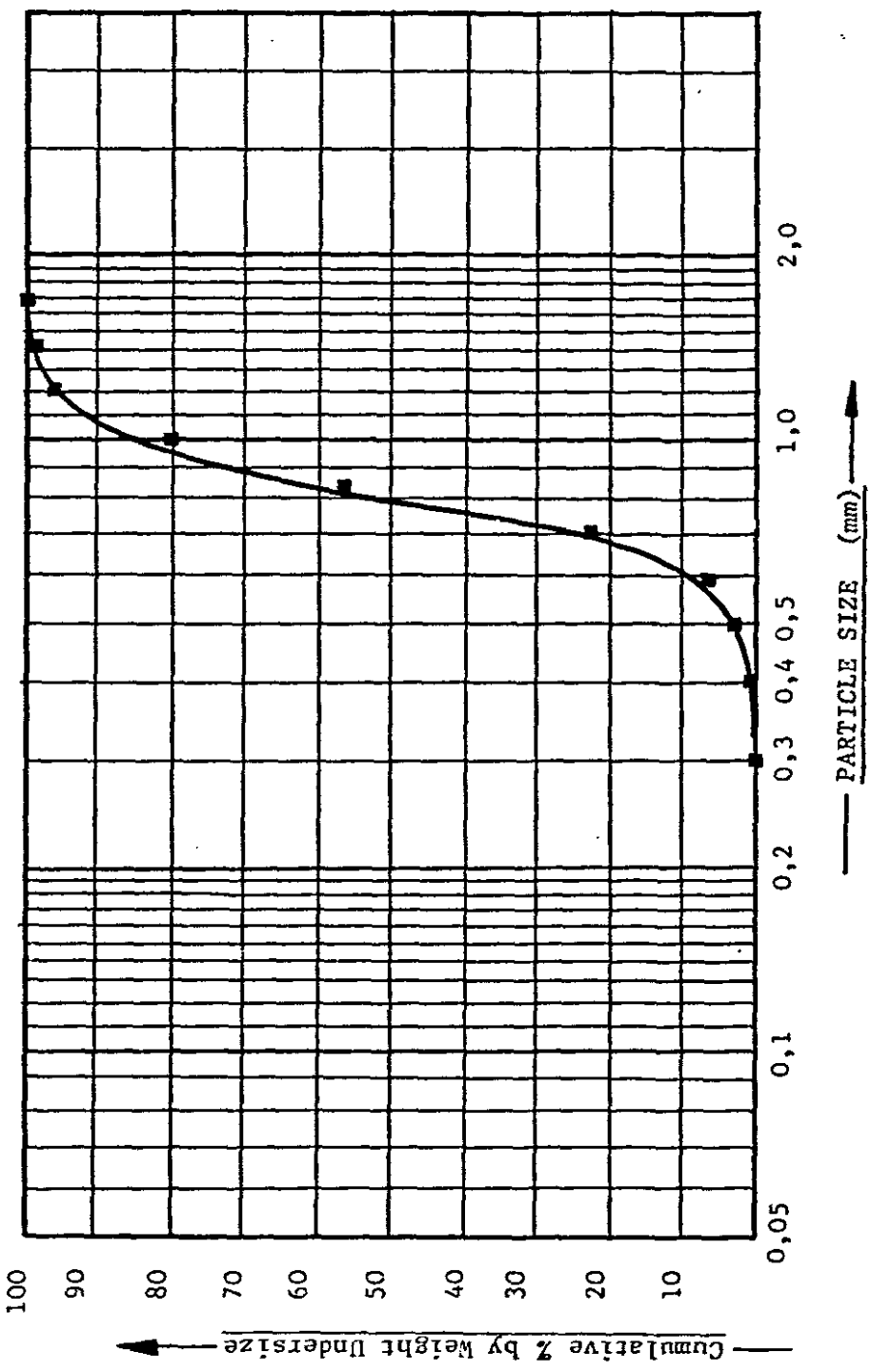

FIGURE 16 : Size Grading of Silica Sand used as Bed Material for Runs 7,8,9 and 10

Table 2.1 a : Summary of Operating Conditions with an Inert Bed Weight of 30 kg.

Velocity (m/s)	Temperature (°C)						
	650	700	750	800	850	900	950
0,9				6			
1,1			7C	7A		7B	
1,3			8E	8A		8F	
1,5	8H		8D	8B		8C	8G

Table 2.1 b : Summary of Operating Conditions with an Inert Bed Weight of 20 kg.

Velocity (m/s)	Temperature (°C)						
	700	750	800	850	900	950	1000
1,1		10C	9B		9D	9E	
1,3	10D			10B			
1,5		10A	9A		9C		10E

2.4.3. Test Procedure

Prior to each run, the combustor vessel was emptied and the pressure drop across the distributor was determined at a number of different velocities. The layer of refractory stones was placed on top of the distributor plate and a second series of pressure drop velocity measurements were taken. The bed pressure probes and thermo-couples were then placed

in position and the respective amount of silica sand was introduced to form the inert bed. A fluidization study was then conducted in order to determine at what superficial gas velocity the bed was fluidized. Once the minimum fluidizing velocity was established, preparations for igniting the fuel in the combustor were made.

The bed was raised to the ignition temperature of the coal by means of gas combustion. Once the coal combustion is self sustaining, the gas is shut down, and the particular velocity and temperature conditions for the test are chosen. The velocity is obtained by setting the fan discharge dampers, or valves, so regulating the flow from the fan. The required temperature is obtained by adjusting the coal flow. Once steady conditions have been maintained for about fifteen minutes the test is commenced. During the test, ash is collected in the cyclone for analysis at a later stage, whilst pressure, temperature and flow rates are monitored. The resulting ash was tested at Athlone Power Station to determine the amount of unburnt carbon contained in the ash, whilst another sample was used to determine the size grading of the ash. This size grading has been determined by sieving and by employing a sedimentation technique based on the incremental method as outlined in BS 3406 : Part 2 of 1963.

Only one type of coal, Douglas duff, with a top size of 6 mm has been used for the tests. An analysis of the coal grading and properties is presented in Appendix C.

CHAPTER 3

EXPERIMENTAL RESULTS

The major objectives of the tests were to assess the effect of a few of the main variables of the fluidized-bed combustion process on the combustion efficiency and the entrainment rate. It was felt that the system variables which would have a major affect on these two parameters, and in particular on the combustion efficiency could be limited to bed temperature, superficial gas velocity and bed depth. The experiments are therefore made up of these three factors, (a brief description of the more important statistical relationships used in this thesis is contained in Appendix F), and initially combustion efficiencies were determined at two levels of each of these factors. These levels are given below:

Temperature	:	800°C, 900°C
Velocity	:	1,1 m/s, 1,5 m/s
Bed Height	:	230 mm, 150 mm

This yields a 2^3 factorial design. An analysis-of-variance table was determined, from which it was deduced that all three factors had a significant effect on the combustion efficiency within the ranges given above. Therefore the number of test points were extended by performing additional experiments to determine the combustion efficiency for extra combinations of velocity temperature and bed height, in order to enable a multiple regression analysis to be performed. The temperatures were varied in approximate steps of 50°C from 650°C to 1000°C, whilst the velocity was varied from 0,9 m/s to 1,5 m/s. Only two bed heights were used throughout the test series, i.e. static bed heights of approximately 230 mm and 150 mm. For ease of reference the

tests at the two different bed heights have been designated as deep and shallow bed tests.

3.1 GENERAL DESCRIPTION OF RESULTS

3.1.1 Deep Bed Tests

Runs 6, 7 and 8 were conducted with an inert bed weight of 30 kg and having a bed height of about 230 mm. This results in a bed pressure drop of about 400 mm W.g. and a pressure drop across the distributor plate of about 70 mm W.g. An accurate assessment of the bed pressures is difficult due to oscillations of the water manometer levels. With these beds, violent splashing occurs resulting in much bed material being carried over into the cyclone. This material is of a size well in excess of the maximum which could be elutriated by the gas stream. It is felt that with the low pressure drop distributor large gas bubbles may be generated at the distributor surface, i.e. on top of the refractory stones, with the result that through coalescence large bubbles approaching the size of the bed diameter may be formed. On bursting at the upper surface of the bed, large particles of sand are ejected into the freeboard space, resulting in particles larger than those which would normally be elutriated, being entrained by the off gases. During Run 8 large quantities of bed material were collected in the cyclone, particularly during tests conducted at superficial gas velocities of 1,5 m/s. A total of 5 kg of sand had to be added to the bed at different intervals during the test to restore the bed level. The run lasted for a little over 10 hours. Although the original static bed heights were 230 mm, these heights change continuously during the tests. An estimate of the static bed height for each individual test was therefore made by measuring the initial and final bed heights for each test run, and considering the amount and time during which

bed material was added and by finally measuring the average bed pressure drop during each individual test of the total test run.

3.1.2 Shallow Bed Tests

Tests 9 and 10 were conducted with an inert bed material weight of 20 kg resulting in a bed depth of 150 mm. The pressure drop across the bed was about 270 mm W.g. whilst the distributor pressure drop was about 70 mm W.g., similar to that for the deep bed. The amount of sand lost as carry-over to the cyclone was much less than that for the deep bed under all conditions. This is most likely due to the generation of smaller bubbles within the bed causing a reduction in the quantity of material carried over as a result of splashing.

Steady temperature control of the shallow beds was considerably more difficult to maintain than that of the deep bed. This may be ascribed to the reduced thermal inertia of the smaller mass of heated bed material. On the other hand the bed temperature may be reduced and increased more rapidly with the shallow bed.

3.2 EXPERIMENTAL DETERMINATION OF MAIN PARAMETERS

3.2.1 Minimum Fluidizing Velocity

Before the commencement of any test a fluidization study was performed in order to establish the minimum fluidizing velocity. The bed pressure velocity relationship as well as the bed density to velocity relationship during the initial cycle of increasing velocity and subsequent decreasing of velocity are illustrated in Figure 17. The bed density is defined as the difference in pressure between the two static pressure tappings located within the bed, 150 mm apart as indicated in Figure 19.

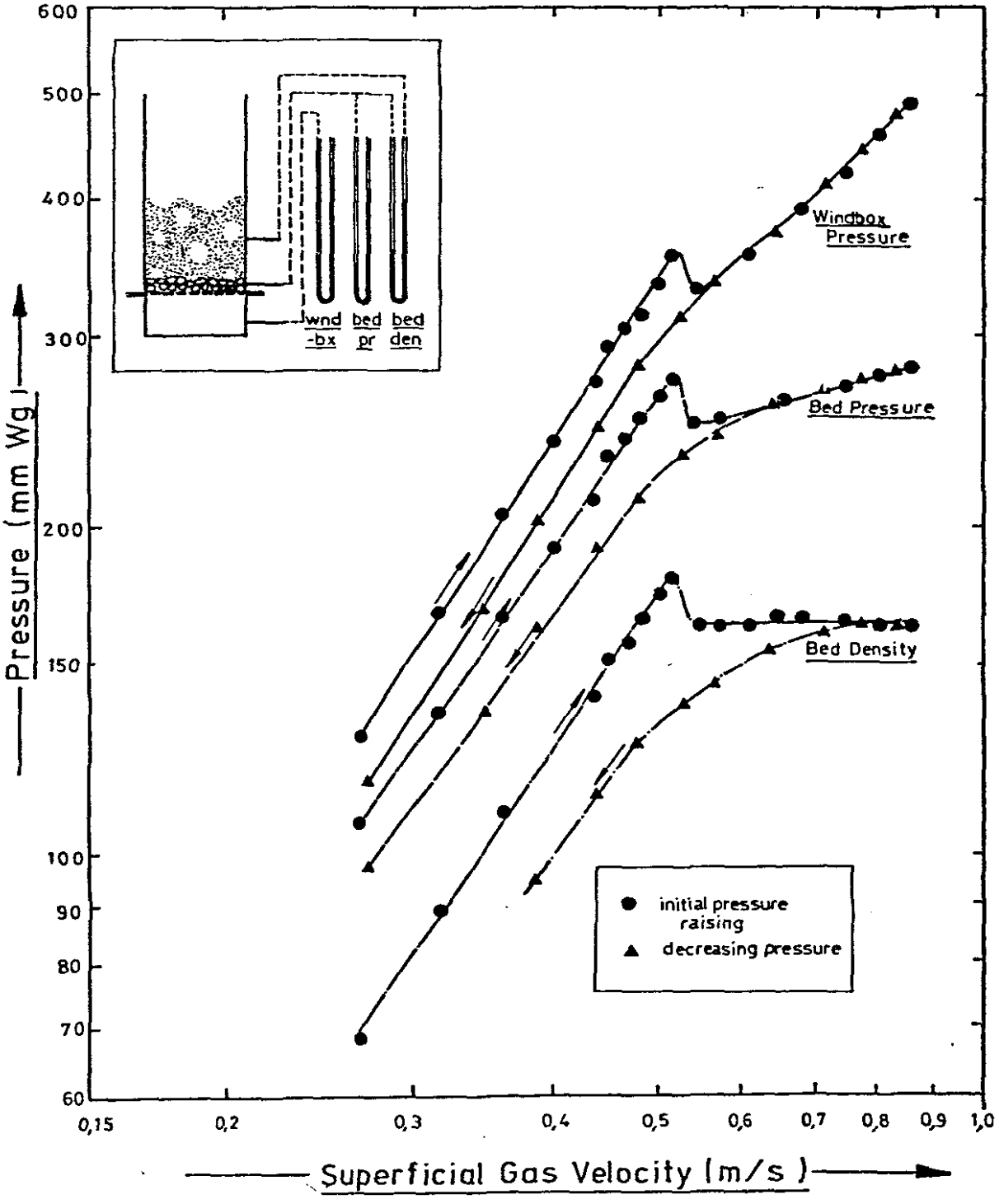

Figure 17 : Pressure-Drop Velocity Characteristic for a Typical Fluidization Study with a 170 mm Deep Bed.

The fluidization study illustrated by Figure 17 is for a bed of silica sand of size grading given by Figure 16 of depth 170 mm. This sand was used for all but one of the tests as mentioned earlier. On increasing the gas velocity it is seen that the pressure increases steadily in the fixed bed region. The slope of this curve on the logarithmic co-ordinates is found to be 1,453, which indicates a pressure velocity relationship in the fixed bed region of

$$\Delta p = c \cdot u^{1,453} \qquad (13)$$

By averaging all of the results this exponent is found to be 1,488, having a standard deviation equal to 0,067. As the exponent is neither unity, as would be expected for laminar flow or for a fixed bed made up of small particles, nor does it have a value of two, as would be expected for large particles or turbulent flow, the flow through the bed material prior to fluidization is in the transition flow regime.

Referring to Section 1.2.2, it was stated that the minimum fluidizing velocity could be obtained by applying a fixed bed correlation, such as that given by Ergun at incipient fluidization conditions. This relationship given by equation (5) is repeated below for ease of reference:

$$Ga = \frac{150 \cdot (1 - \varepsilon_{mf})}{\phi_s^2 \cdot \varepsilon_{mf}^3} \cdot Re_{mf} + \frac{1,75}{\phi_s \cdot \varepsilon_{mf}^3} \cdot Re_{mf}^2 \qquad (5)$$

This equation may be written as

$$Ga = A \cdot Re_{mf} + B \cdot Re_{mf}^2 \qquad (14)$$

where A and B are constants dependent only on the particle sphericity and the voidage at incipient fluidization. Both of these latter two parameters are not easily determined and have not been specifically evaluated in this thesis, though the voidage could be approximated from the bed pressure to

velocity relationship of Figure 17 for the case of decreasing velocity. Wen and Yu (17), cf Section 1.2.2, have approximated the values of A and B in equation (14) as 1650 and 24,5 respectively.

The minimum fluidizing velocity was experimentally determined at low temperatures of about 40°C. Since the temperatures at which fluidized-bed combustion takes place range from about 650°C to 1000°C, a means must be found for extrapolating the information to the higher temperatures or of using a generally acceptable relationship. An attempt was made to establish the constants of equation (14) from the experimental work on fluidizing the inert sand particles. This was done by equating equation (13) to the form of equation (5) given by equation (9) of Section 2.4.1. The values of A and B were evaluated as 600 and 34,2 respectively. It should be noted that the resulting relationship results in a reduced value of the viscous component ($A \cdot Re$) whilst the kinetic component ($B \cdot Re^2$) remains much the same as that given by Wen and Yu (17), cf equation (6).

At 40°C, and at a velocity of 0,5 m/s, the Reynolds number is about 24. On increasing the temperature, due to the decrease in density and the increase in viscosity, the Reynolds number decreases to values of about 1,8 at 700°C and 1,0 at 1000°C at the respective minimum fluidizing velocities. In view of the findings of Broughton (21), cf Section 1.2.2, and as Re_{mf} would be much less than 20 for fluidized-bed combustion, a simple relationship such as that given by equation (7) might be used. Indeed, two forms of equation (14), and one of equation (7) as used by Avedesian and Davidson (10) are plotted in Figure 18 to illustrate the variation of minimum fluidizing velocity with temperature. For easy reference these equations are written below:

$$Ga = 1650 \cdot Re_{mf} + 24,5 \cdot Re_{mf}^2 \qquad (6)$$

$$Ga = 600 \cdot Re_{mf} + 34,2 \cdot Re_{mf}^2 \qquad (15)$$

$$Ga = 1650 \cdot Re_{mf} \qquad (16)$$

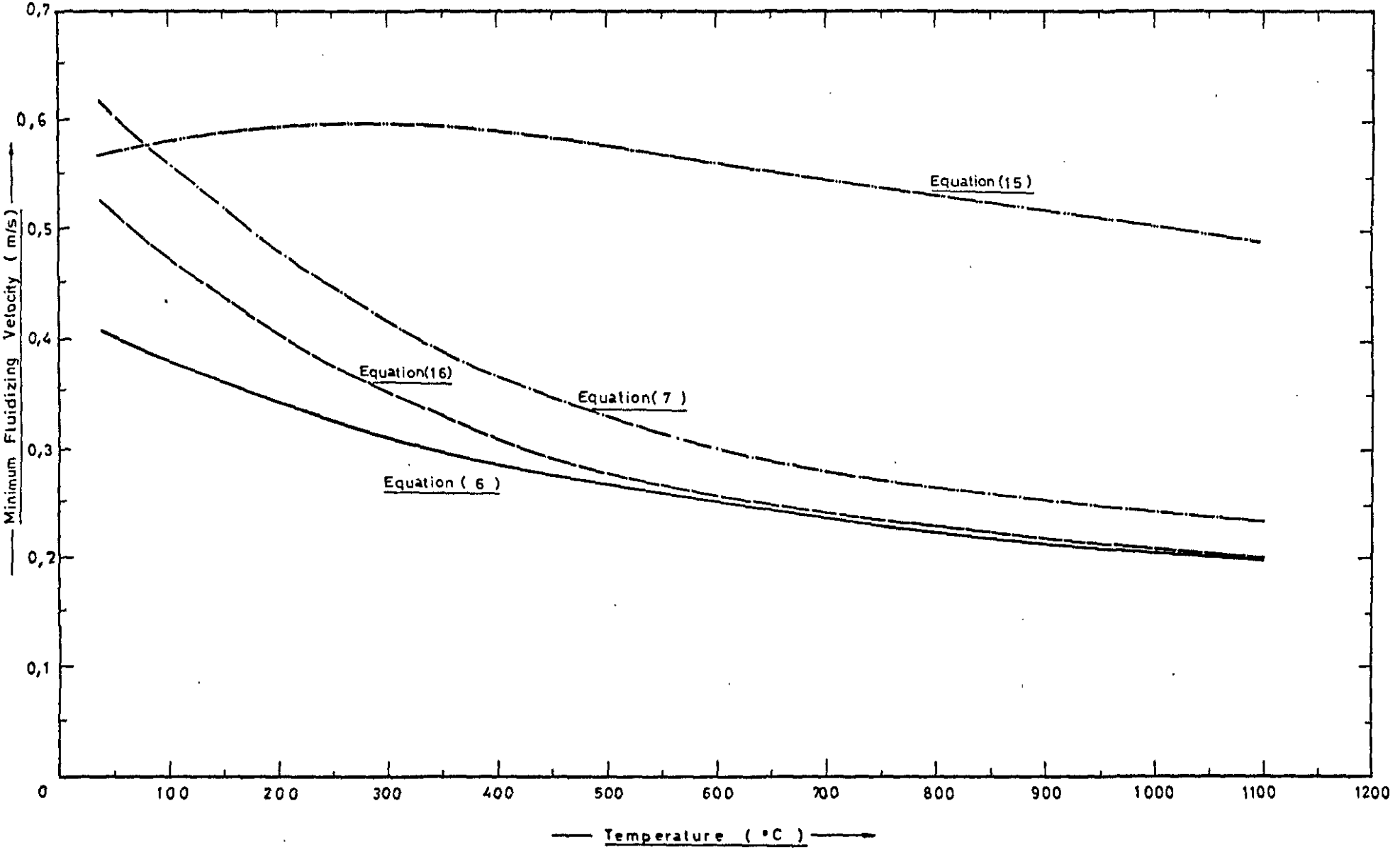

Figure 18 : Variation of u_{mf} with Temperature for the bed material given by Figure 16

From Figure 18, it is evident that equation (15) as derived from the fluidization study is in error due to a peak value for U_{mf} being evident between 200 and 300°C. Equation (6) predicts a value somewhat lower than the average value of 0,53 determined experimentally whilst equation (16) predicts a value of 0,52 at 40°C. Further, equations (6) and (16) tend to predict the same values as the temperature increases ie the Reynolds number decreases.

From the above, it was decided to use equation (16) in the evaluation of the minimum fluidizing velocity for the inert bed used in the tests.

Once the bed has been fluidized, the pressure drop through the bed remains almost constant as the velocity increases. Reference to Figure 17 indicates that the pressure increases. However, it is to be noted that the bed pressure probe also measures a small pressure drop due to the fixed bed of refractory stones above. Subtracting this value would produce a flatter curve, similar to curve of the density. From Figure 17, the characteristic 'hump' during the first pressure raising cycle is evident, whilst a distinct cut off on defluidizing as the bed changes from the fluidized to the fixed bed regime is evidence suggesting localized channelling and defluidization as the velocity approaches the minimum fluidization velocity.

3.2.2 Measurement of the Dynamic Bed Height

The pressure measurements associated with the combustor plenum chamber and the bed sections fluctuated continuously during the tests as a result of bubbles bursting at the surface. This made an accurate measurement of these readings difficult. Pressure probes were placed in the bed at two different heights, from which an assessment of the dynamic bed height should be possible. A diagram to indicate the precise positioning of the bed pressure probes

and illustrating their connection to water manometers is given in Figure 19. The bed density is simply taken as the difference between the pressures of the two probes. The dynamic bed height can therefore be estimated by equation (17), where the constants 'a' and 'b' are as defined in Figure 19.

$$H_{dyn} = a + b.\frac{(bed\ pressure)}{(bed\ \ density)} \qquad (17)$$

Table H.2 of Appendix H contains details of the different pressure drops as well as details of the static and dynamic bed heights for each of the tests. The static bed height has been determined by measuring the bed heights at the beginning of and at the end of a particular test run and by considering the amount of bed material added in conjunction with the pressure drop through the bed.

Referring to Appendix J, the fraction of bubbles 'f' in the bed can be determined by equation (J.6) whilst the absolute velocity of rise of the bubble 'U_{BS}' is given by the Davidson and Harrison (12, pg 100) relation of equation (J.8). These equations are reproduced below:

$$f = (H - H_{mf}) / H \qquad (J.6)$$

$$u_{BS} = (u_f - u_{mf}) + u_B \qquad (J.8)$$

The various velocities, and the values of dynamic and static bed height are included in Table H.3 of Appendix H. From these values, the fraction of bubbles in the bed as well as the bubble velocities have been determined. From Table H.3 it is clear that according to the slug flow criterion of Appendix J.3, the bed is in a slugging flow regime. However, as discussed in Appendix J, slugging flow probably does not occur in the shallow beds. This is discussed further in Section 3.4.3.

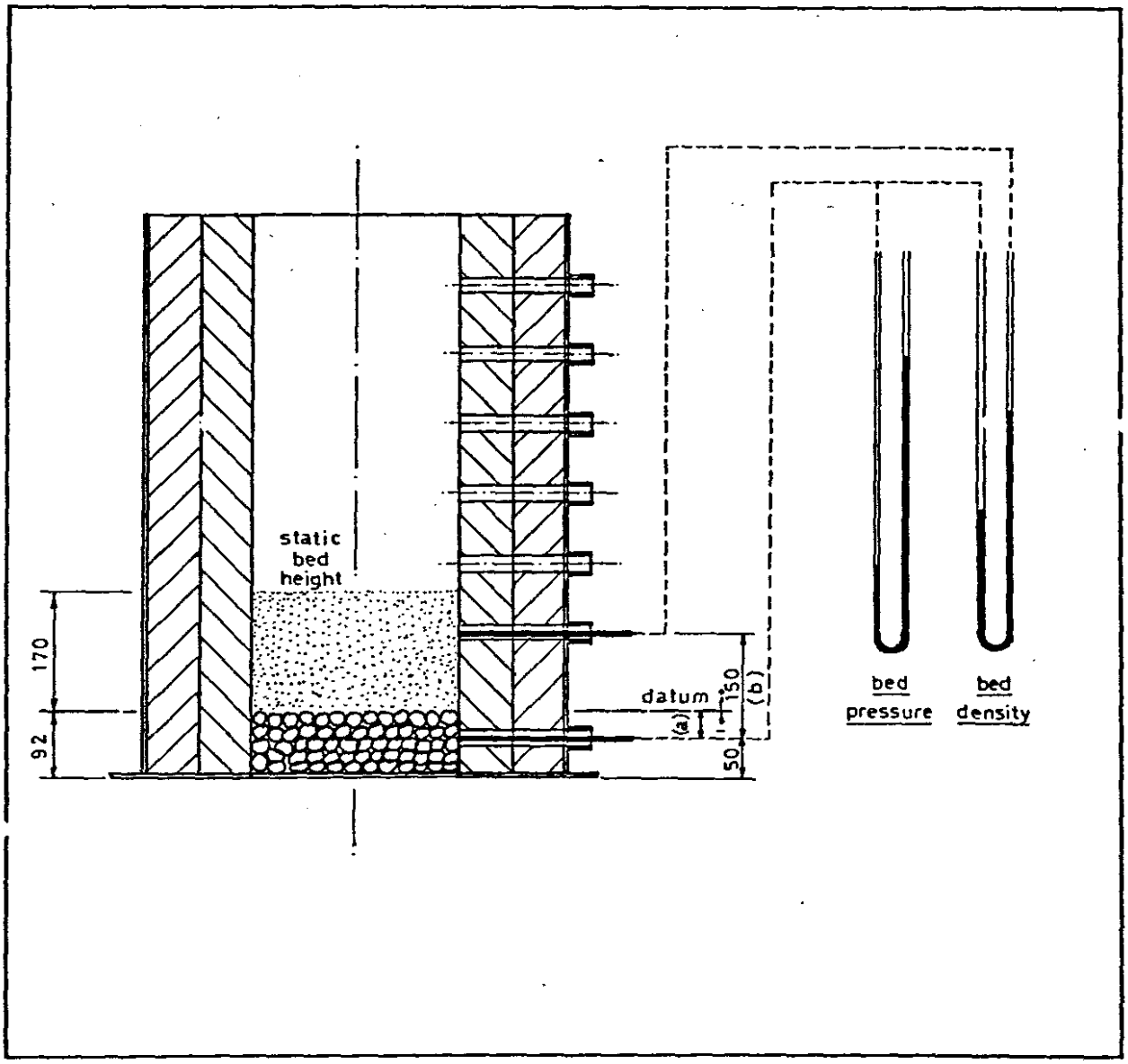

Figure 19 : Diagram to Illustrate the Location of the Bed Pressure Probes.

The bed expansions which have been deduced from the evaluation of the dynamic bed heights, result in small values of f, ie the fraction of bubbles in the bed. In view of the high excess gas velocity $U_f - U_{mf}$, a higher proportion of the bed would be taken up as bubbles than is indicated by Table H.3. The calculated value of the dynamic bed height is suspected to be in error. This is further vindicated, as it can be shown statistically that no correlation exists between, the bed height, or the bed expansion R, or the fraction of bubbles in the bed f, and the excess gas velocity $U_f - U_{mf}$. Finally, the resulting evaluation of the bubble diameters from the bed height measurements are well in excess of the rig diameter indicating that the use of the bed measurements for determining bed heights has not been satisfactory.

3.3 COMBUSTION EFFICIENCY

Complete combustion of coal is assumed to have taken place when all of the coal is burnt in the presence of oxygen to form carbon dioxide, sulphur dioxide and water vapour. The reactions taking place during the formation of these products are all exothermic, resulting in a corresponding release of heat. The nitrogen present in the coal is assumed to leave the reaction zone as gaseous nitrogen, as the formation of NO_x is assumed to be small. The definition of the combustion efficiency has been defined in Appendix B, as the ratio of the rate of heat liberated to the rate of heat input. This latter quantity, the rate of heat input, is the rate at which heat could be generated should complete combustion of the entire coal feed be effected. The rate of heat liberated is less than this quantity as a result of:

a) incomplete combustion, and

b) unburnt carbon remaining in the ash.

Incomplete combustion of the coal generally refers to the combustion of the carbon component of the coal to carbon monoxide instead of carbon dioxide which is accompanied by a reduction in the heat released due to the smaller heat of formation of carbon monoxide. As the combustion efficiency is to be related only to the bed section, the combustion process is considered to take place within the fluidized bed, and therefore any combustion above the bed section would be as the result of incomplete combustion within the fluidized bed. The combustion of the volatile component, or of carbon monoxide to carbon dioxide, above the bed would be as a result of the incomplete combustion of volatile or fixed carbon components of the coal within the fluidized bed. Incomplete combustion generally takes place in oxygen deficient regions, or at low combustion temperatures due to the slow reaction rates prevailing at these lower temperatures.

In order to ensure that all the carbon presented in the coal feed is burnt, this carbon must remain in the high temperature combustion zone for a finite length of time. In a fluidized-bed combustion system, once the particle has been reduced to a specific size as a result of the combined action of attrition and combustion, it may be entrained in the off gases. Indeed, Skinner (8, pg 81) states that the coal should be crushed so that it has as small a proportion as possible below 120 microns, so as to reduce the proportion of particles of high carbon content entrained from the bed. The unburnt carbon loss from a fluidized-bed combustion system, therefore manifests itself as carbon in the entrained ash, or in the carbon contained in the bed material which may be withdrawn from the combustor.

The test rig used for the experiments reported consists of a refractory lined combustor vessel, with cooling being effected by means of the fluidizing air. The air supplied to the combustor is therefore about three times that required

for stoichiometric combustion. The formation of carbon monoxide, or incomplete combustion of the volatiles, in the bed section is not likely to occur due to the abundance of oxygen supplied to the rig resulting in no oxygen deficient regions in the bed. Visual observation of the rig when operating between 700°C and 1000°C indicated an absence of the combustion of carbon monoxide in the freeboard, whilst a small volatile flame appeared sporadically in the freeboard area above the position of the coal feed aperture at temperatures above 900°C. This is probably caused due to the rapid evolution and combustion of the volatiles at high temperatures. However, at temperatures slightly above 600°C, a blue flame was evident in the freeboard section indicating the combustion of carbon monoxide. Yellow flashes were also observed above the bed, indicating the combustion of volatiles above the bed at these low temperatures. In view of the above observations, and further as a result of the high oxygen concentration prevalent in the fluidized bed, it is clear that the volatiles are burned within the bed section, whilst the carbon component of the coal burns to carbon dioxide in this section. Therefore no measurements to assess the loss due to incomplete combustion have been undertaken.

As no provision was made during the tests for removal of the bed material as overflow from a weir or any similar device, ash and bed material can only be removed from the rig as a result of the entrainment process. The unburnt carbon loss is therefore limited to the carbon entrained in the off gases. The proportion of carbon contained in the ash collected by the cyclone has been determined in order to evaluate the unburnt carbon loss. In fact, this represents the only combustion loss from the fluidized-bed combustion test rig, and the combustion efficiency can be determined directly from it as given by equation (B.2) below:

$$\eta_c = 1 - h_c \qquad (B.2)$$

3.3.1 Methods of Determining the Combustion Efficiency

If the unburnt carbon in the entrained ash is considered to be the only combustion loss in the fluidized-bed combustion section, then the combustion efficiency may be determined by one of two methods:

a) by means of a heat balance

b) by determination of the unburnt carbon in the entrained ash.

a) The Heat Balance

By considering a heat balance about the fluidized-bed combustion section of the rig the following equations from Appendix E are formed

$$(\text{heat input}) = (\text{heat in off gases}) + (\text{heat loss through combustor walls}) \qquad (E.1)$$

which can be reduced to

$$M_f \cdot NCV = M_g \cdot c_p \cdot \Delta T + 0{,}473 \cdot 10^{-3} \cdot \Delta T \qquad (E.5)$$

or

$$\eta_c \cdot M_{fo} \cdot NCV = M_g \cdot c_p \cdot \Delta T + 0{,}473 \cdot 10^{-3} \cdot \Delta T \qquad (E.6)$$

In the determination of the combustion efficiency from equations (E.5) and (E.6), all the quantities, except for the gas flow rates can easily be determined. However, the gas flow rate can be approximated in terms of the air flow rate, the rate of fuel burnt and the ash content of fuel by the following equation

$$M_g = M_a + (1 - a) \cdot M_f \qquad (18)$$

and hence from equations (E.5) and (18), the fuel burnt can be shown to be

$$M_f = f(NCV, a, M_a, \Delta T) \qquad (19)$$

The net calorific value (NCV) and the ash content (a) have been determined from samples for a series of different tests, cf Appendix D, and small variations from test to test may occur. Further the values used for these two parameters in the solution of equation (19) are average values. However the deviation is not expected to significantly affect the estimation of the fuel burnt. The values for air flow (M_a) and the difference between the bed temperature and the surrounding air temperature have been measured to a sufficient accuracy to permit an accurate assessment of the fuel burnt (M_f).

The combustion efficiency may be determined as the ratio of the rate of fuel burnt to the rate of fuel supplied as given by equation (20).

$$\eta_c = M_f / M_{fo} \qquad (20)$$

The rate at which the fuel is supplied to the combustor can be determined from the feeder speed to a very high degree of accuracy cf Section 2.4.1. However, during each test the feeder speed had to be varied continuously in order to maintain the bed temperature within acceptable limits. Further, coal wedging between the feeder screw and locating sleeve resulted in retardation of the feed flow rate. As continuous monitoring of the feeder speed was not undertaken, the speed was noted after each adjustment and at regular intervals. During a large number of the tests the feeder had to be adjusted quite frequently thus reducing the accuracy of the integrated feed flow.

The combustion efficiencies were determined in accordance with equation (20). The resulting values are contained in Tables 3.1a and 3.1b with the approximate temperature and velocity conditions for easy reference.

Table 3.1 a : Table of Combustion Efficiencies determined from a Heat Balance at approximate Temperature and Velocity Conditions for an Inert Bed Weight of 30 kg.

Velocity (m/s)	Temperature (°C)						
	650	700	750	800	850	900	950
0,9				75,5			
1,1			78,7	67,0		69,7	
1,3			78,5	69,4		78,9	
1,5	62,1		78,7	72,2		71,1	77,5

Table 3.1 b : Table of Combustion Efficiencies determined from a Heat Balance at approximate Temperature and Velocity Conditions for an Inert Bed Weight of 20 kg.

Velocity (m/s)	Temperature (°C)						
	700	750	800	850	900	950	1000
1,1		90,7	86,1		88,0	80,9	
1,3	77,0			80,7			
1,5		75,8	77,6		81,1		83,8

The results presented in Tables 3.1 a and 3.1 b are very poor, with virtually no correlation between temperature and efficiency, whilst a relationship between velocity and efficiency is only evident for a shallower bed. Further, in contrast to general expectations, the efficiencies obtained from the shallower bed are higher than those for the deeper bed. These results were deemed to be in error, due to the unreliable value for the integrated value of the coal feed.

The instantaneous coal feed rate can be determined to a high degree of accuracy. As the coal feed was changed continuously during each test, instantaneous values had to be measured and integrated over the duration of the test. The method of determining this integrated value was not very satisfactory and it is felt that an instantaneous recording of the feed flow every 30 seconds is necessary to achieve any meaningful results. Further, the adjustment of the coal feed would only manifest itself on the combustion system after a time delay of between two to five minutes, and coal feed rates immediately prior to the commencement of the test may also be necessary.

This approach has been discarded for these tests in preference for the determination of the combustion efficiency from the estimation of the unburnt carbon in the entrained ash which is described below.

b) Unburnt Carbon in the Entrained Ash

The ash entrained in the gas stream leaving the fluidized-bed combustor is removed via a low pressure drop cyclone. The efficiency of dust extraction would be of the order of 75% cf Section 3.4 and Appendix K. Therefore about 25% of the ash will not be collected by the cyclone, and the carbon content of this ash has not been assessed. However the carbon content of these finer ash particles would have to be considerably different from that collected by the cyclone to have a marked effect on the overall result. The combustion efficiency can be determined by the unburnt carbon loss as defined in BS 2885 : 1974 from equation (B.2).

$$\eta_c = 1 - h_c \qquad (B.2)$$

where the unburnt carbon loss referred to the net calorific value of the fuel can be found from equation (21)

$$h_c = \frac{c_c}{1 - c_c} \cdot a \cdot \frac{33\ 820}{NCV} \qquad (21)$$

Or the combustion efficiency can be determined in terms of the carbon content of the entrained ash and the ash content and calorific value of the coal i.e.

$$\eta_c = f(NCV, a, c_c) \qquad (22)$$

From equation (22), it is clear that the combustion efficiency is independent of the direct measurement of any of the main operating variables during each individual test. Provided a representative ash sample is analysed, and that the main operating variables remain within acceptable limits, a good assessment of the combustion efficiency as defined by equation (22) can be obtained. The resulting values are contained in Tables 3.2 a and 3.2 b with the approximate temperature and velocity conditions for ease of reference. Accurate values for velocity and temperature as well as more detailed results are contained in Table H.1 of Appendix H.

Table 3.2 a Table of Combustion Efficiencies determined from the Carbon in Ash Analyses at approximate Temperature and Velocity Conditions for an Inert Bed Weight of 30 kg.

Velocity (m/s)	Temperature (°C)						
	650	700	750	800	850	900	950
0,9				88,6			
1,1			81,8	88,3		83,4*	
1,3			76,9	83,0		87,8	
1,5	52,0*		76,6	84,3		88,9	89,7

Table 3.2 b Table of Combustion Efficiencies determined from the Carbon in Ash Analyses at approximate Temperature and Velocity Conditions for an Inert Bed Weight of 20 kg.

Velocity (m/s)	Temperature (°C)						
	700	750	800	850	900	950	1000
1,1		79,6	80,2		87,7	88,0	
1,3	71,7			85,6			
1,5		79,6*	73,1		79,8		91,4

The results of Tables 3.2 a and 3.2 b indicate increasing combustion efficiency with increasing temperature and increasing bed height, whilst the combustion efficiency tends to decrease as the superficial gas velocity increases. Those values marked with an asterisk (*) have been omitted from the regression analysis as they are apparently in error. In each of these three tests, large adjustments to the coal feed rate had to be made to maintain the bed temperature at an acceptable value.

3.3.2 Statistical Analysis of Results

The experimental work has been conducted by considering variations in the main independent variables, temperature, superficial gas velocity and the static bed height. The temperature was continuously recorded by means of three chromel-alumel thermo-couples, cf Section 2.2.7. The mean value of the temperature has been evaluated for each test from about 120 equally spaced individual readings. Table H.1 of Appendix H contains details of the mean, maximum and minimum temperature levels recorded during each test, as well as the standard deviation from the mean. This latter value has been included to illustrate the degree of deviation

from the mean, and higher values for the standard deviation recorded during the shallow bed tests indicate the increased difficulty in maintaining steady temperature conditions with these shallower beds.

Superficial gas velocities and the static bed heights are obtained indirectly from other measurements. The former has been obtained by measuring the air flow to the rig and adding the small component from the resulting combustion gases when the coal is burnt within the rig. The static bed height is determined from measurements of the bed height prior to and at the end of each test run, eg Run 8, and by relating these values to the individual bed pressure drop measurements for each test, eg 8C or 9E etc. Values of the superficial gas velocities are contained in Table H.1 in Appendix H, whilst those of the static bed height are contained in Table H.2 of the same Appendix.

In view of the fact that Ehrlich (28) used other independent variables, viz coal flow rate, air flow rate and inert feed rate, it was decided to estimate the effect of other independent variables on the combustion efficiency. A list of the independant variables considered is quoted below:

bed temperature
superficial gas velocity
static bed height
coal feed rate
gas flow rate
ratio of the bed to distributor pressure drops
vigorousness of bubbling as given by: $(U_f - U_{mf})/U_{mf}$
splashing rate, cf Section 3.4

The measured value of the coal feed rate has been found to be of poor accuracy. A better value for the coal feed rate can however be deduced from the evaluation of the rate at which the coal is burnt and the combustion efficiency. Therefore the coal feed rate cannot be used in the regression analysis.

further, as the rig is cooled by the fluidizing air, the gas flow rate is almost proportional to the superficial gas velocity, and can therefore be omitted from the analysis.

The remaining six quantities from the original eight listed above will be used in a multiple linear regression analysis. A brief outline of the statistical method employed in the analysis is contained in Appendix F.

The ratio of the bed to distributor pressure drop is obtained directly from the measured values quoted in Table H2 of Appendix H. This value has been included in order to include some parameter which may quantify the quality of fluidization. Similarly the velocity ratio, termed the vigorousness of bubbling by Merrick and Highley (22) has also been included. The splashing rate which is discussed in Section 3.4 may also be related to the quality of fluidization, and therefore this parameter will also be assessed in the regression analysis.

The Regression Analysis

Table H.4 of Appendix H includes all the values to be used in the regression analysis. It should be noted that the results for tests 7B, 8H and 10A have not been included for reasons as set out in Section 3.3.1 (b). The first step of the analysis is the evaluation of the bivariate correlation coefficients, r_{zi}. These have been determined and tabulated in Table 3.3 overleaf.

Table 3.3 : Bivariate Correlation Coefficients between the various Parameters as defined in the Table

	Temperature r_{i1}	Gas Velocity r_{i2}	Bed Height r_{i3}	Pressure Ratio r_{i4}	Velocity Ratio r_{i5}	Splashing Rate r_{i6}	Efficiency r_{iY}
Temperature r_{1j}	1,0000	0,3015	-0,1856	0,0531	0,5957	-0,1468	0,7474
Gas Velocity r_{2j}	0,3015	1,0000	0,0673	-0,8002	0,8644	0,3500	-0,1775
Bed Height r_{3j}	-0,1856	0,0673	1,0000	0,1558	0,0426	0,6969	0,1847
Pressure Ratio r_{4j}	0,0531	-0,8002	0,1558	1,0000	-0,6299	-0,1912	0,5210
Velocity Ratio r_{5j}	0,5957	0,8644	0,0426	-0,6299	1,0000	0,2943	0,1746
Splashing Rate r_{6j}	-0,1468	0,3500	0,6969	-0,1912	0,2943	1,0000	0,0716
Efficiency r_{Yj}	0,7474	-0,1775	0,1847	0,5210	0,1746	0,0716	1,0000

Nineteen data points have been used in the analysis. It is of interest to determine whether a significant correlation exists between any two parameters. From Appendix F, it is seen that the hypothesis that the correlation does not differ significantly from zero can be tested by the analog given by

$$r_{ij}\sqrt{\frac{n-2}{1-r_{ij}^2}}$$

distributed under the null hypothesis as t (19-2), i.e. with seventeen degrees of freedom.

For 95% confidence limits, and seventeen degrees of freedom

$$t_{0,025} = -2,110$$

and

$$t_{0,975} = 2,110$$

or for there to be no significant correlation between any two parameters, the following inequality must be satisfied:

$$-2,110 < r_{ij}\sqrt{\frac{17}{1-r_{ij}^2}} < 2,110 \qquad (23)$$

or

$$r_{ij} < 0,342 \qquad (24)$$

Reference to equation (24) and Table 3.3 indicates that a significant correlation exists between the following parameters:

Temperature	:	and velocity ratio
Gas Velocity	:	and pressure ratio, velocity ratio, splashing rate
Bed Height	:	and splashing rate
Pressure Ratio	:	and gas velocity, velocity ratio
Velocity Ratio	:	and temperature, gas velocity, pressure ratio
Splashing Rate	:	and gas velocity, bed height

In order to determine the significance of each of the dependent variables on the combustion efficiency, the standard normal correlation coefficient, B_i, for each of these parameters must be determined. These are found from the components of the inverted matrix formed from the matrix comprising the bivariate correlation coefficients between the independent variables of Table 3.3, i.e. all the components of Table 3.3 except for the correlation coefficients between efficiency and each of the independent variables. This inverted matrix is given in Table 3.4

Table 3.4 : Inverted Matrix of the Bivariate Correlation Coefficients between the Independent Variables.

	g_{i1}	g_{i2}	g_{i3}	g_{i4}	g_{i5}	g_{i6}
g_{1j}	4,8679	-0,3564	1,1918	-3,9603	-5,3829	0,8356
g_{2j}	-0,3564	7,6277	-0,7614	3,7138	-3,9123	-0,3295
g_{3j}	1,1918	-0,7614	2,6907	-1,9986	-0,9755	-1,5287
g_{4j}	-3,9603	3,7138	-1,9986	6,6468	3,4931	-0,2453
g_{5j}	-5,3829	-3,9123	-0,9755	3,4931	10,142	-1,0579
g_{6j}	0,8356	-0,3295	-1,5287	-0,2453	-1,0579	2,5677

From the above table, the following standard normal correlation coefficients are determined:

1) Temperature : $B_1 = 0,9782$
2) Gas Velocity : $B_2 = 0,5329$
3) Bed Height : $B_3 = 0,2019$
4) Ratio of bed to distributor Pressure Drops : $B_4 = 0,1023$
5) Gas Velocity Ratio, $(U_f-U_{mf})/U_{mf}$: $B_5 = 0,0063$
6) Splashing Rate : $B_6 = 0,2720$

The multiple correlation coefficient has been calculated as:

$$R = 0,9679$$

indicating that the regression equation which could be determined from the six independent variables fits the data rather well. However the contribution of some of the independent variables may not be significantly different from zero. By taking 95% confidence limits the interval estimates, B^1, for each of the standard partial correlation coefficients can be determined from equations (F.11) and (F.12) of Appendix F. The calculated interval estimates are given below:

$$\begin{aligned}
0,6295 &< B'_1 < 1,3269 \\
-0,9694 &< B'_2 < -0,0964 \\
-0,0574 &< B'_3 < 0,4612 \\
-0,3052 &< B'_4 < 0,5098 \\
-0,4971 &< B'_5 < 0,5097 \\
0,0187 &< B'_6 < 0,5253
\end{aligned}$$

From the above it is evident that the effect of the ratio of the bed to distributor plate pressure drop (B_4), and the gas velocity ratio (B_5) have little significance in the regression analysis and can be eliminated. The splashing rate (B_6) appears to be of significance, whilst the contribution due to the static bed height (B_3) is apparently insignificant. However, it was previously noted that a correlation exists between the bed height and the splashing rate, and thus the elimination of the splashing rate would increase the significance of the bed height. Further, a positive value of the standard partial correlation coefficient for the splashing rate, indicates that as the splashing rate increases the combustion efficiency increases. This is contrary to expectations, and further as the measurement of the static bed height is easier than that of the splashing rate, this latter variable has also been eliminated.

The analysis has been performed to obtain a regression equation using temperature, superficial gas velocity and bed height. The resulting correlation is given below:

$$\eta_c(\%) = 36,27 + 0,0675 \cdot T - 17,1 \cdot u_f + 65,0 \cdot H \qquad (25)$$

The multiple correlation coefficient, R is found as

$$R = 0,9422$$

The elimination of three of the original six variables has resulted in a decrease of the multiple correlation coefficient from 0,9679 to 0,9422. In order to establish whether this coefficient has been lowered significantly by the elimination of the three variables, the test as presented in Appendix F.2 is applied. From equation (F.13), the following value is obtained:

$$F = 3,1019$$

and

$$F_{0,95}(12,3) = 8,74$$

$$F_{0,05}(12,3) = 0,287$$

and since the value of F lies between 0,287 and 8,74, the multiple correlation coefficient has not been significantly reduced.

Finally it was felt that a regression equation could probably be evaluated with only two independent variables, viz temperature and superficial gas velocity. However, the resulting multiple correlation coefficient was only 0,8586 which can easily be shown to be significantly different from the 0,9422 obtained using three independent variables.

Therefore equation (25) can be taken as the best estimate of the combustion efficiency from the data obtained from the test rig. In the determination of equation (25), the following regression table, given by Table 3.5 was generated:

Table 3.5 : Regression Table from the Analysis resulting in the formation of Equation (25).

	Sum of Squares	Degrees of Freedom	Mean Squares
Regression	551,6	3	183,9
Residual	69,7	15	4,65
Total	621,3	18	

with the following statistical values:

Coefficient of Determination : 0,8878
Standard Error of Estimate : 2,1559
Multiple Correlation Coefficient : 0,9442

3.3.3 Discussion of Results

It has been found that the combustion efficiency can be predicted from the bed temperature, the superficial gas velocity and the static bed height. Although extrapolations could be made beyond the limits for which the results have been obtained, predictions of combustion efficiency with low pressure drop distributors and burning a coal having a high fines component such as the Douglas Duff tested, based on equation (25) should be restricted to the following limits:

Bed Temperature : from 700 to 1000°C
Superficial Gas Velocity : from 0,9 to 1,5 m/s
Static Bed Height : from 150 to 250 mm

The combustion efficiency is most strongly influenced by the combustion temperature, resulting in improved combustion at the higher temperatures due to increased reaction rates. Secondary effects on the combustion efficiency are due to

the superficial gas velocity and the static bed height. As the superficial gas velocity is increased, the combustion efficiency decreases as a result of the increased entrainment rate causing a reduction in the residence time of the particles in the bed. The high fines content of the coal feed may cause the effect of velocity on the combustion efficiency to be a little more emphasized than would normally be the case. The deeper beds tested resulted in higher combustion efficiencies, due to the increased particle residence time.

The combustion efficiencies reported in this thesis are much lower than those reported elsewhere, eg by Waters (30), Ehrlich (28), Jonke et al (63). Though direct comparison is not possible due to the lack of information regarding the basic parameters, the lower efficiency can be attributed to three factors:

a) the use of shallow beds,
b) the low pressure drop distributor, and
c) the high fines content of the coal feed.

It is generally accepted that shallow beds result in lower combustion efficiencies due to the shorter residence time of the coal particle in the high temperature combustion zone. Residence times of particles subject to elutriation are decreased in direct proportion to the total mass of the bed by the following relationship which is discussed in more detail in the theoretical analysis of Chapter 4. If the concentration of solids is designated as 'C', then the rate of change of concentration by elutriation can be approximated by a first order rate equation, eg

$$\frac{dC}{dt} = K \cdot C \qquad (26)$$

$$\frac{dC}{dt} = K^{*} \cdot \frac{A_t}{W} C \qquad (27)$$

where K* is an elutriation rate constant in (kg/m^2s) which is readily obtained from experimental correlations (24). Whilst most published results relate to work done in beds ranging from about 300 to 600 mm in depth, the present series of tests were performed at depths considerably less than these. Equation (27) clearly indicates that the rate of elutriation of solids from the bed increases as the bed weight decreases, i.e. as the bed height decreases.

Although the pressure drop across the distributor should be of the same order as that through the bed, satisfactory results have been obtained using low pressure drop distributors, cf Section 1.2.7. However, the quality of fluidization may be impaired by using such distributors resulting in poor combustion efficiencies. This parameter, the quality of fluidization, is difficult to quantify and attempts were made to assess this quantitatively by introducing some additional factors in the regression analysis of Section 3.3.2. All the factors analysed, resulted in insignificant improvements in the prediction of the combustion efficiency due to the interaction of the various factors upon each other. The precise effect of the pressure drop across the distributor, as well as efforts directed at determining quantitatively the quality of fluidization will only be possible by evaluating combustion efficiencies whilst using both similar and different distributors but having different pressure drop to velocity characteristics.

The high fines content in the coal feed results in these fine particles being entrained in the off gases before combustion can take place. The coal gradings as supplied are given in Appendix C. However, prior to introducing this coal into the rig, the size fraction above 6,35 mm was screened off, resulting in the as fired grading given by Figure 20. Only the coal given as Batch B in Appendix C has been plotted as this was used for eighteen of the twenty-two tests. From Figure 20, it is seen that about

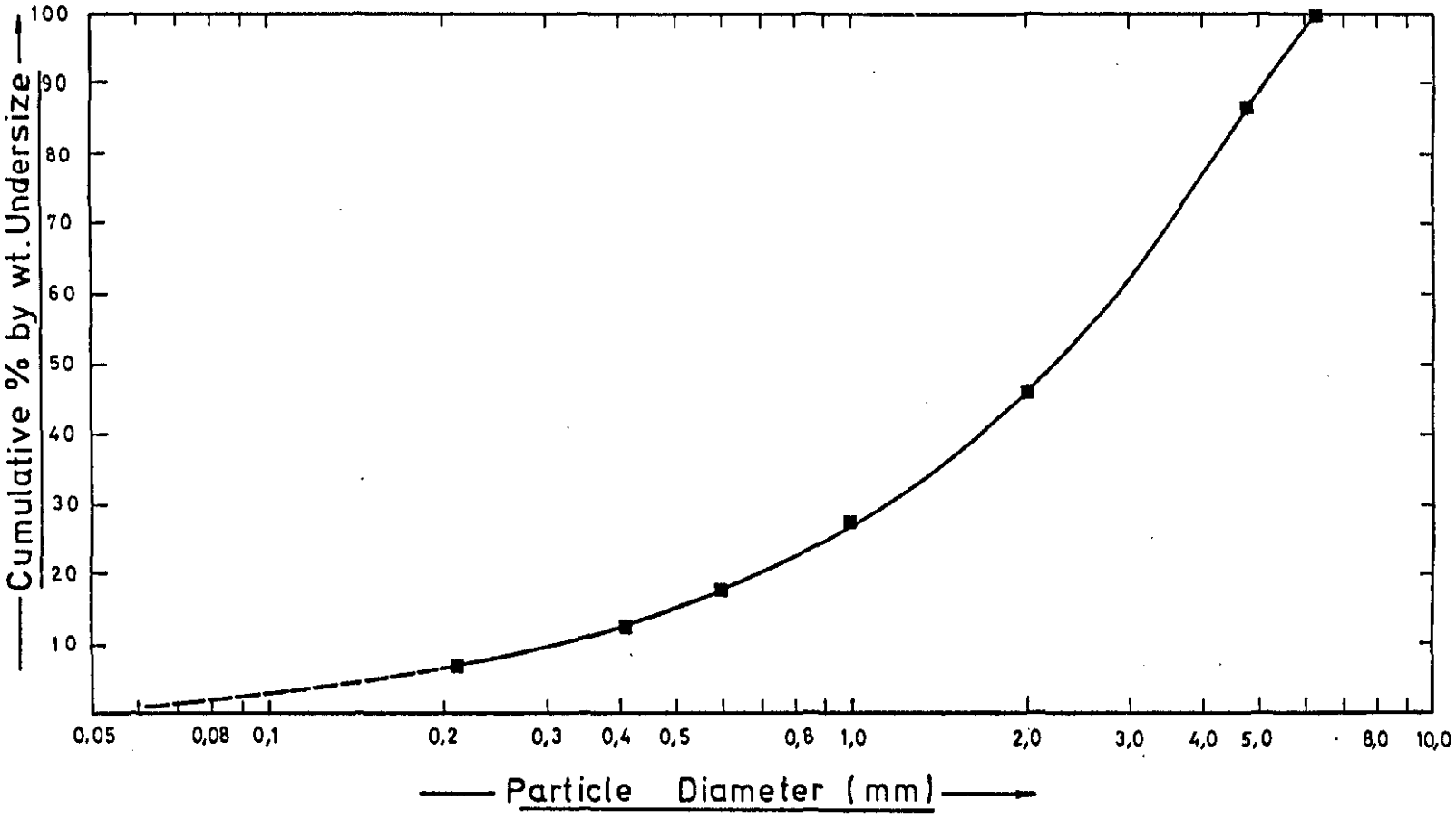

Figure 20 : As Fired Size Distribution of Coal Designated as Batch B (cf App C)

10% of the coal is less than 0,3 mm in diameter, the size for which the terminal velocity would be about 1,5 m/s cf Figure 6.

Finally, it can be said that though the combustion efficiency can be approximated with confidence by a regression equation containing only temperature, gas velocity and bed height, the incorporation of a fourth parameter to quantify the quality of fluidization could probably lead to a more general application which would allow for changes in equipment, in particular the distributor type. A further point is the effect of slugging flow which may have taken place in the deeper beds. This is discussed in more detail in Section 3.4 and is felt to have little effect on the combustion efficiency.

The results of Test Runs 6, 7 and 8 have been plotted in Figure 21, with lines of constant velocity from equation (25) being superimposed on these points. Similarly, Figure 22 has been drawn for the shallow bed tests, ie Test Runs 9 and 10. From these two figures the results of the regression analysis can be compared directly with the points used in the derivation of equation (25).

3.4 ENTRAINMENT

Particles are entrained from the combustor vessel of the fluidized-bed combustion rig and separated from the off gases in a cyclone. The entrainment mechanism can be described by considering it as the sum of two processes, the first due to elutriation of the fine particles, and the other as a result of splashing cf Section 1.2.3. The phenomenon of elutriation has been studied in some detail, whilst the concept of splashing has been introduced to explain the entrainment of those particles too large to be elutriated.

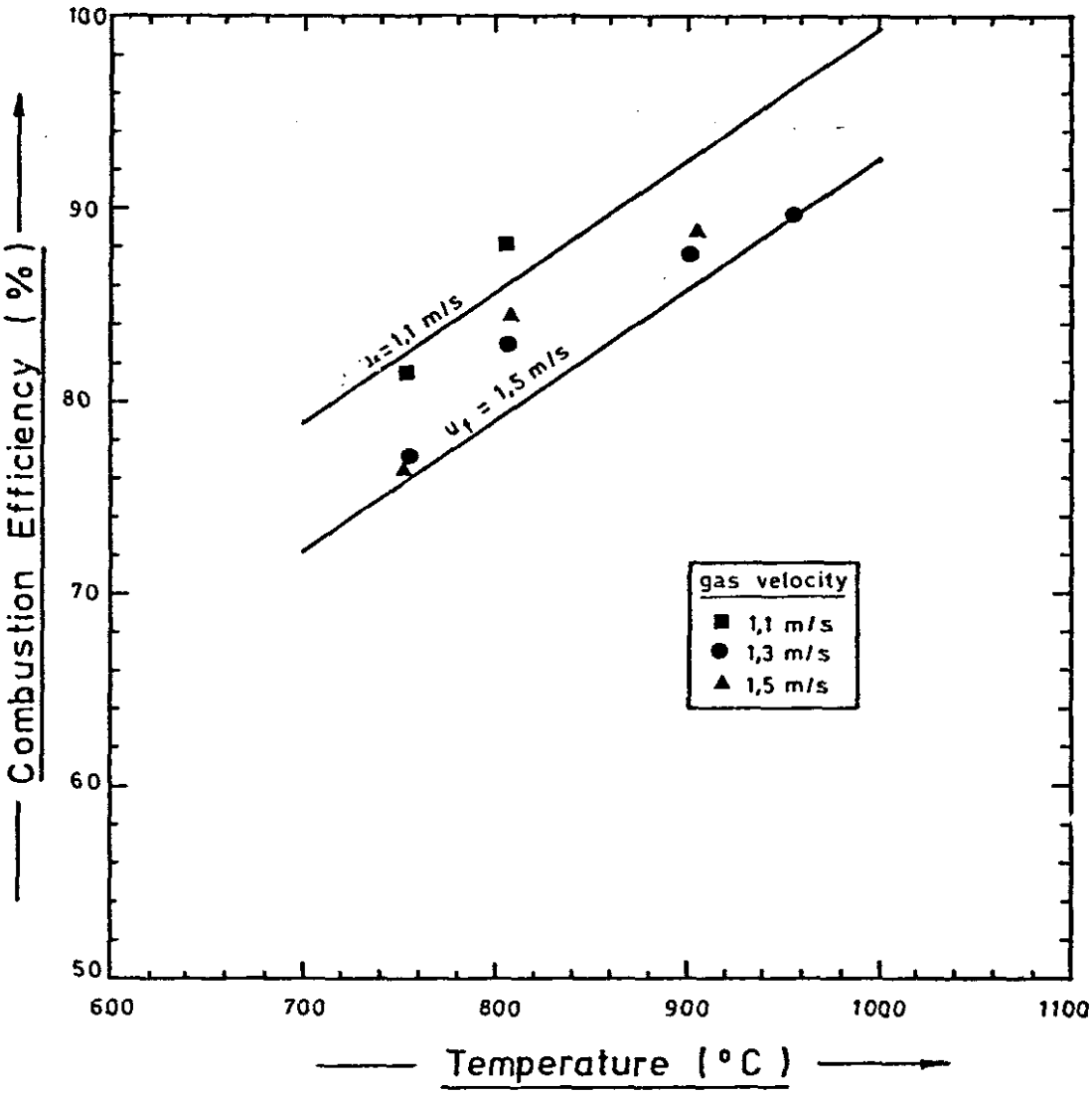

Figure 21 : Combustion Efficiencies when Burning Duff Coal in a 220 mm Deep Bed.

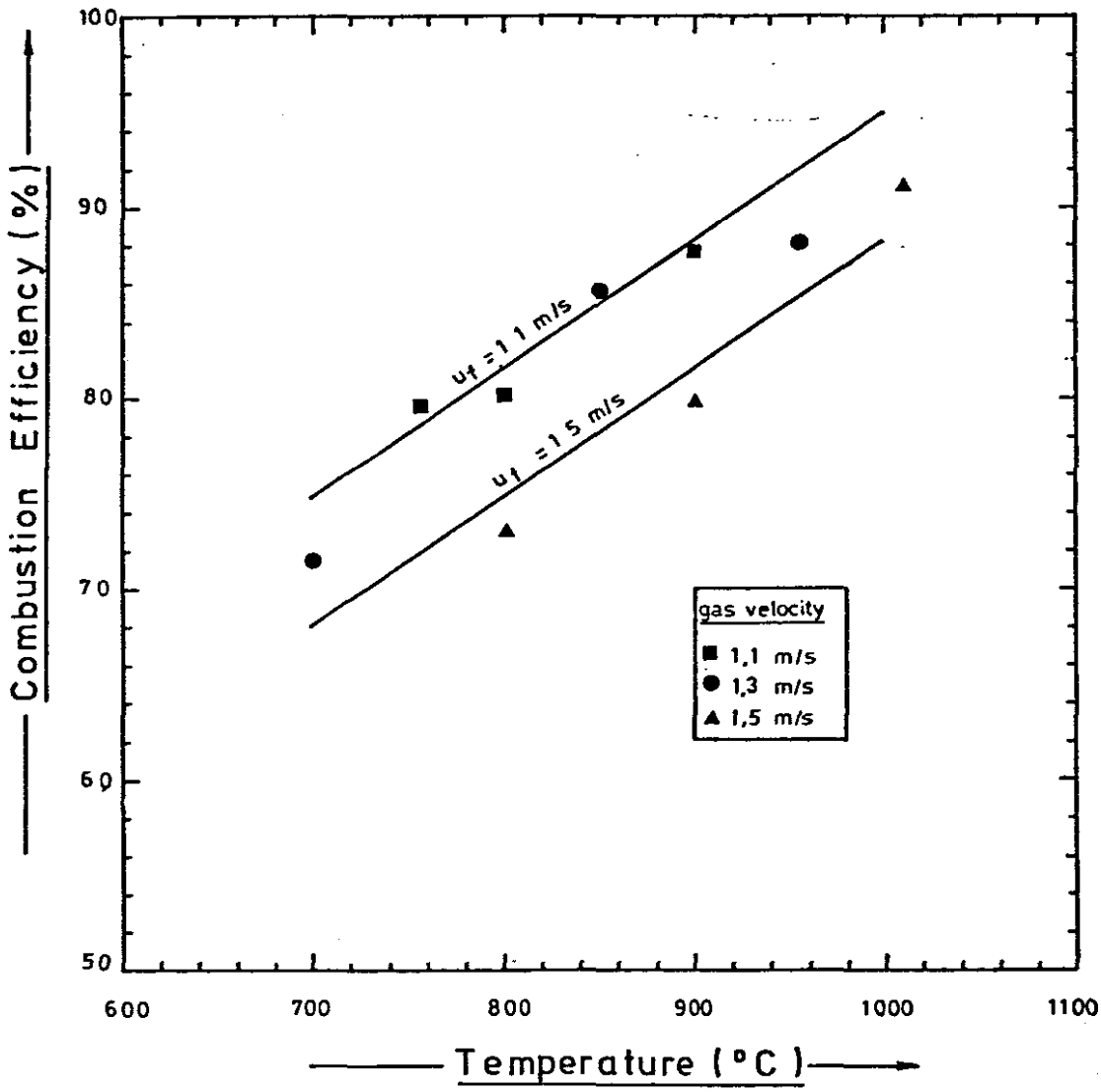

Figure 22 : Combustion Efficiencies when Burning Duff Coal in a 155 mm Deep Bed.

The first analyses of the material collected from the cyclone indicated that the proportion of material larger than 600 microns was consistently greater than anticipated resulting in almost a discontinuity in the grading curves. Further, the quantity of material retained on the 420 and 211 micron sieves was very much lower than that on the 600 micron sieve. On closer examination, it was established that almost all of the material retained on this latter sieve was made up of the silica sand which was used as the inert bed material. These particles of bed material are too large to be elutriated, as the terminal velocity of these particles is well in excess of the 0,9 to 1,5 m/s velocity range used during the tests, cf Figure 6. Further, the bed material used for all but one of the tests has the size grading given by Figure 16 which indicates that about 92% of the bed material has a size greater than 600 microns. During the combustion process, the bed will only comprise between 0,5 to 2% of combustible matter, and therefore any material extracted from the bed during the combustion process will be made up mainly of inert particles. In view of the above it is evident that those particles greater than 600 microns have been entrained from the bed by the splashing mechanism. Therefore it has been assumed in this thesis, that any material greater than 600 microns has been removed by the process of splashing, whilst that below 600 microns has been removed by the elutriation mechanism.

The above assumption is not strictly true, as the splashed material should have a grading identical to that of the bed. However, the quantity of bed material smaller than 600 microns will at worst not exceed 10% of the bed material, being made up of the original bed material comprising about 8% and some combustible matter comprising no more than 2% of the fluidized bed. Further, reference to Figure 6 indicates that particles much larger than 300 microns will not be elutriated. However, from the size gradings

presented later in this section, it is evident that the fraction of material between 300 and 600 microns represents only a small fraction, about 5%, of the total below 300 microns, such that the inclusion of this small fraction in the elutriated quantity will have little effect on the results.

3.4.1 Grading of the Ash

Once the 600 micron fraction has been removed from the material collected by the cyclone, the remaining particles consist almost entirely of ash. This ash fraction has been graded for each of the twenty-two tests by means of sieving, whilst a further eight tests were selected for testing by means of a sedimentation technique. Information on the different means of determining particle sizes as well as the reasoning for adopting the above two methods is given in Appendix G.

Sieving of the material obtained from the cyclone was performed using sieves having the following aperture sizes in two sieve nests as indicated below:

600 micron	150 micron
420 "	106 "
211 "	75 "
	53 "

Particle sizes below 53 microns were determined for eight of the tests by means of a sedimentation technique based on the incremental method as outlined in BS 3406 : Part 2 of 1963 with use being made of an Andreasen pipette. This method allows for the determination of particle sizes from 75 to about 3 microns. The typical form of a size grading for the particles below 75 microns is shown in Figure 23. Distilled water was used as the suspending liquid, and examination of a small drop of the suspension indicated that no coagulation took place. From Figure 23 it is noted

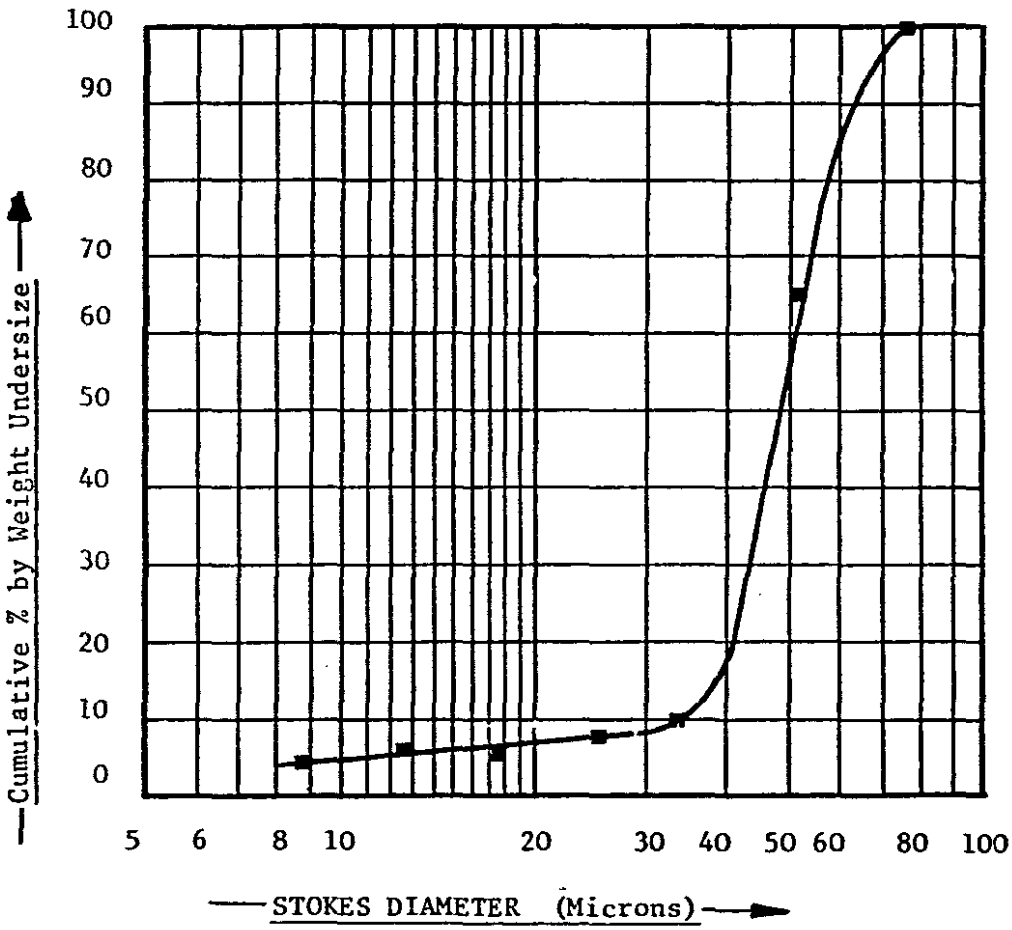

FIGURE 23 : Size Grading of the Ash Fraction Less than 75 Microns Collected in the Cyclone for Test 7B.
(Determination by means of an Andreasen Pipette)

that a sharp decrease in the cumulative percentage takes place between 40 and 55 microns, indicating that a large proportion of the particles are of this size. This is probably due to the natural classifying action of the fluidized bed causing small particles to be elutriated before being reduced too much in size, as well as due to the decreased efficiency of the cyclone in removing the finer ash particles.

As the fluidized-bed combustion process is being investigated, it is of far greater importance to have a knowledge of the size grading of the material leaving the combustor vessel than for that collected by the cyclone. In order to obtain these gradings, iso-kinetic sampling of the dust on leaving the combustor or immediately prior to entering the cyclone will have to be undertaken. However, this would have involved a complex and lengthy procedure rendered difficult due to the short lengths of ducting and relatively confined working area. A second approach was adopted requiring a knowledge of the cyclone performance to deduce the size grading of the incoming dust from the grading of the collected dust. As the cyclone has become almost standard equipment in many dust extraction applications, the performance of these components have been reported in various publications. The performance of the cyclone used for the fluidized-bed combustion tests is discussed in Appendix K.

The size gradings of the collected ash have been used to determine the gradings of the ash on entering the cyclone and hence the ash leaving the cyclone in the following way:

a) The grading of the ash collected from the cyclone is determined by sieving and in some cases the smaller sizes are determined using the incremental pipette method.

b) The grading of the ash at inlet to the cyclone is determined by applying the cyclone efficiencies for the different intervals to the collected ash grading.

c) These results are then "smoothed" by plotting on log-probability (Rosin-Rammler) paper and fitting a straight line to them.

d) The resulting grading for the ash at inlet to the cyclone is then used to determine the "smoothed" collected ash curve from the cyclone efficiencies and hence the grading of the ash leaving the cyclone to the atmosphere.

Figures 24 and 25 illustrate typical curves for the gradings at inlet to and exit from the cyclone as well as the grading of the collected ash. Although there is very little difference between the two sets of curves, Figure 24 is representative of the results obtained from the deep bed tests whilst Figure 25 is representative of the shallow bed tests. In addition to these results, Table H.5 of Appendix H contains some selected smoothed curves of the size gradings of the ash at inlet to, exit from and that collected by the cyclone. The complete sieve analyses from 600 to 53 microns is given in Table H.6 of the same Appendix, whilst Table H.9 contains the results of the size analysis by means of a sedimentation technique for particles of size less than 75 microns. This latter analysis has only been performed on the ash from eight of the tests.

3.4.2 The Splashed Material

All that material entrained in the gas stream from the fluidized-bed combustor greater than 600 microns in size is assumed to be removed by the mechanism of splashing. It is

b) The grading of the ash at inlet to the cyclone is determined by applying the cyclone efficiencies for the different intervals to the collected ash grading.

c) These results are then "smoothed" by plotting on log-probability (Rosin-Rammler) paper and fitting a straight line to them.

d) The resulting grading for the ash at inlet to the cyclone is then used to determine the "smoothed" collected ash curve from the cyclone efficiencies and hence the grading of the ash leaving the cyclone to the atmosphere.

Figures 24 and 25 illustrate typical curves for the gradings at inlet to and exit from the cyclone as well as the grading of the collected ash. Although there is very little difference between the two sets of curves, Figure 24 is representative of the results obtained from the deep bed tests whilst Figure 25 is representative of the shallow bed tests. In addition to these results, Table H.5 of Appendix H contains some selected smoothed curves of the size gradings of the ash at inlet to, exit from and that collected by the cyclone. The complete sieve analyses from 600 to 53 microns is given in Table H.6 of the same Appendix, whilst Table H.9 contains the results of the size analysis by means of a sedimentation technique for particles of size less than 75 microns. This latter analysis has only been performed on the ash from eight of the tests.

3.4.2 The Splashed Material

All that material entrained in the gas stream from the fluidized-bed combustor greater than 600 microns in size is assumed to be removed by the mechanism of splashing. It is

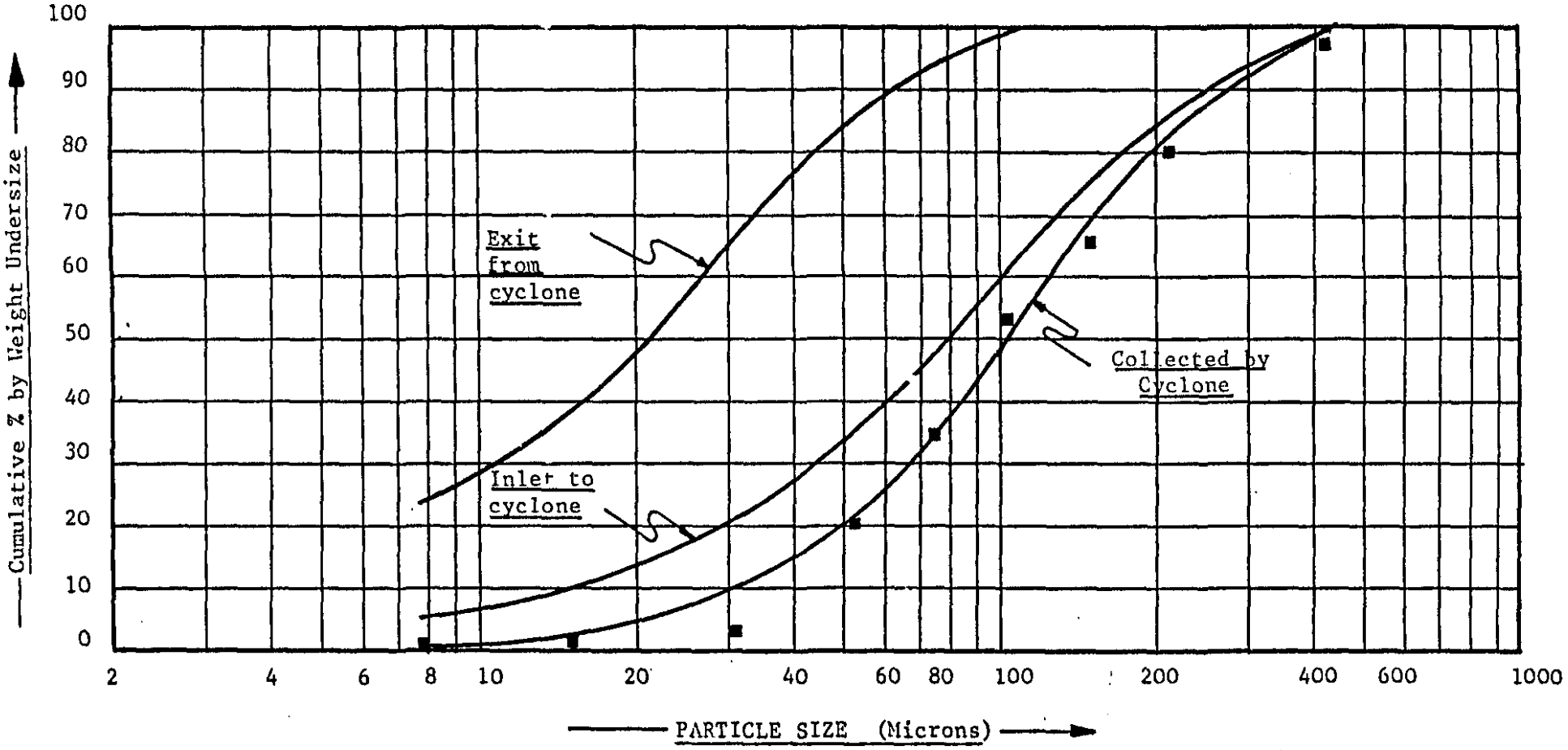

FIGURE 24: Ash Gradings for Flows at Inlet to, Exit from and Collected by the Cyclone for Test 8A.

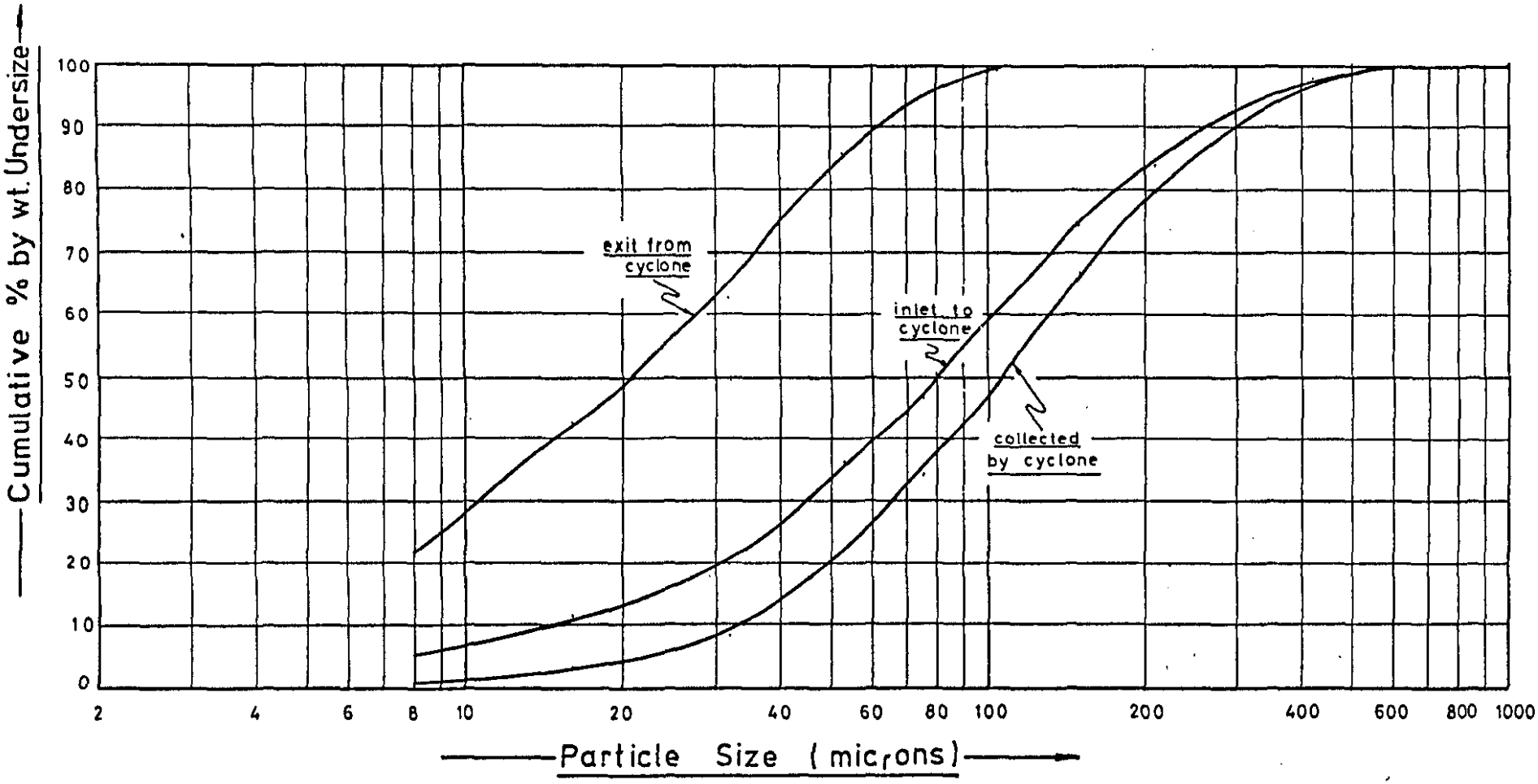

Figure 25 : Ash Gradings for Flows at Inlet to , Exit from and Collected by Cyclone for a Shallow Bed Test (Test 9A)

evident that the splashing rate is a function of the height of freeboard section, and for an infinite freeboard, the splashing rate will be zero. Kunii and Levenspiel (4, Ch 10) consider the entrainment of fines by the elutriation mechanism, whilst the entrainment of coarse particles decreases exponentially in accordance with an equation similar to that given by equation (28).

$$m = F\, e^{-a \cdot H} \qquad (28)$$

This entrainment of the coarse particles has been represented in this thesis by the splashing rate, and as is evident from equation (28) the splashing rate is very much dependent on the rig dimensions, and in particular on the height of the freeboard. The results of this study are therefore referred to a freeboard height of approximately 900 mm, which is well below the figure of about 10 m which is generally quoted as being necessary to eliminate the effect of the entrainment due to causes other than by elutriation.

Examination of the splashed material has shown it to be comprised almost exclusively of the silica sand used as the bed material. Small amounts of ash were evident, but not in any quantity to suggest a build-up of ash in the bed. Reference to Table H.2 of Appendix H shows that the static bed height decreases steadily during a test run. The increase in bed height indicated during Run 8 is due to the addition of some bed material after Test 8E. The bed material was also examined at the end of each run, and besides there being no appreciable build up of ash in the bed, the silica sand forming the inert bed showed almost no sign of degradation. It is clear therefore that the ash formed during combustion at the relatively low bed temperatures, from 700 to 1000^{o}C, is soft and the attrition rate of the ash is high whilst that of the silica sand bed material is very small. This indicates that almost all of the ash introduced into the bed via the coal feed, is broken down in the fluidized bed and removed from the rig by means of the off

gases. The original bed material, i.e. the silica sand, undergoes very little change and is removed by the splashing process. As a result of the removal of the bed material without it being supplemented by ash remaining in the bed from the coal feed, the bed height steadily falls as the Test Run progresses.

3.4.3 Entrainment Rates of the Different Components

Table H.8 of Appendix H contains the entrainment rates of the various components leaving the bed. These are divided into two main components, that due to elutriation represented by the carbon and ash flow rates and the second due to the splashing rate, represented by the sand flow rate. The combined ash and carbon flow rates have been obtained by weighing the sample collected by the cyclone after the removal of the sand (i.e. the component having a diameter in excess of 600 microns), and allowing for the cyclone performance to deduce the flow rate of the incoming particles. The assessment of the percentage carbon in ash enables the ash and carbon flows to be separated. The deduced ash flow rate has been determined directly from the ash content of coal feed rate, assuming that all the ash is entrained from the rig. In comparing this latter flow rate with the measured ash flow rate, it appears that the deduced flow rate, except for two measurements, is always greater than that measured. This would indicate that a small quantity of ash remains in the bed. However, the duration of the tests have been too short to obtain a meaningful result for the measured value, which has further been derived from a simple approach to the cyclone performance. Accurate comparisons could only be obtained from detailed tests on the cyclone. The comparison of the results has little meaning except to indicate that the flow rates are of the same order. However, although the absolute value of the measured entrainment rates is of only marginal importance, the relative values of the elutriated and

splashed components can be determined accurately and are of significance. The fraction of the entrainment rate that occurs as a result of splashing, or the percentage sand of the total entrainment rate, is given in Tables 3.6 a and 3.6 b for each test with the approximate velocity and temperature conditions quoted for ease of reference.

Table 3.6 a : Splashing Rate as a Percentage of Total Entrainment Rate from the Combustor Vessel at Approximate Velocity and Temperature Conditions for a Static Bed Height of 220 mm.

Velocity (m/s)	Temperature (°C)						
	650	700	750	800	850	900	950
0,9				9,2			
1,1			4,7	8,7		6,0	
1,3			4,6	21,1		5,5	
1,5	10,0		13,5	28,9		17,8	9,2

Table 3.6 b : Splashing Rate as a Percentage of Total Entrainment Rate from the Combustor Vessel at Approximate Velocity and Temperature Conditions for a Static Bed Height of 155 mm.

Velocity (m/s)	Temperature (°C)						
	700	750	800	850	900	950	1000
1,1		0,5	1,1		0,4	1,2	
1,3	0,4			0,6			
1,5		1,3	1,6		0,8	1,3	

From Tables 3.6 a and 3.6 b, it is evident that the splashing rate from the deeper bed is far greater than that of the shallower bed. In accordance with the two phase theory of

fluidization, the amount of gas in excess of that required to fluidize the bed passes through the bed as bubbles. From Table H.3 of Appendix H, it is evident that the superficial gas velocity is well in excess of that required to just fluidize the bed. Further, from Stewart's (103) criterion for slug flow given by equation (J.12) below and as discussed in Appendix J.

$$(u_f - u_{mf}) \;/\; 0{,}35 \;/\; (D_t\, g)^{0{,}5} \;>\; 0{,}2 \qquad (J.12)$$

the bed should be in the slugging flow regime. For the shallow beds tested, the coalescence of the bubbles will not have occurred to such an extent for slug flow to occur. The bubbles in the deeper bed probably approach that of the combustor diameter, yet even these deeper beds have a depth of only 230 mm and fully developed slug flow is improbable.

It is felt therefore that the increased entrainment rate for the deeper bed occurs as a result of the increased momentum imparted to particles on the bursting of larger bubbles at the surface. Although Davidson and Harrison (12, pg 19) claim that the two phase theory of fluidization holds for values of $(U_f - U_{mf})/U_{mf}$ in excess of ten, this would appear to be doubtful.

Further examination of Tables 3.6 a and 3.6 b, indicates that increasing velocity increases the splashing rate. However the contribution by splashing at similar velocities but at different temperatures is markedly different, with an apparent maximum being observed at 800°C in four of the five velocity levels noted. This results in a poor correlation being derived between the splashing rate and velocity. It is felt that in order to obtain a quantitative result for the splashing rate a far more comprehensive test series incorporating different distributor types will be necessary as one of the main parameters in the splashing rate would appear to be the bubble diameter.

3.4.4 Discussion of Results

In contrast to quantitative results obtained from the investigation into the combustion efficiency, no such relationship could be derived in the description of the entrainment rates. It is evident, however, that the deeper beds resulted in higher splashing rates as was the result when the velocity was increased. The shallower fluidized beds behave as bubbling beds, whilst the initial phases of slug flow appear to be manifested in the deeper beds investigated. In order to arrive at a quantitative result, the use of the bubble diameter, bubble velocity, fraction of solids in the bubble wake or some other complex phenomenon associated with gas fluidized beds may be necessary. As all these parameters are highly complex, it is evident that a considerable amount of work will have to be done in order to quantify the result even for very specific operating conditions.

CHAPTER 4

THEORETICAL MODEL

The extension of results from experimental or pilot plant for use in large scale equipment or even the comparison of results from one particular arrangement to another requires the formulation of a model to describe the process. Models are particularly useful in establishing the effect of individual parameters on the overall system. However, the combustion of solid fuels in an inert fluidized bed is extremely difficult to describe analytically because of the large number of unknown parameters. Indeed, Pyle (14) reports that models are quite often qualitative or at best semi-quantitative, whilst when some form of correlation is required to predict performance in some other situation, the model may be empirical. No a priori design and analysis of fluidized-bed combustors is presently possible, "nor is it likely to be so in the immediately foreseable future" (14).

A model has been developed based on the theories of different authors to explain the fluidized-bed combustion and entrainment processes under steady state conditions. From a knowledge of the original bed size grading and the grading of the fuel fed into the combustor the eventual gradings of the inert and combustible components within the bed as well as of the entrained material can be predicted. A major objective of the model is the prediction of combustion efficiencies and entrainment rates.

4.1 THE OVERALL CONCEPT

The model commences with an estimate of the combustion efficiency and a determination of one of the three

parameters, superficial gas velocity, temperature or coal flow rate from the remaining two which are used as input. The second stage of the calculation is the determination of the combustion efficiency. This is determined by considering the overall consumption of oxygen in the bed and comparing it with the coal feed rate. The efficiency thus determined is compared with the original estimate, and should they differ by more than 0,5% a new estimate for the efficiency is made based on the previous values. A new value for the unknown of the three parameters, velocity, temperature and coal flow is then determined and the calculation repeated until the desired accuracy is obtained. Elutriation rates, particle shrinkage rates and splashing rates have to be supplied as data. Existing correlations have been used for the first two, whilst a splashing rate constant has been determined from the experimental results. It should be emphasized that the splashing rate constant so determined is rig dependent, the most important influencing parameters being the freeboard height and the existence of baffles above the bed.

The third and final stage is concerned with the determination of particle entrainment rates from the bed. Particles are considered to be abraded in the bed and remain in the bed until they are removed either by elutriation, splashing or in the bed overflow. The major difference between this calculation and that for the determination of the combustion efficiency lies in the manner in which the shrinking particle, caused by combustion or abrasion is considered. In the case of combustion, no attrition is assumed to take place and no fines are produced. As a result the particle shrinks by chemical action only. Further, as the burning particles comprise only a small percentage of the entire bed mass, typically 1%, and therefore the overflow quantity or decrease in bed weight is neglected. In the case of attrition, the fines produced are considered and the mass balance of the system results in a more complex equation which is solved by

considering particles falling into and out of a small size fraction. The splashing rate constant obtained from the previous stage is applied to the third stage, whilst the resulting ash size distribution is correlated with the experimentally determined distribution by applying an attrition rate constant. A simplified block diagram of the overall model is given in Figure 26.

4.2 PRELIMINARY CALCULATIONS

The first stage of the theoretical model consists of performing a heat balance on a fluidized-bed combustor. In particular the heat balance is considered about the fluidized bed section of the test rig as described in Section 3.3.1 (a) and Appendix E. The heat balance is written as :

$$(heat\ input) = \begin{pmatrix} heat\ in \\ off\ gases \end{pmatrix} + \begin{pmatrix} heat\ loss\ through \\ combustor\ walls \end{pmatrix} \qquad (E.1)$$

which reduces to

$$\eta \cdot M_{fo} \cdot NCV = M_g \cdot c_p \cdot \Delta T + Q_w \qquad (29)$$

The heat loss through the combustor walls Q_w is supplied as input. By increasing the value of this parameter, the effect of bed cooling by immersed surfaces can be assessed. The net calorific value may be supplied as input or be deduced from the ultimate analysis of the coal, whilst the specific heat is assumed to be the mean specific heat of air at the respective temperature. The conditions analysed are similar to those for which the tests were carried out i.e. at high excess air levels, and therefore the effect of the carbon dioxide and water vapour components on the specific heat of the flue gases will be small, such that the error introduced by assuming that the specific heat of these gases approximates that of air will be insignificant. The

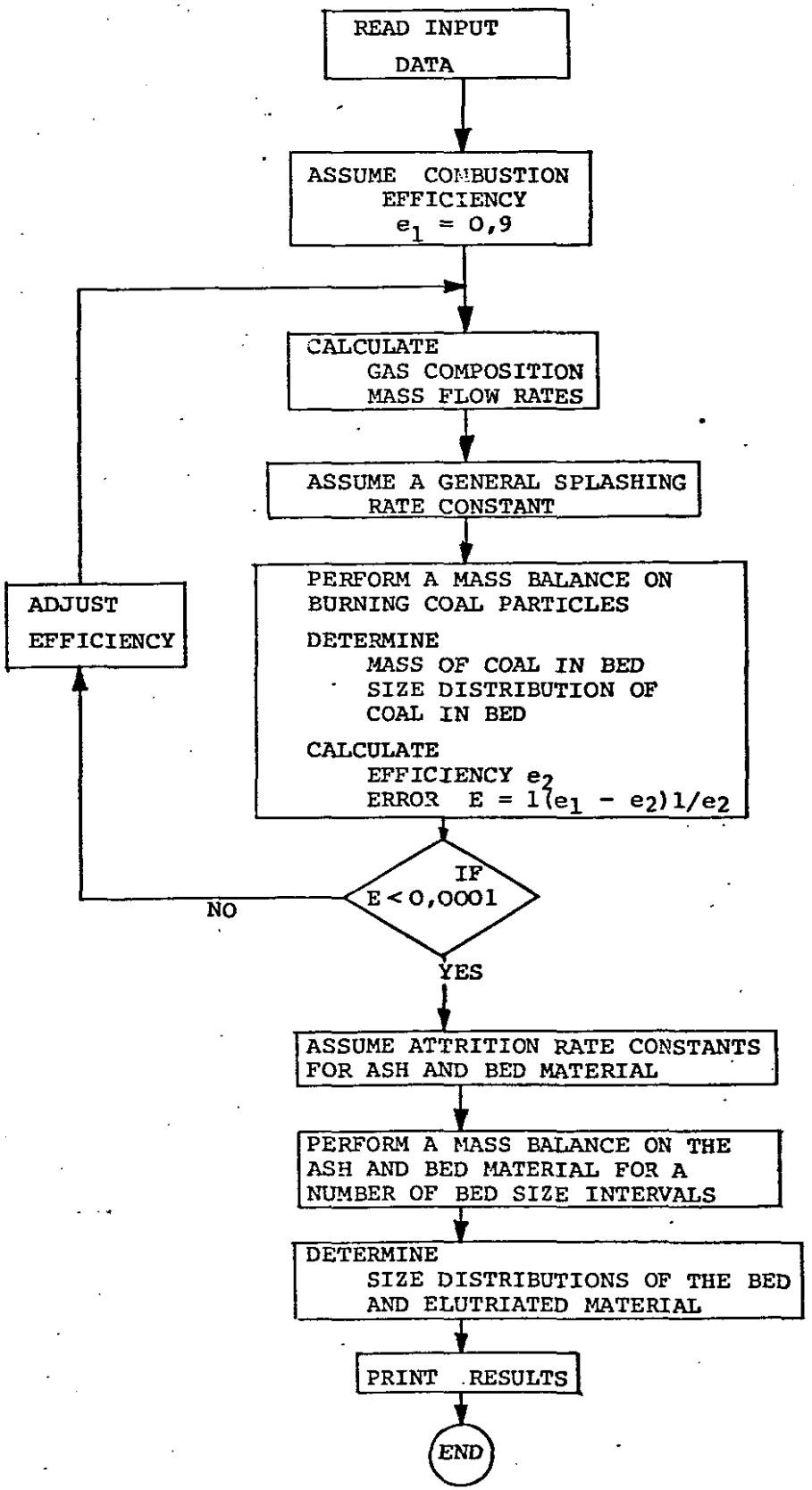

FIGURE 26 : Simplified Flow Chart of Theoretical Model to Predict the Fluidized-Bed Combustor Performance

gas velocity is related to the gas mass flow rate by the simple relationship of equation (30).

$$M_g = \rho_g \cdot A_t \cdot u_f \qquad (30)$$

and equation (29) can be written as

$$\eta = f(T, u_f, M_{fo}) \qquad (31)$$

The combustion calculation commences by assuming a value for combustion efficiency. Any two of the parameters, temperature, velocity or coal feed rate are supplied as input such that the third may be calculated by equation (31). From this the coal, gas and air flows are determined. The ultimate analysis of the coal enables the gas components as well as the specific air required and gas generated per kg of coal burnt to be calculated. A new value for the combustion efficiency is then determined from the combustion model and used in equation (31) to determine the corresponding coal, gas and air flow rates. The value for combustion efficiency is obtained by a method of successive approximations to an accuracy of 0,5% before the iterative procedure is terminated.

4.3 THE COMBUSTION MODEL

Once an estimate of the coal, gas and air flow rates has been made, the combustion efficiency can be determined. Gibbs (23) extended the entrainment model of Kunii and Levenspiel (4, Ch 11) to include the two phase theory of fluidization (12) enabling the evaluation of a combustion efficiency. This model, suggested by Gibbs (23) forms the basis of the combustion model. Other models have been suggested by Campbell and Davidson (13) and also by Becker et al (80). The work of Gibbs attempts to improve on that of the former mentioned (13), whilst the work of Becker et al (80) is an approach to develop a rigorous,

general, inclusive model resulting in a large number of assumptions, some contentions, and an unwieldy and large set of equations which have not as yet been shown to be readily soluble.

In accordance with the two-phase theory of fluidization, the model proposed by Gibbs (23) which has been adopted in this thesis, assumes that the bubble phase is devoid of particles and therefore combustion takes place in the particulate phase. The combustor performance therefore, depends on the rate of transfer of the oxidising reagent from the bubble to the particulate phase and the heterogeneous reaction rate. Avedesian and Davidson (10) have shown that for gas solids contacting these can be measured by two dimensionless groups, the transfer factor X or the number of times a bubble interchanges its volume as it moves through a bed of height H_f, and a dimensionless velocity constant k*. These relationships are represented in equations (32) and (33).

$$X = \frac{Q_B \cdot H_f}{u_{BS} \cdot V_B} \qquad (32a)$$

which can also be written

$$X = K_{bp} \cdot H_f / u_{BS} \qquad (32b)$$

$$\text{and} \quad k^* = k \cdot H_{mf} / u_f \qquad (33)$$

where k is defined as a first order particulate phase velocity constant by writing the rate of oxygen consumption per unit volume of particulate phase (10). From these relationships, it is evident that for high values of X, the transfer of the reagent to the particulate phase is high and the bed combustion reaction rate would be dependent on the heterogeneous reaction rate. Further, low values of X will result in much of the reagent by-passing the bed in the bubbles resulting in decreases in combustion efficiency as a

result of the poor interchange between the bubble and the particulate phases. While the particle shrinks due to the combined action of combustion and attrition, the combustible material is assumed to be removed from the bed in the overflow, by elutriation and splashing.

The combustion model only considers the effect on the combustible matter in the bed. The derivation of the performance equations are summarized below, the complete details may be obtained from References (4, Ch 11), (10) and (23).

4.3.1 Assumptions

The basis for the model is the work on the batch combustion of carbon in a fluidized bed by Avedesian and Davidson (10). By comparing the carbon burn-out time, and carbon dioxide and oxygen concentrations in the off gas with theoretical considerations, they deduced that the combustion process of particles in a fluidized bed is controlled by two diffusional resistances, the diffusion of oxygen from the bubble to the particulate phase and secondly the diffusion of the oxygen through the ash to the burning carbon particle. The combustion of the carbon particle is assumed to take place according to the two film theory of combustion, cf Section 1.1.2. Referring to Figures 3 and 4 which describe this theory, it is seen that carbon dioxide diffuses from the reaction zone towards the carbon particle where the following heterogeneous reaction takes place:

$$C + CO_2 \rightarrow 2CO$$

The resulting carbon monoxide diffuses back to the reaction zone where it reacts with oxygen to form carbon dioxide.

$$2.CO + O_2 \rightarrow 2 \cdot CO_2$$

One part of the carbon dioxide diffuses back towards the carbon particle while the other diffuses into the main stream. Avedesian and Davidson (10) indicate that Reynolds and Grasshof numbers are less than unity thus implying that forced and natural convection effects are small. Mass transfer is thus primarily due to molecular diffusion and by assuming that concentration profiles are quickly established, i.e. fast chemical reactions, the following equation representing concentrations about the particle as the particle shrinks results.

$$\frac{d}{dr}\left(r^2 \cdot \frac{dC}{dr}\right) = 0 \qquad (34)$$

Equation (34) is solved with the boundary conditions imposed by the reactions of the two film theory given above. By comparing the resulting transfer rate with that which would occur with no chemical reaction other than that which would occur at the particle surface, the molar flow of oxygen to the particle is written as

$$n = 2 \cdot \pi \cdot Sh \cdot G \cdot d \cdot C_p \qquad (35)$$

The main assumptions of the model can be stated as follows:

1. The two-phase theory of fluidization as proposed by Davidson and Harrison (12) in which a bubble and a particulate phase exist has been assumed.

2. The particulate phase is completely mixed with regard to both the gas and solids within the phase.

3. The bubbles are in plug flow and of uniform diameter throughout the bed.

4. Coal is fed uniformly to all points on the plane at the base of the bed.

5. Coal particles burn in the particulate phase of the bed. The flow of oxygen to the particles is

dependent on two diffusional resistances such that the molar flow of oxygen to the surface of the combustible particle is given by equation (35).

6. Coal particles shrink due to the combined action of combustion and attrition. The rate of shrinkage by combustion is governed by equation (35) whilst the tiny fragments worn off by attrition are carried away and are not considered as part of the solid population.

7. The volatile component is assumed to be combined with the char and to burn at the same rate as the char.

8. The mass of combustible particles within the bed is much less than the total inert bed mass.

4.3.2 Development of the General Performance Equation

As the gas bubbles pass through the bed, they exchange oxygen with the particulate phase in which the oxygen concentration remains constant and at the same level throughout the fluidized bed at a value 'C_p'. The oxygen concentration of the bubble changes from 'C_o', the value at inlet to the bed, to 'C_b' which is dependent on the height of the bubble within the bed. The overall gas interchange coefficient between the bubble and the particulate phase K_{bp} is defined by equation (36).

$$K_{bp} \cdot (C_p - C_b) = u_{BS} \cdot \frac{dC_b}{dh} \qquad (36)$$

This interchange coefficient can be found by the relationship derived by Davidson and Harrison (12, pg 114) and is given by equation (37).

$$K_{bp} = 4{,}5 \cdot \left(\frac{u_{mf}}{d_B}\right) + 5{,}85 \left(\frac{G^{0{,}5} \cdot g^{0{,}25}}{d_B^{1{,}25}}\right) \qquad (37)$$

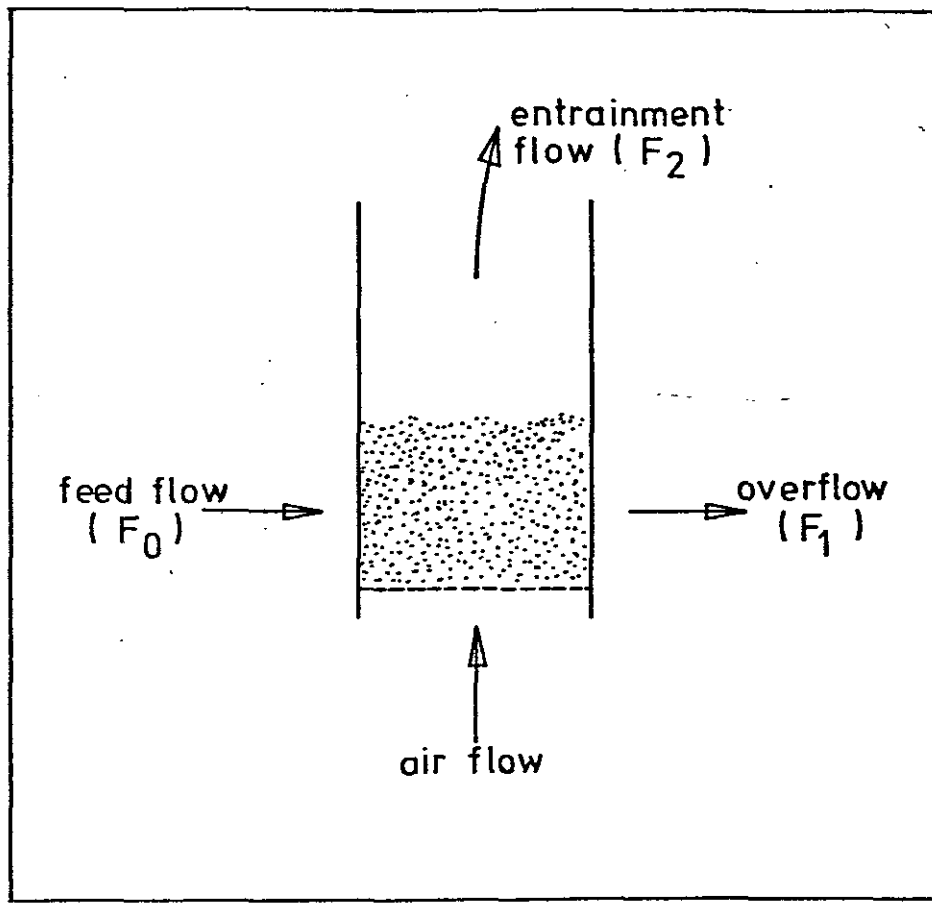

Figure 27 : Diagrammatic Representation of a Fluidized Bed to Illustrate the Components of the Mass Balance.

a) Rate Expressions for Shrinkage

Coal particles shrink as a result of the combustion process and due to attrition. The attrition of the coal particles is assumed to be a fraction of the combustion rate. The overall shrinkage rate can therefore be expressed as the sum of the combustion and attrition rate components.

$$\Gamma(d) = \Gamma_c(d) + \Gamma_a(d) \qquad (41)$$

The rate of shrinkage is assumed to obey a first order rate equation as given by

$$\Gamma(d) = -\frac{dd}{dt} \qquad (42)$$

This rate of shrinkage due to combustion can be assessed by equating the molar flow of oxygen to the particle to the molar consumption of oxygen. From the overall chemical reaction of carbon with oxygen, it is known that one mole of oxygen combines with one mole of carbon to form carbon dioxide. The molar flow of oxygen is obtained from equation (35) whilst the molar consumption of carbon is considered as the rate of shrinkage of the carbon particle.

$$\begin{pmatrix} molar\ flow \\ of\ oxygen \end{pmatrix} = \begin{pmatrix} molar\ consumption \\ of\ carbon \end{pmatrix}$$

$$2 \cdot \pi \cdot Sh \cdot G \cdot d \cdot C_p = -\frac{1}{12} \cdot \rho_c \cdot \frac{\pi \cdot d^2 \cdot dd}{2\ dt}$$

$$\frac{dd}{dt} = -\frac{48 \cdot Sh \cdot G \cdot C_p}{\rho_c \cdot d} \qquad (43)$$

or

$$\Gamma_c(d) = \frac{48 \cdot Sh \cdot G \cdot C_p}{\rho_c \cdot d} \qquad (44)$$

and

$$\Gamma_a(d) = a \cdot \Gamma_c(d) \qquad (45)$$

The rate of shrinkage is assumed to obey a first order rate equation as given by

$$r(d) = -\frac{dd}{dt} \qquad (42)$$

This rate of shrinkage due to combustion can be assessed by equating the molar flow of oxygen to the particle to the molar consumption of oxygen. From the overall chemical reaction of carbon with oxygen, it is known that one mole of oxygen combines with one mole of carbon to form carbon dioxide. The molar flow of oxygen is obtained from equation (35) whilst the molar consumption of carbon is considered as the rate of shrinkage of the carbon particle.

$$\begin{pmatrix} molar\ flow \\ of\ oxygen \end{pmatrix} = \begin{pmatrix} molar\ consumption \\ of\ carbon \end{pmatrix}$$

$$2 \cdot \pi \cdot Sh \cdot G \cdot d \cdot C_p = -\frac{1}{12} \cdot \rho_c \cdot \frac{\pi \cdot d^2 \cdot dd}{2\ dt}$$

$$\frac{dd}{dt} = -\frac{48 \cdot Sh \cdot G \cdot C_p}{\rho_c \cdot d} \qquad (43)$$

or

$$r_c(d) = \frac{48 \cdot Sh \cdot G \cdot C_p}{\rho_c \cdot d} \qquad (44)$$

and

$$r_a(d) = a \cdot r_c(d) \qquad (45)$$

b) Rate Expressions for Entrainment

The entrainment rate is defined as the sum of two components, that due to elutriation, and that due to splashing. The elutriation phenomenon is well understood, and refers to the selective removal of fines by entrainment from a mixture of particle sizes. This elutriation is therefore defined by the following:

$$\begin{pmatrix}\text{rate of removal of}\\ \text{solids of size } d\\ \text{per unit area of bed}\end{pmatrix} = K^{*} \cdot \begin{pmatrix}\text{fraction of bed}\\ \text{of}\\ \text{size } d\end{pmatrix}$$

$$-\frac{1}{A_t} \cdot \frac{d\,m(d)}{dt} = K^{*} \cdot \frac{m(d)}{M} \qquad (46)$$

or it can be defined for a particular system as:

$$\begin{pmatrix}\text{rate of removal of}\\ \text{solids of size } d\end{pmatrix} = K \cdot \begin{pmatrix}\text{weight of solids of}\\ \text{size } d \text{ in bed}\end{pmatrix}$$

$$-\frac{d\,m(d)}{dt} = K \cdot m(d) \qquad (47)$$

where

$$K^{*} = K \cdot M / A_t \qquad (48)$$

The elutriation constant K* can be obtained from a number of correlations by different authors, the one proposed by Wen and Hashinger (24) will however be used for this thesis. The elutriation constant K is then readily obtained from K* by equation (48).

The splashing rate has been introduced to account for those particles lost from the fluidized bed system which are too

large to be removed by the process of elutriation, cf Section 1.2.3. The bursting of bubbles at the bed surface results in these particles being imparted with a high momentum and being lost from the fluidized bed. The splashing rate coefficient has been arbitrarily defined by Gibbs (23) by equation (49).

$$\begin{pmatrix}\text{total combustibles}\\ \text{lost by splashing}\\ \text{in size interval}\\ d \text{ to } (d+\Delta d)\end{pmatrix} = S \cdot M_c \cdot p_c(d) \cdot \Delta d \qquad (49)$$

where the splashing rate constant 'S' is assumed to be a function of particle diameter. Splashing rate constants have been derived from the experimental work for use in the theoretical model. Therefore the total entrainment of solids from the bed in the size interval is given by the sum of the elutriated and splashed components as represented in equation (50).

$$\begin{pmatrix}\text{entrainment of}\\ \text{combustibles in}\\ \text{the size interval}\\ d \text{ to } (d+\Delta d)\end{pmatrix} = (K + S) \cdot M_c \cdot p_c(d) \cdot \Delta d \qquad (50)$$

c) Determination of the Mass of and the Particle Size Distribution of the Burning Particles in the Bed

With a knowledge of the rate equations for particle shrinkage and entrainment, a mass balance can be performed over a small size interval to determine the overall flow rates as well as determine the mass and size distribution of the burning particles in the fluidized bed such that equation (40) can be solved. Steady state conditions are assumed, with constant particle densities throughout the process. Back-mix flow in the bed enables the assumption of equivalent size analyses for both the bed material and the overflow stream to be made, i.e. $p_1(d) = p_c(d)$. Further the

particle shrinkage is given by the general rate expression of equation (42). Referring to Figure 27, Kunii and Levenspiel (4, Ch 11) consider a mass balance on the solids to determine the total particle shrinkage rate, or

$$\begin{pmatrix}\text{total solid shrinkage}\\ \text{in the bed}\end{pmatrix} = F_0 - (F_1 + F_2)$$

$$= \Sigma \begin{pmatrix}\text{shrinkage of solids in the}\\ \text{size interval } d \text{ to } (d+\Delta d)\end{pmatrix}$$

$$= \Sigma \; \rho_s \cdot \left(\frac{M_c \cdot p_c(d) \cdot \Delta d}{\rho_s \cdot \pi \cdot d^2 / 3}\right) \cdot \left(-\frac{\pi d^2 \cdot dd}{dt}\,\Delta t\right)$$

From which on taking the limit as Δd tends to dd, the total solids generation in unit time is found as:

$$\begin{pmatrix}\text{solid shrinkage}\\ \text{in the interval}\end{pmatrix} = \frac{3 \cdot M_c \cdot p_c(d) \cdot \Gamma(d)}{d}\,dd \qquad (51)$$

For which total shrinkage is found as

$$F_0 - (F_1 + F_2) = \int \frac{3 \cdot M_c \cdot p_c(d) \cdot \Gamma(d)}{d}\,dd \qquad (52)$$

Further, a mass balance for coal particles in the size interval d to $d + \Delta d$ is written as follows

$$\begin{pmatrix}\text{total coal}\\ \text{consumption}\\ \text{in the bed}\\ \text{in interval}\\ d \text{ to } (d+\Delta d)\end{pmatrix} = \begin{pmatrix}\text{coal}\\ \text{fed}\\ \text{to the}\\ \text{bed}\end{pmatrix} - \begin{pmatrix}\text{coal}\\ \text{leaving}\\ \text{in the}\\ \text{overflow}\end{pmatrix} + \begin{pmatrix}\text{coal}\\ \text{shrinking}\\ \text{into}\\ \text{interval}\\ \text{from larger}\\ \text{size}\end{pmatrix} - \begin{pmatrix}\text{coal}\\ \text{shrinking}\\ \text{out of}\\ \text{interval}\\ \text{to smaller}\\ \text{size}\end{pmatrix} + \begin{pmatrix}\text{coal}\\ \text{entrained}\\ \text{in off}\\ \text{gases}\end{pmatrix} \qquad (53)$$

By equating equations (53) and (51), and taking limits as Δd tends to zero, Kunii and Levenspiel (4, Ch 11) derive the general differential equation for fluidized beds

Therefore the mass of burning particles is determined from equation (58) whilst the size distribution of the burning particles can be found from equation (55). These parameters are then substituted into equation (40) which is then solved for the resulting particulate oxygen concentration.

4.3.3 Discussion of the Combustion Model

The use of simple shrinkage rate equations has enabled these to be integrated to yield expressions which are easily solved numerically. Development of the equations has been limited to the case where particles shrink steadily and therefore cannot be used where particles break apart or agglomerate into large lumps.

The combustibles loss, and hence the combustion efficiency is determined from the entrained carbon flow. Higher superficial gas velocities result in higher elutriation and hence higher entrainment rates. An important factor affecting the entrainment rate, however, is the mass of coal or carbon particles contained in the bed. High oxygen transfer rates, and the associated high combustion rates will result in the residence time of the carbon within the bed being small and therefore a smaller mass of carbon will be retained in the fluidized bed. Therefore fast reaction rates will result in high efficiencies. Gibbs (23) has shown that when operating near to stoichiometric conditions, the combustibles loss remains small for bubble diameters up to 100 mm, on increasing the diameter above this value, the combustibles loss increases rapidly. This is due mainly to the decrease in the transfer factor X, cf equation (32), i.e. the number of times the bubble interchanges its volume as it moves through bed, as the bubble diameter increases. This transfer factor determines the diffusional resistance of the oxygen transfer from the bubble phase to the particulate phase.

In the case of high excess air, as was prevelant during all of the tests performed on the fluidized-bed combustor, the oxygen concentration throughout the bubble and particulate phases would be high since only a small amount of oxygen would be consumed. The combustion would therefore be controlled by local diffusion near the particle, with the transfer from the bubbles having only a small effect.

4.4 THE ENTRAINMENT MODEL

Entrainment has been considered to be made up of a splashing and an elutriation component, cf Section 1.2.3. The entrainment is considered independently of the combustion process. In this model, inert ash and bed material are assumed to be fed to the bed separately from the carbon flow. The coal flow is assumed to be made up of two components, a pure coal flow which is used in the combustion model, and a pure ash flow which is used in the entrainment model.

The entrainment model is based on the work of Merrick and Highley (22). Although they (22) developed a new expression for entrainment to account for the loss of particles which are larger than those which would be removed by the elutriation mechanism, this approach has not been used in this thesis. Entrainment has been divided into splashing and elutriation as was done in the combustion model. Ash and inert bed material are fed into the bed in which the individual particles are reduced in size until they are eventually entrained in the off gases. Both the fine particles abraded away from the core particles and these reduced core particles are considered in the mass balance.

Attrition in a fluidized bed is therefore the result of the abrasion of the coarse particles to form fine particles with a corresponding reduction in the size of the coarse

particles. Merrick and Highley (22) have found that the size distribution of the fines produced is almost constant for a particular bed material, and independent of the bed size distribution or operating conditions. A typical size distribution of the fines produced by attrition is given in Figure 28 from the data supplied by Merrick and Highley (22). They correlate the production of fines by the following equation

$$F_a = A \cdot (u_f - u_{mf}) \cdot M_b \qquad (59)$$

However the use of equation (59) for individual size fractions resulted in the predicted bed size distributions being considerably coarser than found experimentally (22). A correction factor was applied to account for the fact that though the coarser particles are continually in contact with each other, the fines spend some time in the voids created by the larger particles. Therefore a new rate equation was developed including a second abrasion rate constant A* and the proportion of particles in the bed smaller than the size d. The following equation for the production of fines by abrasion of particles of size d results:

$$\frac{d M_d}{dt} = - F_{ad} = - A^* \cdot f_d \cdot (u_f - u_{mf}) \cdot M_d \qquad (60)$$

such that the sum of all the abrasion rates is the same as that given by equation (59).

In the development of the mathematical model, the size distributions of the various components are divided up into a number of size fractions, where i refers to the i th size fraction and where i=1 represents that fraction having the largest mean diameter. A mass balance is then performed on the system for the i th size interval, which results in equation (61). Figure 29 diagramatically

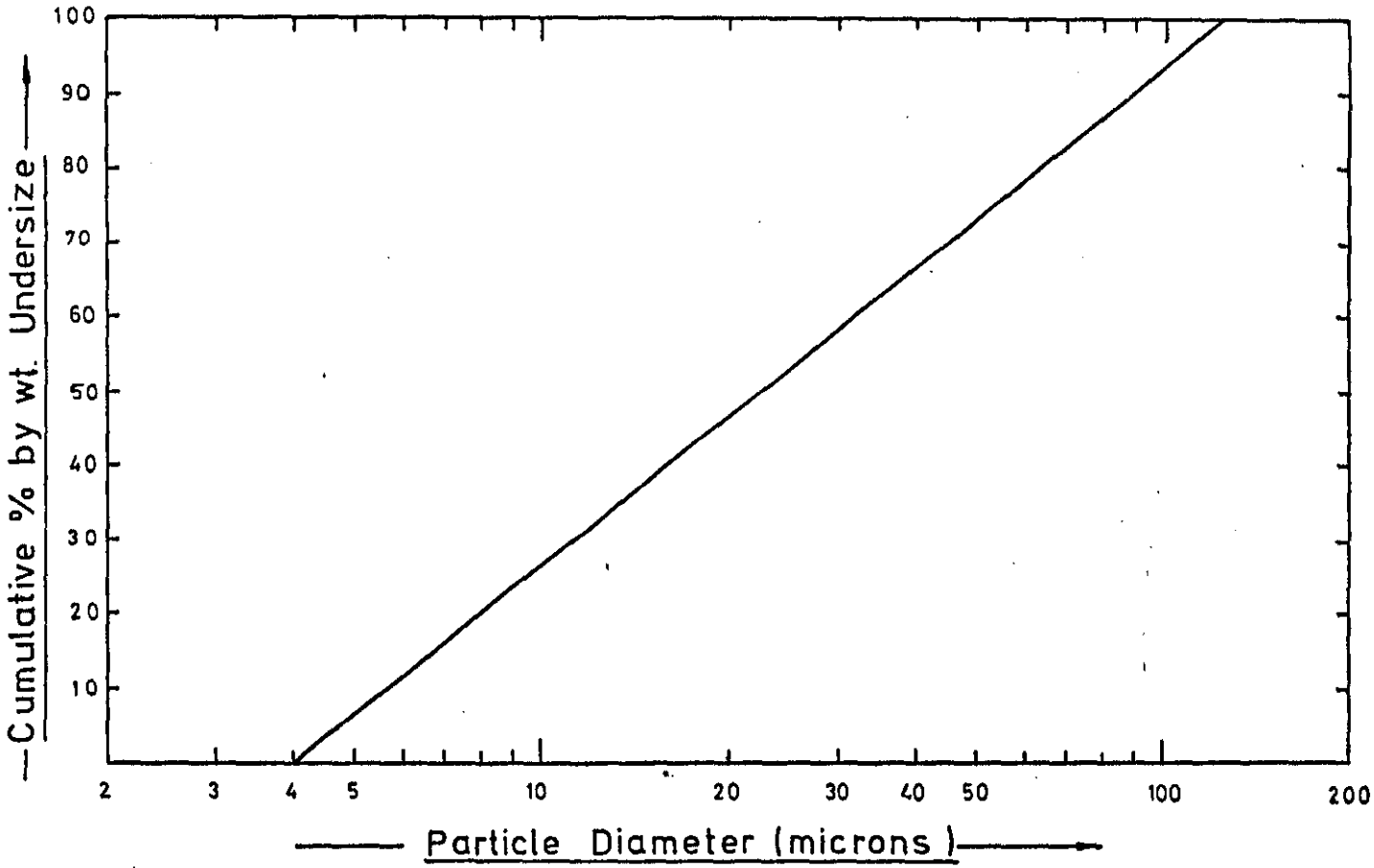

Figure 28 : Typical Size Distribution of Fines Produced by Attrition from the Results of Merrick and Highley (22)

represents the various components of the mass balance.

$$\begin{pmatrix}\text{inert feed rate } F_i\end{pmatrix} + \begin{pmatrix}\text{gain of particles from next largest size due to size reduction } w_{i-1}\end{pmatrix} + \begin{pmatrix}\text{gain of fines by abrasion}\end{pmatrix} = \begin{pmatrix}\text{overflow rate}\end{pmatrix} + \begin{pmatrix}\text{loss of weight due to fines production}\end{pmatrix} + \begin{pmatrix}\text{entrainment rate}\end{pmatrix} + \begin{pmatrix}\text{loss of particles to next smallest size by size reduction } w_i\end{pmatrix} \quad (61)$$

The only parameter which requires special calculation, is the rate of loss of particles to the next smallest size W_i. A mean removal rate constant, Z_m, is defined (22) by equations (62) and (63).

$$\frac{d\,M}{dt} = -\,Z_m \cdot M \quad (62)$$

where

$$Z_i = A_i^* + K_i + S_i + O / M_b \quad (63)$$

from which Merrick and Highley (22) deduce an expression for the rate of loss of particles to the next smallest size.

The final flow rates and size gradings are solved by an iterative procedure. The iteration is commenced by estimating the overflow rate and the bed size grading. A mass balance on each size grading is performed resulting in the mass of each size fraction being deduced. Summing each of these individual fractions results in a total bed weight being obtained which is then compared with the desired bed weight. The overflow rate is then adjusted until the bed weight is obtained to the desired accuracy.

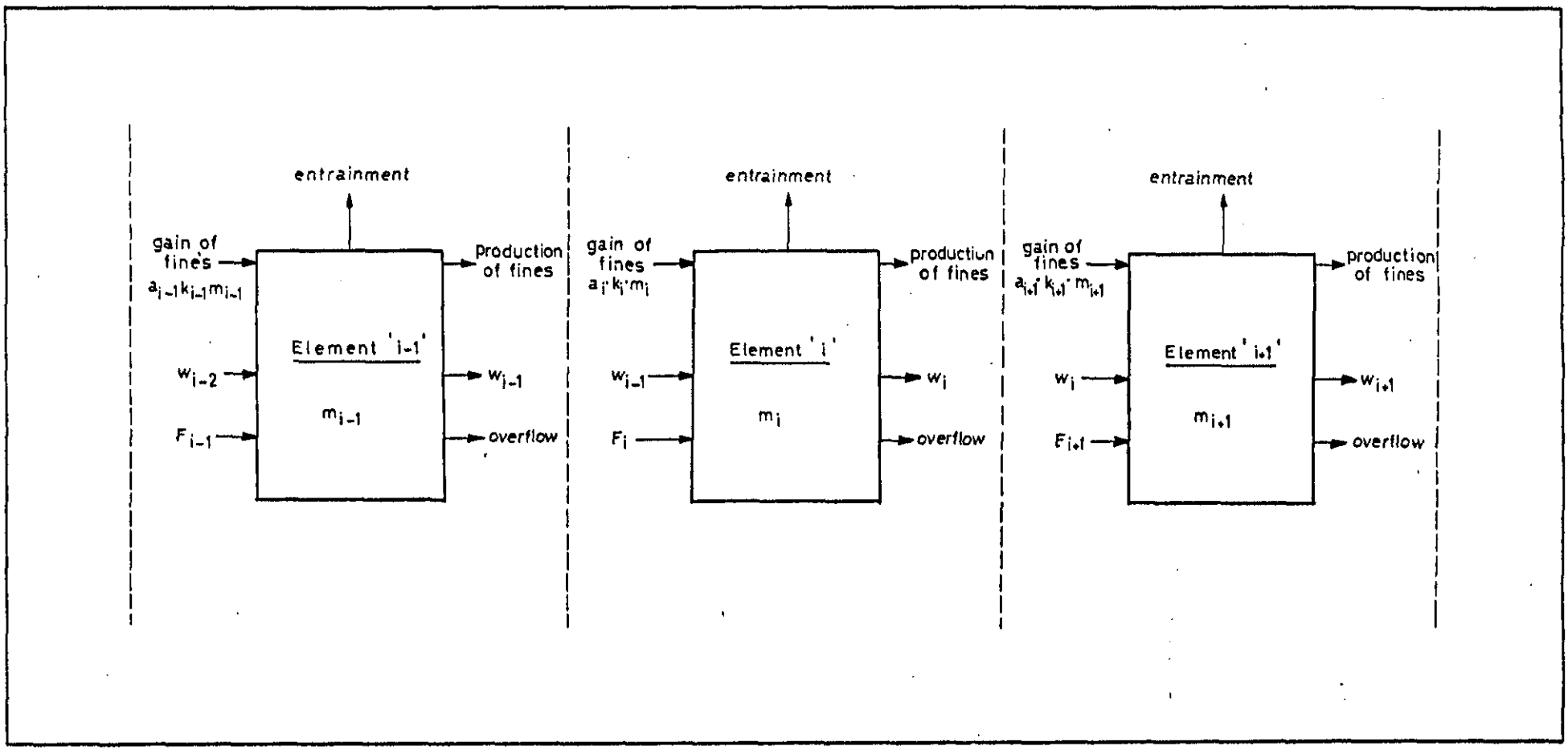

Figure 29 : Diagram to Illustrate the Mass Balance Performed on the i'th Size Fraction of the Fluidized Bed System

4.5 DESIGN OF THE COMPUTER PROGRAMME

A suite of fifteen subroutines and a main "calling" programme have been developed for use on the UNIVAC computer for solving the theoretical model. Details of the numerical methods employed, viz for interpolation, integration and iteration are contained in Appendix I.

Input to the programme consists mainly of the coal and inert feed size gradings on a cumulative percent by weight undersize basis. The particle sizes have a range, typically from about 50 microns to 10,0 mm. In the combustion model, these input size gradings are supplied at arbitrary intervals between each size. For the entrainment model, however, the particle sizes increase as a geometric progression given by equation (64), where each of the values, namely the minimum diameter, the number of points and the exponent for the progression are supplied as input:

$$d_i = d_{min} \cdot (\ 2\ )^{e \cdot (i-1)} \qquad (64)$$

Intermediate points are obtained by means of Aitken's method of interpolation, cf Appendix I. The integrations required for the solution of equation (40) have been performed by means of Gregory's formula for numerical integration. It has been found that the use of a 75 micron step in the integration formula results in satisfactory results, though the computational time is extremely high, about 30 minutes due to the relatively inefficient integration technique. Use of a central difference formula for the integration would improve the computation substantially.

The efficiency is derived from the evaluation of particulate oxygen concentration deduced from equation (40). The solution of equation (40) was performed by means of the method of successive approximations (82, Ch 5). This method requires an initial estimate of the oxygen

concentration from which a revised value is determined.

Therefore equation (40) has to be rewritten in the form given below:

$$C_{p_n} = f(C_{p_{n-1}}) \qquad (65)$$

where n refers to the n th iterate. However, C_{p_n} will only converge to a solution if the derivative of $f(C_{p_{n-1}})$ is less than unity in absolute value or symbolically if

$$\left| \frac{d\, f(C_{p_{n-1}})}{dC_p} \right| < 1 \qquad (66)$$

It should be evident that a number of different expressions can be found for equation (65). A few of these expressions were tested, and the one given by equation (67) is found to converge to a solution to equation (40), i.e. the condition represented by equation (66) is met.

$$C_{p_n} = C_0 \,/\, (1 + D/A) \qquad (67)$$

where

$$D = \frac{M_c\, p_c(d)}{d^2}\, dd$$

and

$$A = \frac{A_t \cdot \rho_s}{12 \cdot Sh \cdot G} \cdot \left[(1-f) \cdot u_{mf} + f \cdot u_{BS} \cdot (1-e^{-X})\right]$$

where D can be shown to be a function of $C_{p_{n-1}}$ from equations (41), (44) and (55).

Equation (67) converges to a value of C_p such that the efficiency is evaluated to within $\frac{1}{2}\%$ within four to five iterations.

Once the combustion efficiency has been evaluated, the coal feed rate and hence the inert ash flow rate is established. In order to establish the resulting bed size analysis and the entrainment rates, the coal feed is assumed to be divided into two streams each of identical size analyses. The first comprises only combustible matter and is used exclusively in the combustion calculation, whilst the second is made up of the inert material in the coal and is only used in the entrainment model. Replenishment of the bed material is accommodated by considering the introduction of bed material as a separate flow entering the bed. The entrainment model therefore uses an inert ash flow rate with a size grading equivalent to the original coal, and an inert bed material flow rate. The attrition rate of the inert bed material is assumed to be two orders of magnitude less than the attrition of the resulting ash. This results in very little degradation of the inert bed taking place, whilst almost all of the ash is removed as a result of the entrainment process.

4.6 DISCUSSION AND CORRELATION OF THE MODEL WITH EXPERIMENTAL RESULTS

4.6.1 The Combustion Model

A major limitation of the combustion model lies in the requirement that the size distribution function of the input coal stream, $p_o(d)$, be a smooth curve. Although the curve of the cumulative percent by weight undersize versus the particle diameter almost invariably yields a smooth curve, the resulting size distribution $p_o(d)$ may be irregular. Indeed, the cumulative size distributions of the coals used in the experimental work result in very irregular size distribution functions, $p_o(d)$, as is evident from Figure C.3 of Appendix C. The smoothed size distribution function and resulting cumulative distribution are

illustrated in Figures C.3 and C.4 of the same Appendix. This smoothed function was used as input to the computer model, resulting in combustion efficiencies somewhat higher than anticipated from the experimental work. However by artificially adjusting the attrition rate of the coal, expressed as a fraction of the combustion rate resulted in values for combustion efficiency approaching those achieved during the experimental work. By changing the gas velocities, changes in the combustion efficiency of the same order as those found by the regression relationship of equation (25) were found. Variations in the operating temperature have only a minor effect on the resulting combustion efficiency. Adjustment of bubble velocity and diameter effected the required change in the combustion efficiency. These adjustments in fact alter the transfer factor 'X', given by equation (32).

It is clear therefore that adequate answers are provided by the combustion model. More work is required to establish the precise nature of the attrition and possibly the combustion rate. An improved model for the prediction of bubble diameters and velocities is also required so that the transfer factor 'X' can be derived from first principles rather than having this parameter artificially suppressed or exaggerated, dependent on the bed operating temperature.

4.6.2 The Entrainment Model

The resulting size grading of the entrained material flow predicted by the entrainment model are somewhat coarser than those obtained from the experimental work. However, adjustment of the attrition rates of the ash and bed material alter the entrained size gradings. A further complication is the fact that the size grading of the resulting ash on combustion of the coal particle has been assumed to be similar to that of the original coal feed.

This is probably an over simplification, as the ash of most South African coals is generally inherent or homogeneously dispersed in the coal body. Further the coal feed did not appear to contain complete inert lumps of ash the size of the coal particle. Therefore the ash feed size distribution would on average be smaller than that of the coal feed. It is therefore evident, that much additional information is necessary to be able to fully utilize the entrainment model.

CHAPTER 5

CONCLUSIONS AND RECOMMENDATIONS FOR FURTHER WORK

Coal having a high fines content is in abundant supply as a result of the limited demand for this fuel. Such a coal has been successfully burned in a fluidized-bed combustion test rig. In order to enhance the commercial application of the fluidized-bed combustion process, the coal has been burnt in relatively shallow beds with a correspondingly low pressure drop across the distributor. A shallow bed, though reducing the combustion efficiency, results in a reduction of the fluidizing air fan power consumption which is normally considerably higher than the auxiliary power consumption of conventional solid fuel combustion equipment. As no cooling surface has been supplied to the combustion test rig, the bed temperature is maintained within acceptable limits by increasing the air flow rate in excess of that required for the combustion of the coal. This results in about three times the air which would be required for stoichiometric combustion being present in the fluidized-bed. As a consequence, complete combustion of both the volatile and fixed carbon components is accomplished in the bed section. The following conclusions have been drawn:

5.1 CONCLUSIONS

Combustion Efficiency

a) Combustion efficiencies are lower than has been reported in the literature. This is attributed to the large proportion of fines contained in the coal feed which are entrained in the gas stream without having had sufficient time to burn in the high temperature fluidized bed section.

b) The resulting combustion efficiencies have been correlated with the bed temperature, superficial gas velocity and static bed height by the following relationship having a correlation coefficient of 0,9422 :

$$\eta_c(\%) = 36,27 + 0,0675 \cdot T - 17,1 \cdot u_f + 65,0 \cdot H \qquad (25)$$

The above equation has been derived over the following ranges of the independent variables:

Bed Temperature	:	700 to 1000°C
Gas Velocity	:	0,9 to 1,5 m/s
Bed Height	:	150 to 230 mm

c) Some parameter describing the quality of fluidization would enable a more general application of equation (25) which is limited to fluidized beds with similar distributors and fluidizing conditions.

d) The combustion efficiency determined from the regression relationship of b) above, is almost independent of the freeboard height because of the small quantity of combustible matter contained in the splashed material.

Entrainment

e) The use of a separate bed material with a narrow size distribution and an attrition rate considerably less than that of the combustible material enabled the entrained material to be divided into splashing rate and elutriation rate components.

f) Only a qualitative assessment of the splashing rate has been possible. A considerable number of further tests under several different operating conditions

would be necessary to obtain a quantitative assessment of the splashing rate.

g) Increases in splashing rates with increasing bed depths may partially be attributed to the change in the bed flow regime from that of a bubbling bed to that of a slugging bed flow regime.

Theoretical Model

h) At best the theoretical model can be described as semi-quantitative. Trends are correctly predicted, however theory can only be correlated with experiment by artificially adjusting the bubble diameters, or the attrition rates.

i) The two-phase theory of fluidization may not adequately describe the fluidized-bed combustion process when the superficial gas velocity is about five times the minimum fluidizing velocity.

General

j) The coal burnt has an ash content of about 15%, and is easily reduced in size in the bed such that the loss of bed material by splashing is greater than the rate of ash build-up in the bed. Therefore the bed height decreased steadily throughout the tests.

5.2 RECOMMENDATIONS FOR FURTHER WORK

a) Cooling surfaces should be introduced into the bed to enable the combustion process to be conducted at conditions closer to the stoichiometric combustion condition. This will enable a study of the combustion of the volatile component within or

immediately above the bed, as well as establishing whether carbon monoxide is formed within the bed as a result of oxygen deficient regions, to be burnt to carbon dioxide above the bed.

b) Different distributors should be employed, whilst at the same time the range of pressure drops across the distributor be increased, to attempt to establish a parameter for describing the quality of fluidization.

c) It is recommended that more intensive testing be undertaken to quantify the splashing rate phenomenon. At the same time an improved method of determining the bubble diameters should be investigated for possible use in explaining the splashing rate.

d) Tests on different types of South African coals and solid fuels should be undertaken. In particular the high ash coals or those fuels for which there is no immediate market, should be tested for possible use as a feedstock for industrial or utility type steam raising plant. This would enable the better utilization of high grade coals for the metallurgical or chemical industries.

e) It is finally recommended that extensive tests be conducted using different solid fuels to establish such basic parameters as ignition temperatures, susceptibility to fusing in the bed, attrition rates and corrosion or erosion of immersed surfaces in the bed at different operating conditions for each of the fuels.

REFERENCES

1. EHRLICH, S. "History of the Development of the Fluidized-Bed Boiler", *Fourth International Conference on Fluidized-Bed Combustion*, McLean (Virginia), USA, 9-11 December 1975.

2. DAVIDSON, J.F. AND HARRISON, D. "Fluidization", Academic Press, London and New York, 1971.

3. HARRISON, D., DAVIDSON, J.F. AND DE KOCK, J.W. "On the Nature of Aggregative and Particulate Fluidization", Transactions of the Institution of Chemical Engineers, Vol.39, 1961, Pp 202-211.

4. KUNII, D. AND LEVENSPIEL, O. "Fluidization Engineering", John Wiley and Sons Inc. 1969.

5. ZENZ, F.A. AND OTHMER, D.F. "Fluidization and Fluid Particle Systems", Rheinhold Publishing Corporation, New York, 1960.

6. FIELD, M.A., GILL, D.W., MORGAN, B.B. AND HAWKESLY, P.G.W. "Combustion of Pulverised Coal", British Coal Utilization Research Association, Leatherhead (Surrey), Great Britain, 1967.

7. PITT, G.J. "The Kinetics of the Evolution of Volatile Products from Coal", Fuel, Vol.41, 1962, Pp 267-274.

8. SKINNER, D.G. "The Fluidized Combustion of Coal", National Coal Board Research and Development Department, 1970.

9. BISHOP, J.W., ROBINSON, E.B., EHRLICH, S., JAIN, A.K., CHEN, P.M. "Status of the Direct Contact Heat Transferring Boiler", Fuels Division of the ASME; ASME Winter Annual General Meeting and Energy Systems Exposition, New York, 1-5 December 1968.

10. AVEDESIAN, M.M. AND DAVIDSON, J.F. "Combustion of Carbon Particles in a Fluidized Bed". Transactions Institute Chemical Engineers, Vol.51, 1973, Pg 121-131.

11. BASU, P., BROUGHTON, J. AND ELLIOT, D.E. "Combustion of Single Coal Particles in Fluidized Beds". Fluidized Combustion, Vol.1 Institute of Fuel Symposium Series No. 1, London, September 1975.

12. DAVIDSON, J.F. AND HARRISON, D. "Fluidized Particles", Cambridge University Press, 1963.

13. CAMPBELL, E.K. AND DAVIDSON, J.F. "The Combustion of Coal in Fluidized Beds", Fluidized Combustion, Vol.1 Institute of Fuel Symposium Series No. 1, London, September 1975.

14. PYLE, D.L. "Fluidized Combustion Models : Rapporteur's Report", Fluidized Combustion Vol.2, Institute of Fuel Symposium Series No. 1, London, September 1975.

15. BOTTERILL, J.S.M. "Fluid-Bed Heat Transfer", Academic Press, London 1975.

16. REH, L. "Verbrennung in der Wirbelschicht", Chemie Ingenieur Technik, Vol.40, No. 11, 1968.

17. WEN, C.Y. AND YU, Y.H. "Mechanics of Fluidization", AIChE Symposium Series No. 62, Vol. 62, 1966.

18. LEWIS, W.K., GILLILAND, E.R. AND BAUER, W.C. "Characteristics of Fluidized Particles", Industrial and Engineering Chemistry, Vol. 41, No. 6, June 1949, Pp 1104-1117.

19. BARNEA, E. AND MEDNICK, R.L. "Correlation for Minimum Fluidization Velocity", Transactions Institution of Chemical Engineers, Vol. 53, No. 4, October 1975, Pp 278-281.

20. LEVA, M. "Fluidization", McGraw Hill Book Company Inc, 1959.

21. BROUGHTON, J. "The Influence of Bed Temperature and Particle Size Distribution on Incipient Fluidization" Transactions Institute of Chemical Engineers, Vol. 52, 1974, Pp 105-107.

22. MERRICK, D. AND HIGHLEY, J. "Particle Size Reduction and Elutriation in a Fluidized-Bed Process", AIChE Symposium Series No. 137, Vol. 70, 1974.

23. GIBBS, B.M. "A Mechanistic Model for Predicting the Performance of a Fluidized-Bed Coal Combustor", Fluidized Combustion Conference Vol. 1, Institute of Fuel Symposium Series No. 1, London, September 1975.

24. WEN, C. AND HASHINGER, R.F. "Elutriation of Solid Particles from a Dense-Phase Fluidized Bed", AIChE Journal, Vol. 6, No. 2, June, 1960 Pp 220-226.

25. McLAREN, J. AND WILLIAMS, D.F. "Combustion Efficiency, Sulphur Retention and Heat Transfer in Pilot Plant Fluidized Bed Combustors", Journal of the Institute of Fuel, August 1969, Pp 303-308.

26. BISHOP, J.W. "Process and Apparatus for Reduction of Unburned Combustible in Fly Ash", US Patent No. 3 508 506, 28 April 1970.

27. WRIGHT, S.J. "Fluidized Combustion : Results Obtained from a Water-Cooled Combustion Pot", BCURA (Private and Confidential) Document No. R16/32, 18 March 1965.

28. EHRLICH, S. "A Coal Fired Fluidized-Bed Boiler", Fluidized Combustion Conference, Vol. 1, Institute of Fuel, Symposium Series No. 1, London, September 1975.

29. VOGEL, G.J., SWIFT, W.M., MONTAGNA, J.C., LENC, J.F. AND JONKE, A.A. "Recent ANL Bench Scale, Pressurised Fluidized-Bed Studies", Fourth International Conference on Fluidized-Bed Combustion, McLean (Virginia), USA, 9-11 December 1975.

30. WATERS, P.L. "Factors Influencing the Fluidized Combustion of Low Grade Solid and Liquid Fuels", Fluidized Combustion Conference, Vol. 1, Institute of Fuel, Symposium Series No. 1, London, September 1975.

31. WRIGHT, S.J. "Experiments on the BCURA Pilot-Scale Fluidized-Bed Combustor", Combustion of Coal in Fluidized Beds, Symposium held at the Coal Research Establishment, NCB, May 1968.

32. VREEDENBERG, H.A. "Heat Transfer between a Fluidized-Bed and a Horizontal Tube", Chemical Engineering Science, Vol. 9, No. 1, 1958.

33. SIEGEL, R. "Effect of Distributor-Plate-to-Bed Resistance Ratio on onset of Fluidized-Bed Channeling", AIChE Journal, Vol. 22, No. 3, May 1976, Pp 590-592.

34. WRIGHT, S.J. "The Design of Fluidized Combustion Systems Burning Solid Fuel", Institution of Chemical Engineers, London, Symposium Series No. 27, 1968.

35. RAMA PRASAD, V.R. "Combustion of High Ash, Indian Coals", Fluidized Combustion Conference, Vol. 1, Institute of Fuel, Symposium Series No. 1, London, September 1975.

36. THURLOW, G.G. "Fluidized-Bed Combustion : The Present Position", Discussion to the paper presented to The Combustion Engineering Association, Slough, Buckinghamshire, Document No. 9463, 3 October 1974.

37. THURLOW, G.G. "Coal as a Fuel for Boiler Furnaces", Journal of the Institute of Fuel, August/September 1972, Pp 453-459.

38. COOKE, M.J. AND ROGERS, E.A. "Investigations of Fireside Corrosion in Fluidized Combustion Systems", Fluidized Combustion Conference, Vol. 1, Institute of Fuel, Symposium Series No. 1, London, September 1975.

39. HIGHLEY, J., KAYE, W.G., CHIBA, T., NIENOW, A.W. AND ROWE, P.N. "The Application of Fluidized Combustion to Industrial Boilers and Furnaces", Fluidized Combustion Conference, Vol. 1, Institute of Fuel, Symposium Series No. 1, London, September 1975.

40. PILLAI, K.K. "Premixed Gas Combustion in Shallow Fluidized Beds", Journal of the Institute of Fuel, December 1976, Pp 200-205.

41. PILLAI, K.K. "The Feasibility of Heavy Oil Combustion in Shallow Fluid Beds", Journal of the Institute of Fuel, December 1976, Pp 206-210.

42. TEAGUE, D.S. AND WRIGHT, S.J. "Fluidized Combustion: a Preliminary Appraisal of Fluidization Data and the Possibilities of Further Development", BCURA, Document No. R16/7, August 1963.

43. LOCKE, H.B., LUNN, H.G., HOY, H.R. AND ROBERTS, A.G. "Fluidized Combustion in Great Britain - Environmentally Clean Steam and Power Generation from Coal, Heavy Oil and Dirty Fuels", Fourth International Conference on Fluidized-Bed Combustion, McLean (Virginia), USA, 9-11 December 1975.

44. SQUIRES, A.M. "Clean Fuels from Coal Gasification", Science, Vol. 184, April 1974.

45. GODEL, A.A. "The Ignifluid, a new System of Combustion", The Combustion Engineering Association, London, Document No. 7624, 28 May 1963.

46. DEMMY, R.H. "Ignifluid Boilers for Utilities", Chemical Engineering Progress, Vol. 68, No. 2, February 1972.

47. GODELL, A.A. AND COSAR, P. "The Scale-up of a Fluidized-Bed Combustion System to Utility Boilers", AIChE Symposium Series No. 116, Vol. 67, 1971, Pp 210-218.

48. HEALEY, E.M. AND STOCKWELL, D.H. "Fluidized-Bed Combustion - Test Rig Provides Important Data", Process Engineering, June 1969, Pp 76-77.

49. GIBSON, J. "Fluidized-Bed Combustion", Coal and Energy Quarterly, No. 7, Winter 1975, Pp 9-17.

50. GIBSON, J. "Fluidized Combustion", ICCR Conference, London, October 1974.

51. THURLOW, G.G. "Fluidized Combustion : The Present Position", The Heating and Air Conditioning Journal, March and April 1975.

52. HIGHLEY, J. "Report on Progress at the NCB Coal Research Establishment", Fourth International Conference on Fluidized-Bed Combustion, McLean (Virginia), USA, 9-11 December 1975.

53. COOKE, M.J. AND HODGKINSON, N. "The Fluidized Combustion of Low Grade Materials", Fluidized Combustion Conference, Vol. 1, Institute of Fuel, Symposium Series No. 1, London, September 1975.

54. NAUDÉ, D.P. Private Communication with NCB, October 1976.

55. HOY, H.R. "FBC Power Generation from Coal and Heavy Oils : Clean Uses for Dirty Fuels", Fourth International Conference on Fluidized-Bed Combustion, McLean (Virginia), USA, 9-11 December 1975.

56. LAIRD, R. "Coal Board is Climbing into the Wrong Fluid Bed", The Engineer, 17 March 1977, Pp 30-31.

57. ANON. "Fluid-Bed Shell Boiler", The Heating and Air Conditioning Journal, November 1975, Pp 7.

58. KAYE, W.G. "New Developments in Coal Burning Equipment", Solid Fuel, No. 256, 28th January 1976.

59. McKENZIE, E.C. "Fluidized-Bed Firing Boilers", The Heating and Air Conditioning Journal, Vol. 47, No. 542, March 1977.

60. IAMMARTINO, N.R. "Fluidized-Bed Combustion : A Better Way to Burn Coal", Chemical Engineering, Vol. 83, No. 12, 7 June 1976.

61. GAMBLE, R.L. AND WARSHANY, F.R. "Commercial Development of Atmospheric Fluidized-Bed Utility Steam Generators", Joint Power Generation Conference, sponsored by ASME Power and Fuels Division and IEEE Power Engineering Society, Portland, Oregon, USA, 28 September - 2 October 1975.

62. ANON. "TVA to Test Fluidized-Bed Coal Burning", Electrical World, 1 March 1977, Pp 28.

63a. JONKE, A.A., SWIFT, M.M. AND VOGEL, G.J. "Fluidized-Bed Combustion : Development Status", Society of Mining Engineers, AIME Transactions, Vol. 258, June 1975, Pp 159-167.

63b. REH, L. "Einsatzmöglichkeiten der Wirbelschicht-feuerung als Kraftwerkfeuerung", VGB Kraftwerks-technik, Vol. 56 No. 8, August 1976, Pp 509-518.

64. BOWLING, K.McG. AND WATERS, P.L. "Fuel Processing in Fluidized Beds", British Chemical Engineering, Vol. 13, No. 8, August 1968.

65. ANON. "Coal Burning Fluidized-Bed Combustion System", Coal Research in the CSIRO, No. 34, April 1968.

66. WATERS, P.L. "Factors Influencing the Fluidized Combustion of Low Grade Solid and Liquid Fuels", Fluidized Combustion Conference, Vol. 1, Institute of Fuel, Symposium Series No. 1, London, September 1975.

67. GILMOUR, I.A. "Fluidized-Bed Combustion of Coal", New Zealand Engineering, 15 June 1975.

68. DU TOIT, P. "A Progress Report on Preliminary Investigations into the Fluidized-Bed Combustion of Large Coal", Fuel Research Institute of South Africa, Report No. 33 of 1976, 6 May 1976.

69. HOLSTEYN, H.W. "Fluidized Combustion", The Clean Air Journal, Vol. 3, No. 1, November 1976.

70. PERRY, R.H. AND CHILTON, C.H. (Editors), Chemical Engineers' Handbook, Fifth Edition, McGraw-Hill Kogakusha, 1973.

71. NATIONAL COAL BOARD, Coal Research Establishment, Stoke Orchard, Gloucestershire, Annual Report, April 1975 to March 1976.

72. RIGBY, G.R., CALCOTT, T.G., SINGH, B. AND EVANS B.R. "New Distributor for Gas Fluidized Beds", Transactions of the Institution of Chemical Engineers, Vol. 55, 1977, Pp 68-70.

73. BLINICHEV, V.N., STREL'STOV, V.V. AND LEBEDEVA, E.S. "An Investigation of the Size Reduction of Granular Materials during their Processing in Fluidized Beds", International Chemical Engineering, Vol. 8, No. 4, October 1968.

74. AGARWAL, J.C., DAVIS, W.L. AND KING, D.T. "Fluidized-Bed Coal Drier", Chemical Engineering Progress, Vol. 58, No. 11, November 1962.

75. NORMAN, P. "Combustion of Colliery Shale in a Fluidized Bed", Energy World, July 1975.

76. WRIGHT, S.J. "Fluidized Combustion : Results obtained from a Water-Cooled Combustion Pot", BCURA (Private and Confidential) Document Number R16/32, 18 March 1965.

77. RICHARDSON, D.R. "How to Design Fluid Flow Distributors", Chemical Engineering, 1 May 1961.

78. NONHEBEL, G. (Editor), "Gas Purification Processes for Air Pollution Control", Newnes-Butterworths, Second Edition, London 1972.

79. HESKETH, H.E. "Understanding and Controlling Pollution", Ann Arbor Science Publishers, Ann Arbor, Michigan, USA, 1972.

80. BECKER, H.A., BEER, J.M. AND GIBBS, B.M. "A Model for Fluidized-Bed Combustion of Coal", Fluidized-Bed Combustion, Vol. 1, Institute of Fuel Symposium Series No. 1, London, September 1975.

81. LEVENSPIEL, O., KUNII, D. AND FITZGERALD, T. "The Processing of Solids of Changing Size in Bubbling Fluidized Beds", Powder Technology, Vol. 2, 1968/69, Pp 87-96.

82. McCRACKEN, D.D. AND DORN, W.S. "Numerical Methods and Fortran Programming", John Wiley and Sons Inc., New York, 1965.

83. DUBBELS, "Taschenbuch für den Maschinenbau", 11th Edition, 1958.

84. VDI - WÄRMEATLAS, VDI - Verlag Gmb H, 1963.

85. BRANDT, F. "Eine Allgemeine Darstellung der Stoffwerte von Rauchgasen für beliebige Brennstoffen", Brennstoff-Wärme-Kraft, Vol. 16, No. 2, February 1964.

86. SCHUMACHER, A. AND WALDMANN, H. "Wärme und Strömungstechnik im Dampferzeugerbau", Vulkan-Verlag, 1973.

87. ANDERSON, V.L. AND McLEAN, R.A. "Design of Experiments : A Realistic Approach", Marcel Dekker Inc., New York, 1974.

88. BROWNLEE, K.A. "Statistical Theory and Methodology in Science and Engineering", John Wiley and Sons Inc., Second Edition, 1965.

89. DAVIES, O.L. "The Design and Analysis of Industrial Experiments", Published for Imperial Chemical Industries by Oliver and Boyd (London and Edinburgh), 1963.

90. MORONEY, M.J. "Facts from Figures", Penguin Books Ltd., Great Britain, Third edition, 1956.

91. WILLIAMS, E.J. "Regression Analysis", John Wiley and Sons, 1959.

92. CADLE, R.D. "Particle Size Determination", Inter-science Publishers Inc., New York, 1955.

93. DALLEVALLE, J.M. "Micromeritics : the Technology of Fine Particles", Pitman Publishing Corporation, 1943.

94. SCHEID, F., "Theory and Problems of Numerical Analysis", Schaum's Outline Series, McGraw-Hill Book Company, 1968.

95. KHABAZA, I.M. "Numerical Analysis", Pergamon Press, 1965.

96. HILDEBRAND, F.B. "Introduction to Numerical Analysis", McGraw-Hill Book Company, Second Edition, 1974.

97. WYLIE, C.R. "Advanced Engineering Mathematics", McGraw-Hill, Kogakusha Book Company, Third Edition, 1966.

98. BOTTERILL, J.S.M., GEORGE, J.S. AND BESFORD, H. "Bubble Chains in Gas Fluidized Beds", AIChE Symposium Series Vol. 62, No. 62, 1966.

99. MORI, S. AND WEN, C.Y. "Estimation of Bubble Diameter in Gaseous Fluidized Beds", AIChE Journal, Vol. 25, No. 1, January 1975, Pp 109-115.

100. GELDART, D. "The Effect of Particle Size and Size Distribution on the Behaviour of Gas-Fluidized-Beds", Powder Technology Vol. 6, 1972, Pp 201-215.

101. LEWIS, J.B. AND PARTRIDGE, B.A. "Fluidization", Nature, Vol. 216, 14 October 1967, Pp 124-127.

102. GELDART, D. "The Expansion of Bubbling Fluidized Beds", Powder Technology, Vol. 1, 1967/8, Pp 355-368.

103. STEWART, P.S.B. AND DAVIDSON, J.F. "Slug Flow in Fluidized Beds", Powder Technology, Vol. 1, 1967, Pp 61-80.

STANDARDS REFERRED TO :

BS 1016 : Methods for the Analysis and Testing of Coal and Coke
Part 3 : 1965 Proximate Analysis of Coal
Part 5 : 1972 Gross Calorific Value of Coal and Coke.
Part 14: 1963 Analysis of Coal Ash and Coke Ash
Part 16: 1971 Reporting of Results.

BS 1017 : 1972 and 1942 The Sampling of Coal and Coke.

BS 1377 : 1975 Methods of Test for Soils for Engineering Purposes.

BS 1796 : 1976 Methods for the use of B.S. Fine-Mesh Test Sieves

BS 1916 : Limits and Fits for Engineering
Part 1 : 1953 Limits and Tolerances
Part 2 : 1953 Guide to the Selection of Fits.

BS 2885 : 1974 Code for Acceptance Tests on Stationary Steam Generators of the Power Station Type

BS 3406 : Methods for the Determination of Particle Size of Powders
Part 1 : 1961 Subdivision of Gross Sample down to 0,2 ml
Part 2 : 1963 Liquid Sedimentation Methods.

APPENDICES

APPENDIX A : Detailed Design of Components.

APPENDIX B : Definitions.

APPENDIX C : Coal Properties and Coal Gradings.

APPENDIX D : Sampling Procedures.

APPENDIX E : General Calculations.

APPENDIX F : Statistical Analysis.

APPENDIX G : Particle Size Analysis.

APPENDIX H : Tabulation of Results.

APPENDIX I : Numerical Analysis.

APPENDIX J : Some Consequences of the Two-Phase Theory of Fluidization.

APPENDIX K : Cyclone Performance.

APPENDIX L : Complete Table of Contents.

APPENDIX A

DETAILED DESIGN OF COMPONENTS

A number of details pertaining to different components of the rig are included on the following pages. These details are not necessary for the general understanding of the operation of the rig but provide information which may be of value when comparing results with similar forms of equipment. A brief explanatory note is produced below for each of the following drawings.

A.1 Combustor Vessel

Figure A.1 represents various sections taken through the combustor vessel to indicate the location of instrumentation apertures, positioning of the coal feeder and the gas ignition pilot burner.

A.2 Distributor

Figure A.2.a represents the final layout of the orifices in the distributor, after some of the original holes had been blocked. Figure A.2.b illustrates the method of attachment of the distributor to the combustor vessel. An asbestos tape seal is used between the distributor plate and the combustor vessel, with the distributor tightly clamped to the vessel by means of six bolts.

A.3 Coal Feeder

The coal feeder has been designed to facilitate maintenance and is made up of four basic components; the feeder housing, the locating sleeve and sleeve carrier, the screw shaft and the bearing housing. The screw shaft is press-fitted into the self-aligning bearing located in the bearing

housing, thus allowing some movement of the shaft. The bearing housing has a guide spigot machined such as to form a loose fit with the sleeve carrier, this is a H11h11 fit. This then locates the screw with the locating sleeve, and the whole assembly is then bolted onto the feeder housing. All limits and fits have been toleranced in accordance with the recommendations and requirements of BS 1916 of 1953.

A.4 Circuit Diagram for DC Motor Control

Figure A.4 illustrates the method in which the speed control of the DC Motor is achieved by varying the armature voltage. It will also be noted that a 220V/6V transformer is used to provide a low voltage power source to engage the clutch of the DC motor.

A.5 Cyclone

The basic dimensions of the cyclone which is fabricated from 1,6 mm (16 gauge) steel plate is illustrated by Figure A.5.

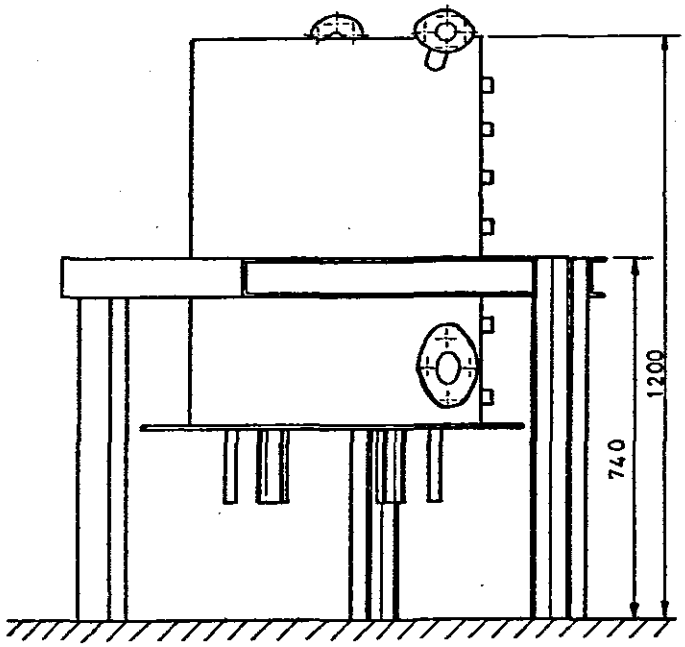

SIDE ELEVATION

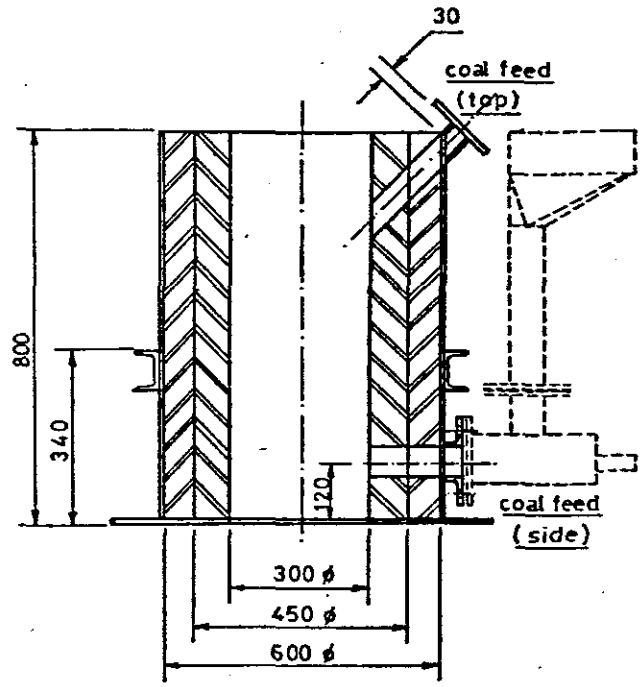

SECTION 'A-A'

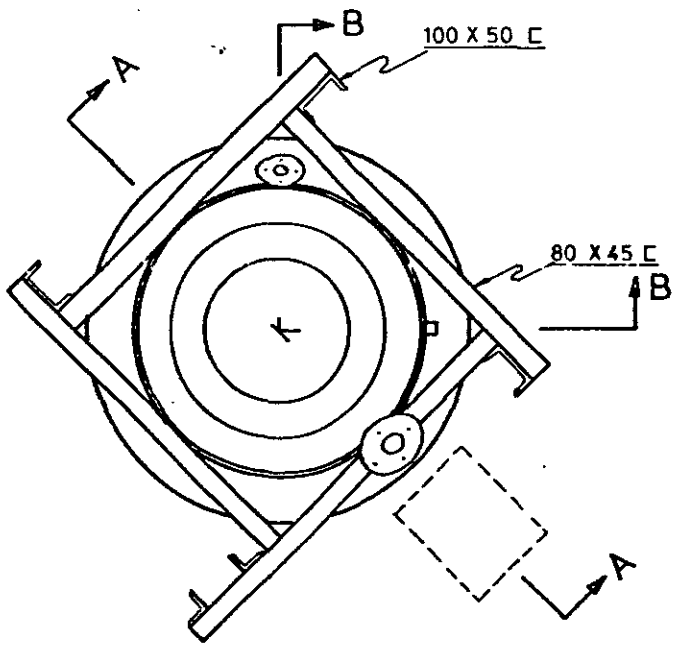

PLAN

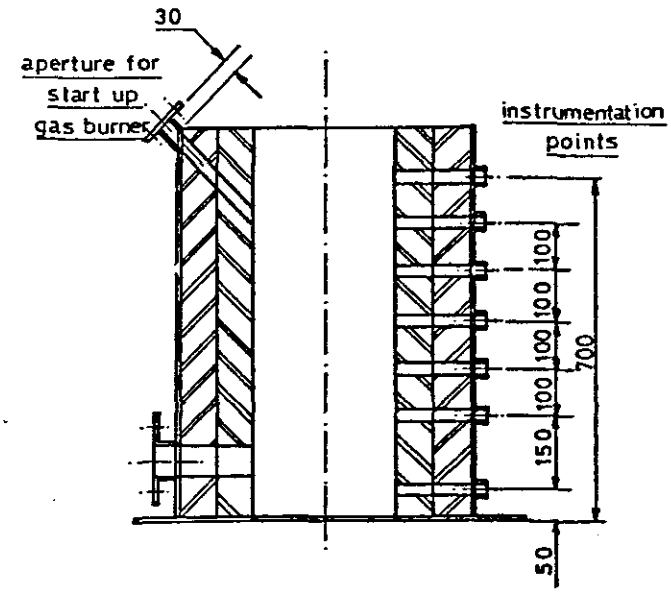

SECTION 'B-B'

Figure A1 : The Basic Combustor Vessel

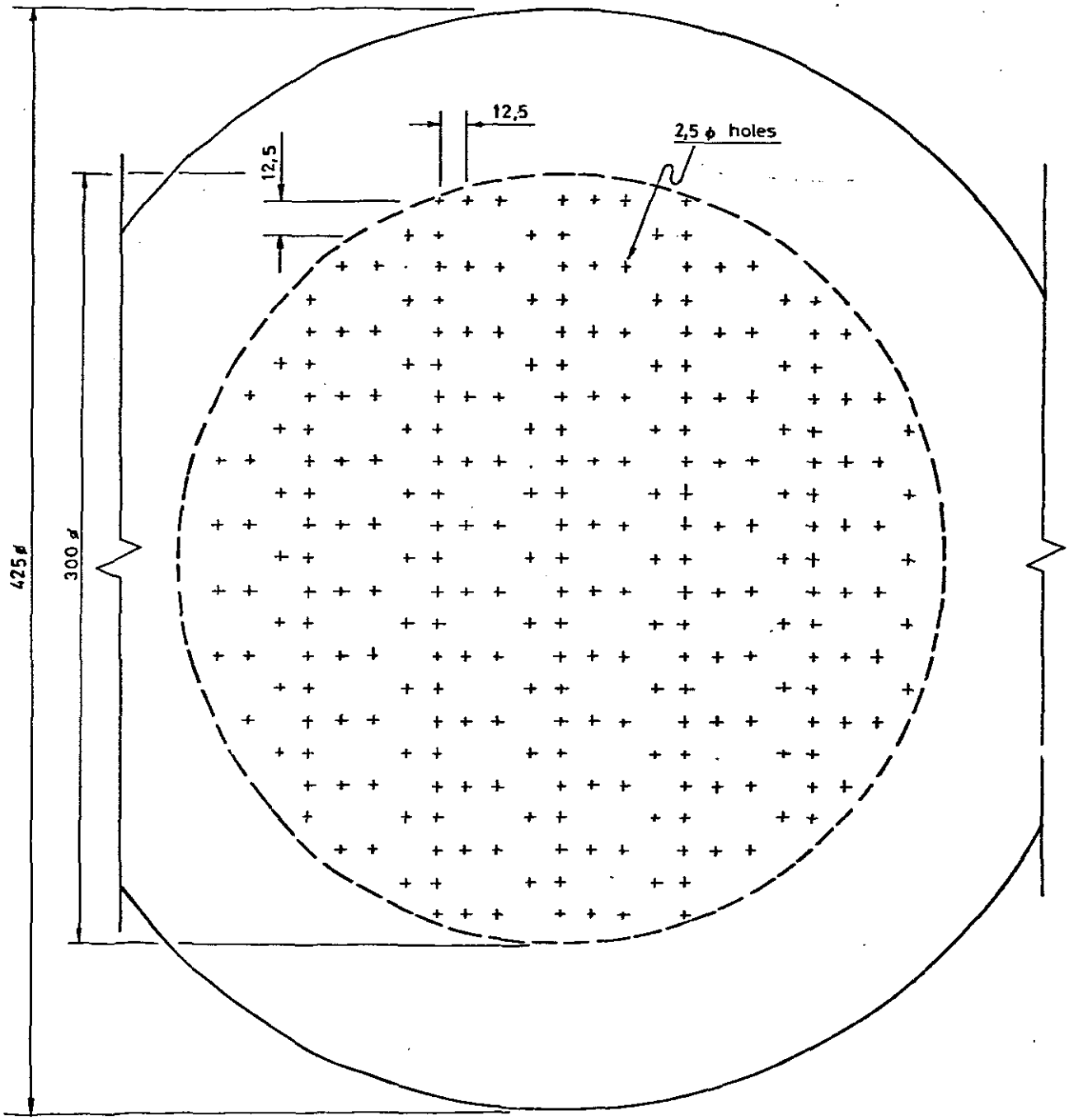

DISTRIBUTOR

Figure A2a : Distributor Plate Illustrating the Positioning of the Orifices.

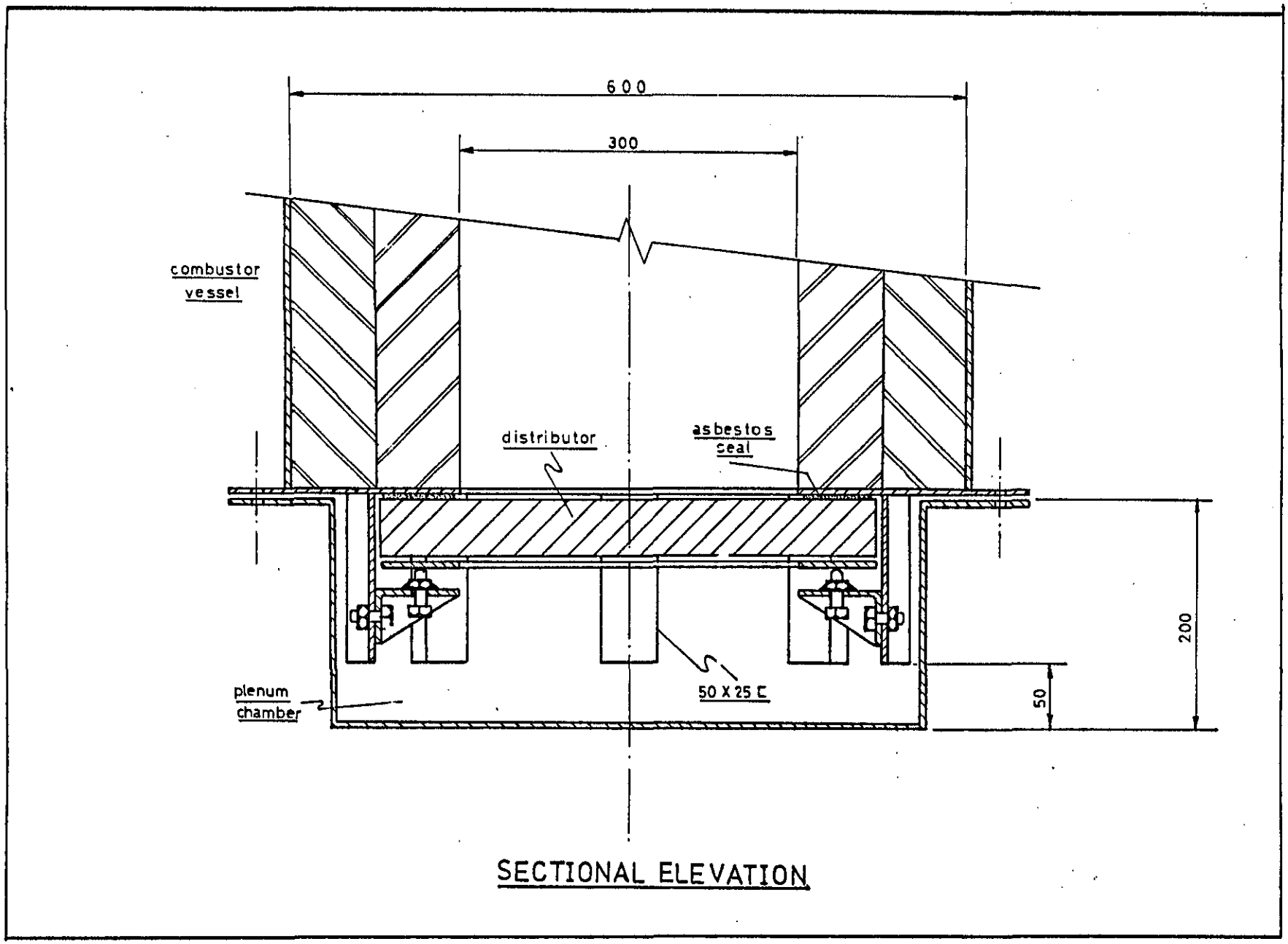

Figure A2b : Attachment of the Distributor to the Combustor Vessel

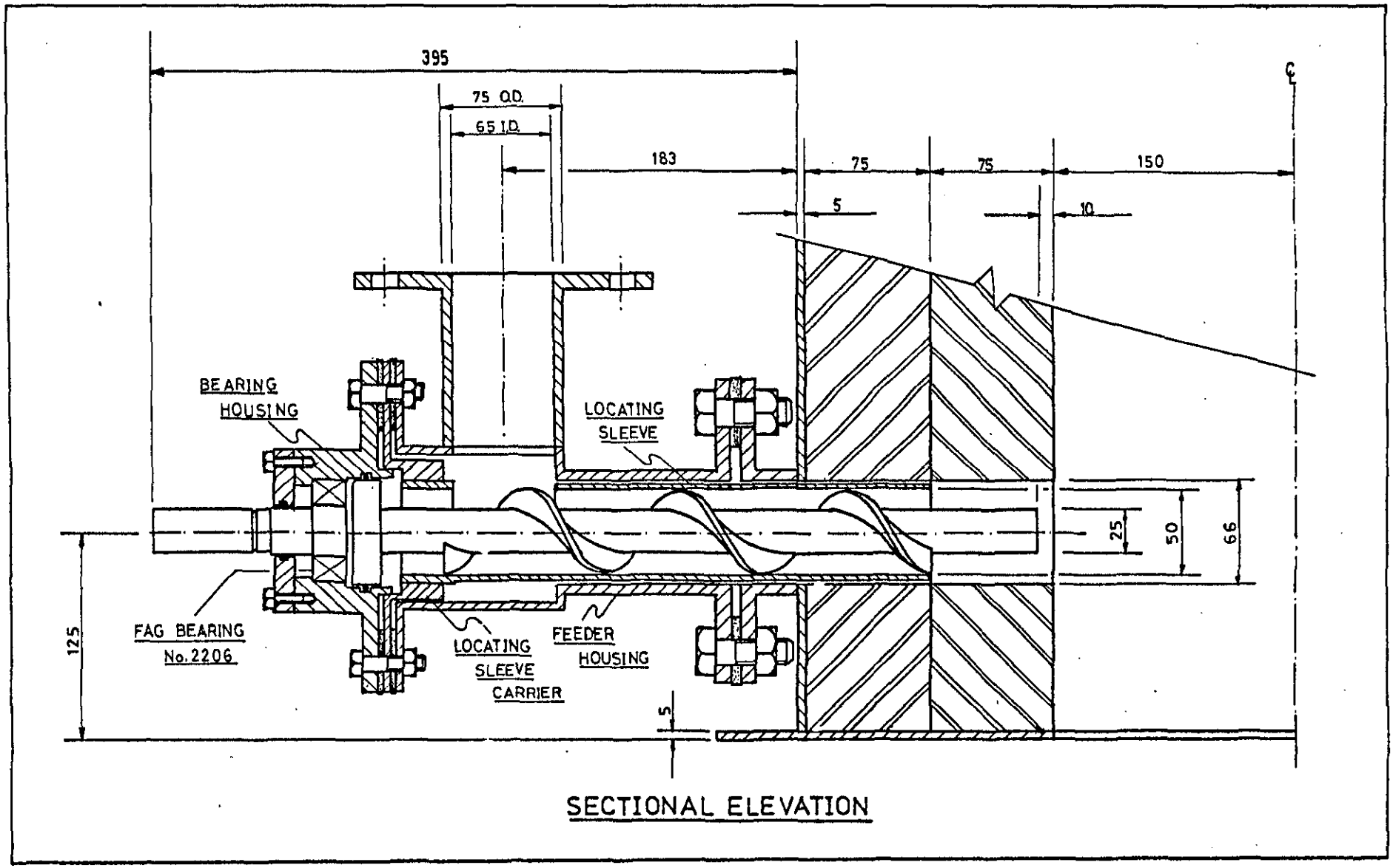

Figure A3 : Sectional Elevation of the Coal Feeder

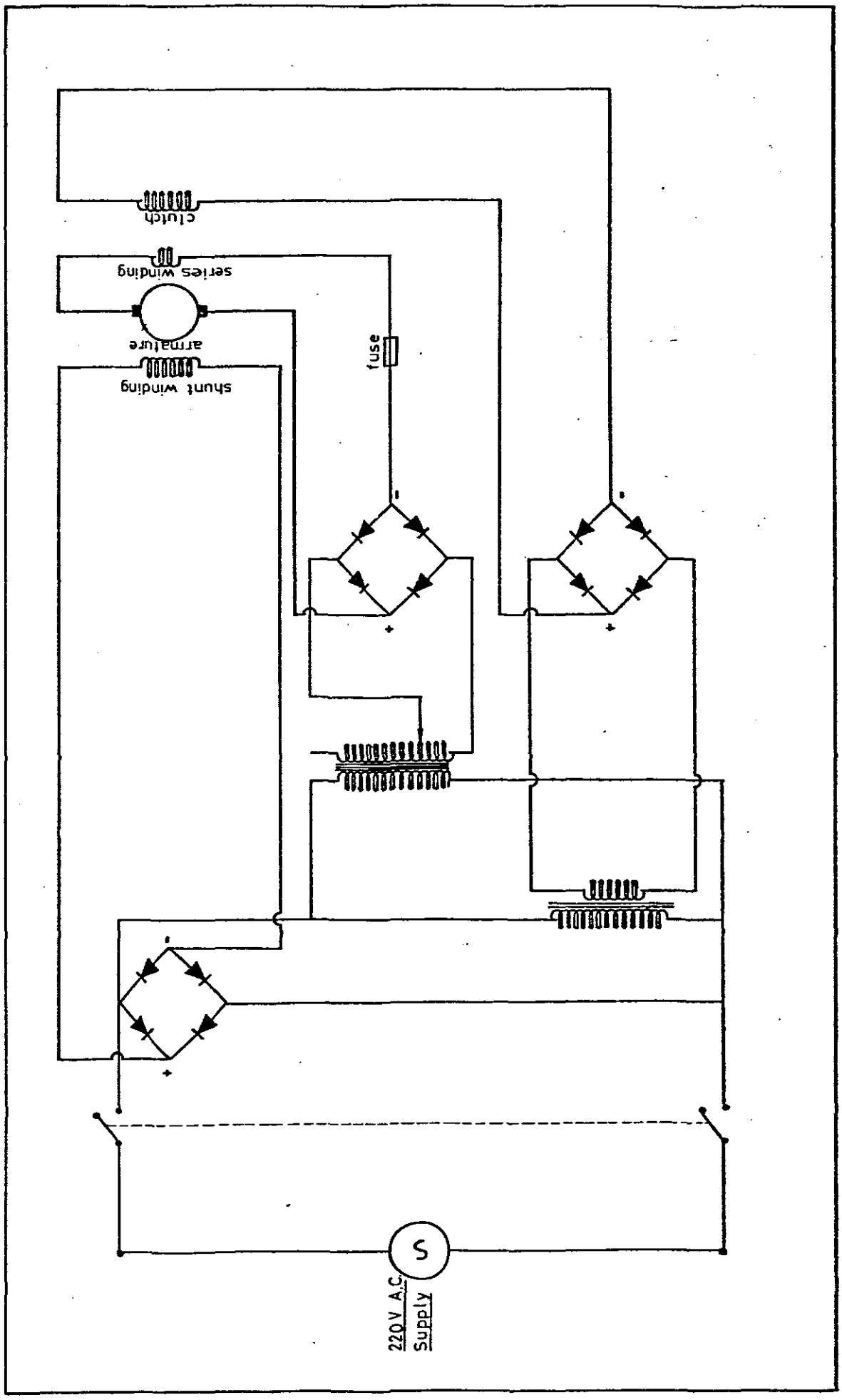

Figure A4 : Circuit Diagram for DC Motor Control

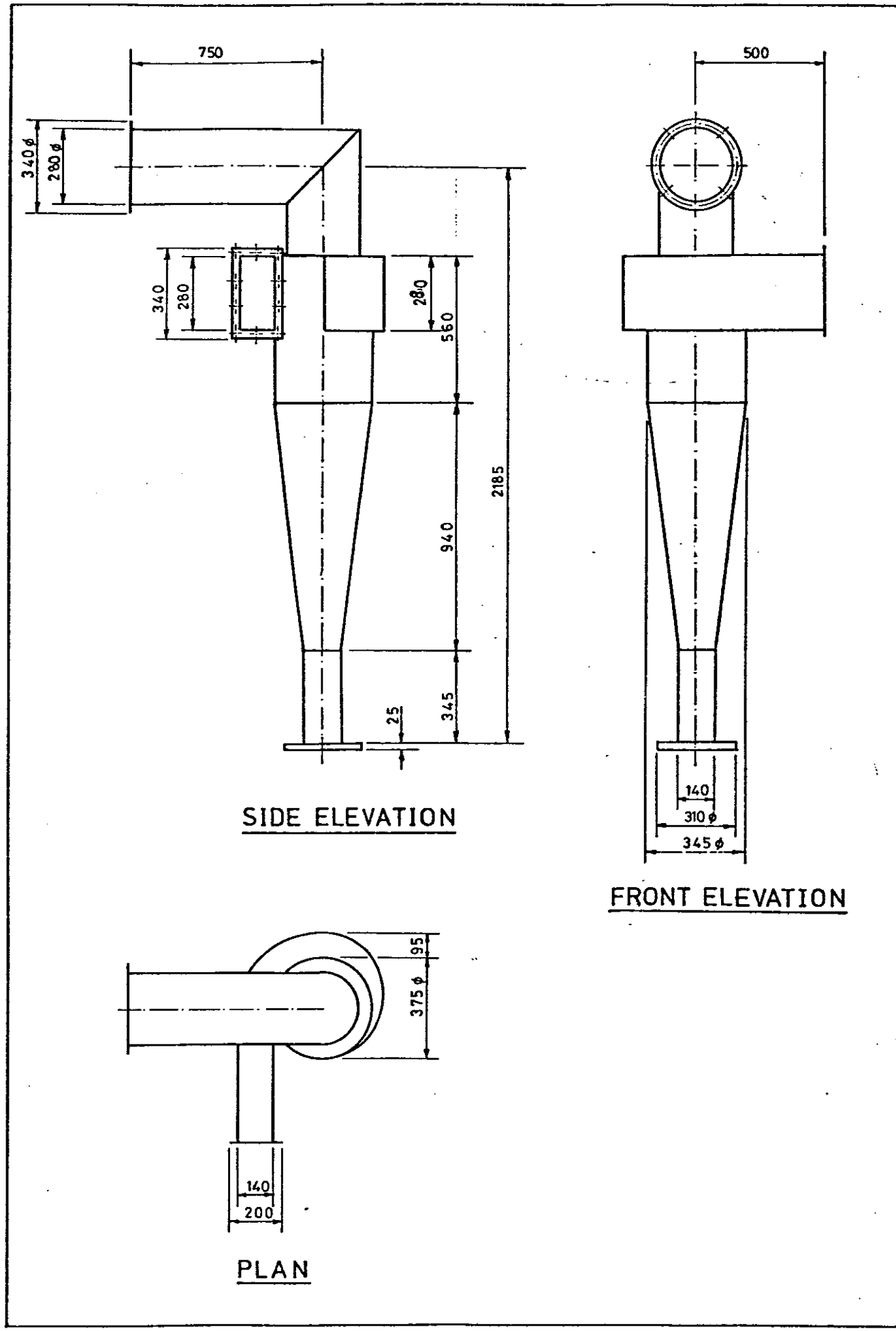

Figure A5 : Cyclone Fabricated from 1,6 mm thick Steel Plate.

APPENDIX B

DEFINITIONS

B.1 Combustion Efficiency

The combustion efficiency of the fluidized-bed combustion chamber is defined as the ratio of the rate of heat liberated to the rate of heat input. This ratio can be shown to be equal to the rate at which the coal is burnt to rate of coal fed into the rig, or:

$$\eta_c = M_f / M_{fo} \qquad (B.1)$$

where η_c, M_f and M_{fo} are the combustion efficiency, fuel burnt and fuel feed rate respectively.

This can also be written as:

$$\eta_c = 1 - h_c \qquad (B.2)$$

where h_c is the unburnt carbon loss as defined by a boiler acceptance test standard, eg BS 2885 : 1974.

APPENDIX C

COAL PROPERTIES AND COAL GRADINGS

Only two batches of Douglas Duff have been used for the tests. The first, designated as Batch A, was used for Runs 6 and 7; and the second designated as Batch B, was used for Runs 8, 9 and 10. Size gradings and a proximate analysis were performed for both batches, whilst a separate proximate analysis (without the determination of the calorific value) and ultimate analysis was undertaken by Muller Laboratories on Batch B. An important feature of any coal or ash analysis is the sampling procedure, and the method in which the samples were obtained has been included in Appendix D.

C.1 Size Gradings

The gradings have been determined on a cumulative percent by weight undersize, and are listed below. Figure C.1 graphically illustrates these gradings as smoothed curves as required by BS 1796 of 1976, whilst these same curves have also been plotted on Rosin-Rammler paper as Figure C.2, to facilitate their interpretation. Included in both these curves is the size distribution of the bed material, i.e. the silica sand as given by Figure 16, to enable an easy comparison to be made of the size gradings of the different materials.

Sieve Aperture Size (mm)	Cumulative % by weight Undersize	
	Batch A	Batch B
6,35	90,4	86,9
4,76	80,6	75,1
2,00	47,8	40,9
1,003	29,0	24,0
0,600	19,8	15,5
0,420	14,4	11,1
0,211	7,1	5,8

C.2 Coal Analysis

The coal analyses quoted below are each on an air dried basis. As all the coal was air dried prior to testing to eliminate any problems due to poor coal feeding from the storage hopper to the coal feeder as a result of possible coal 'hang-ups' in the feed pipe, the air dried coal is equivalent to the as fired coal. These analyses are given below:

Proximate Analysis (air dried basis)

	Batch A	Batch B
Gross Calorific Value (MJ/kg)	26,84	27,82
Inherent Moisture (%)	1,60	1,45
Volatile Matter (%)	25,55	23,85
Ash (%)	16,03	14,43
Fixed Carbon (%)	56,82	60,27

Analysis by Muller Laboratories

Proximate Analysis	%
Ash	15,28
Water	2,96
Volatile Matter	23,86
Fixed Carbon	57,90
Ultimate Analysis	**%**
Moisture	2,96
Ash	15,28
Carbon	68,39
Hydrogen	3,67
Nitrogen	1,78
Sulphur	0,68
Oxygen	7,24

Using the formula proposed by Dubbels (83, pg 454), a value for the net calorific value can be determined. By applying

the formula on page 19 of BS 1016 : Part 16 : 1971, the gross calorific value can be deduced. These values have been calculated from the preceding ultimate coal analysis as:

NCV = 26,48 MJ/kg
GCV = 27,37 MJ/kg

As only small differences exist between batches A and B, they have been assumed to be similar with respect to their analyses. Therefore the proximate and ultimate analyses as found by Muller Laboratories as well as the last mentioned calorific values which have been determined from the ultimate analysis, have been used in all the calculations.

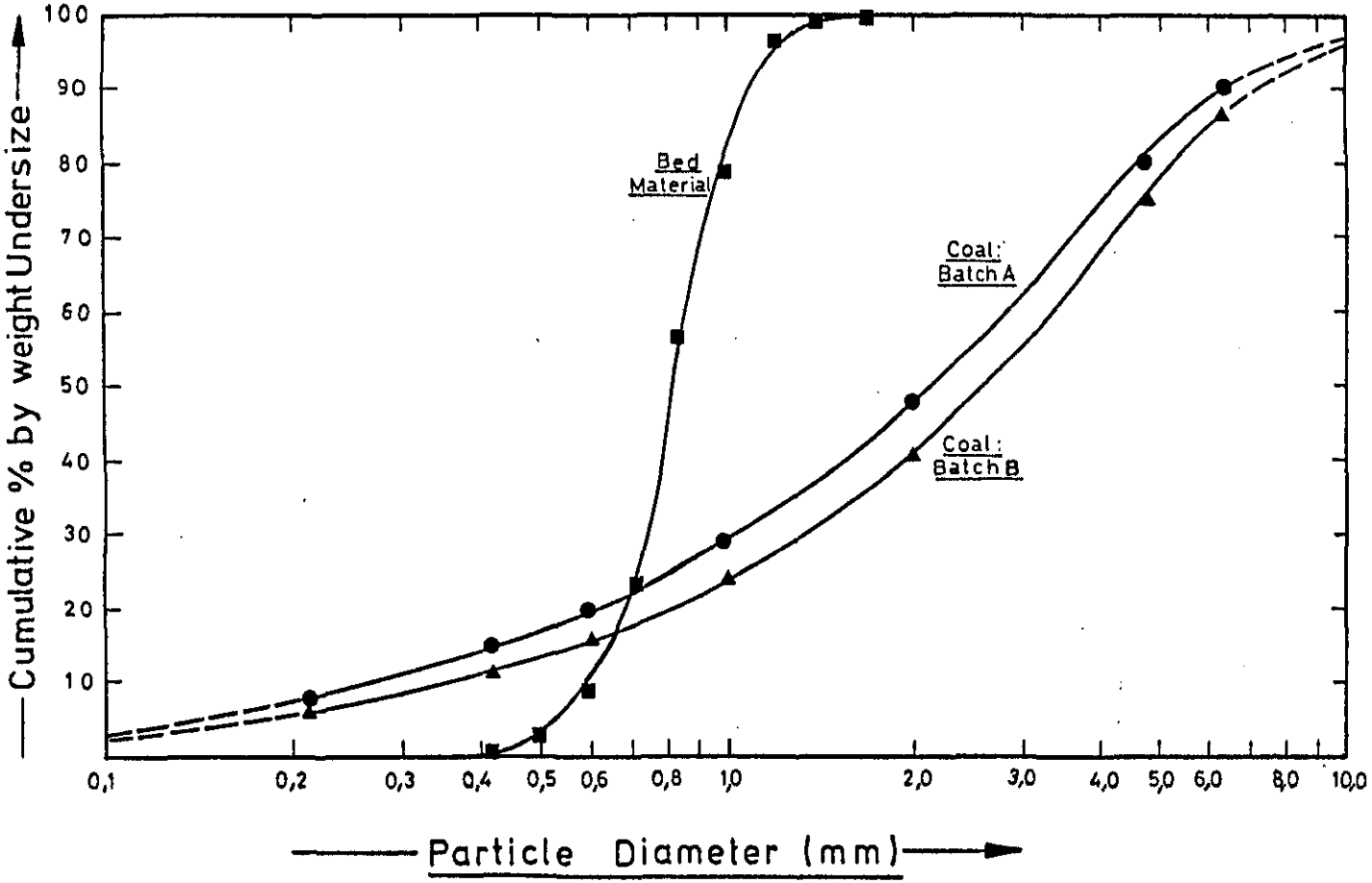

Figure C1 : As Received Size Gradings of the Coal and Bed Material prior to the Removal of the Size Fraction Greater than 6,35 mm

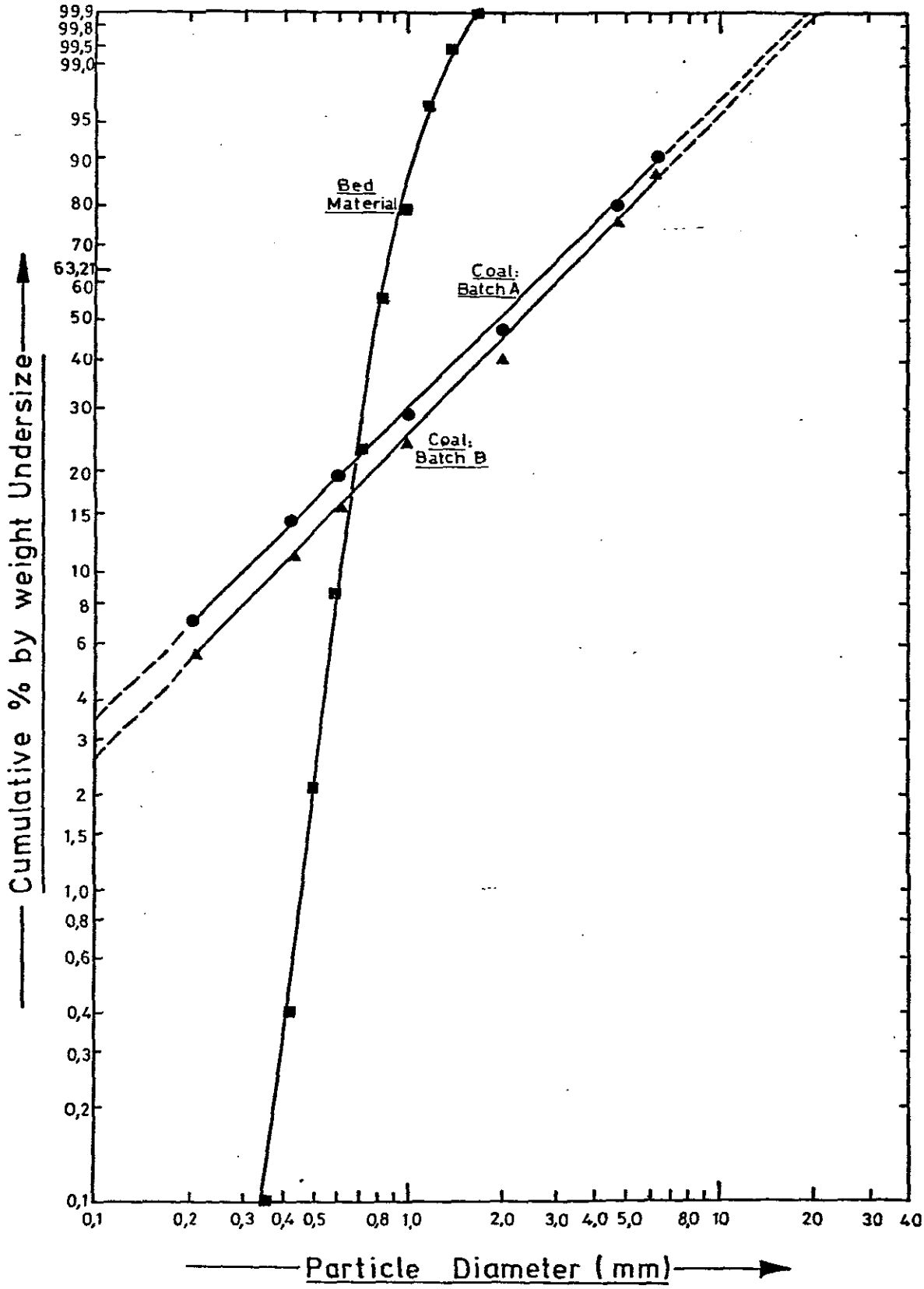

Figure C2 : Size Gradings of the Coal and Bed Material Plotted on Rosin-Rammler Paper.

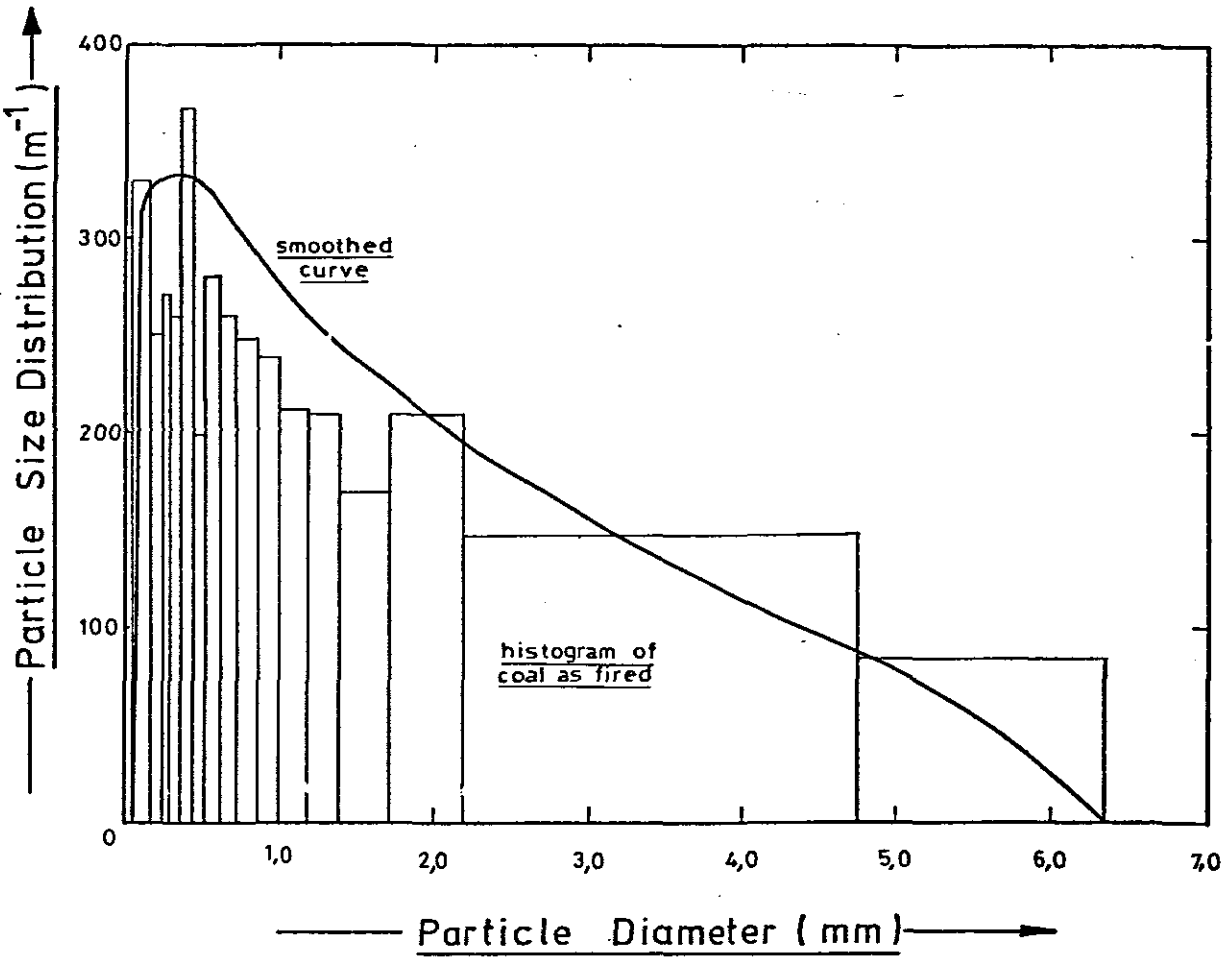

Figure C3 : Particle Size Distribution Function for the Coal as Fired (i.e. $p_o(d)$ for Coal of Batch A) and Smoothed Distribution Function used as Input for the Theoretical Model.

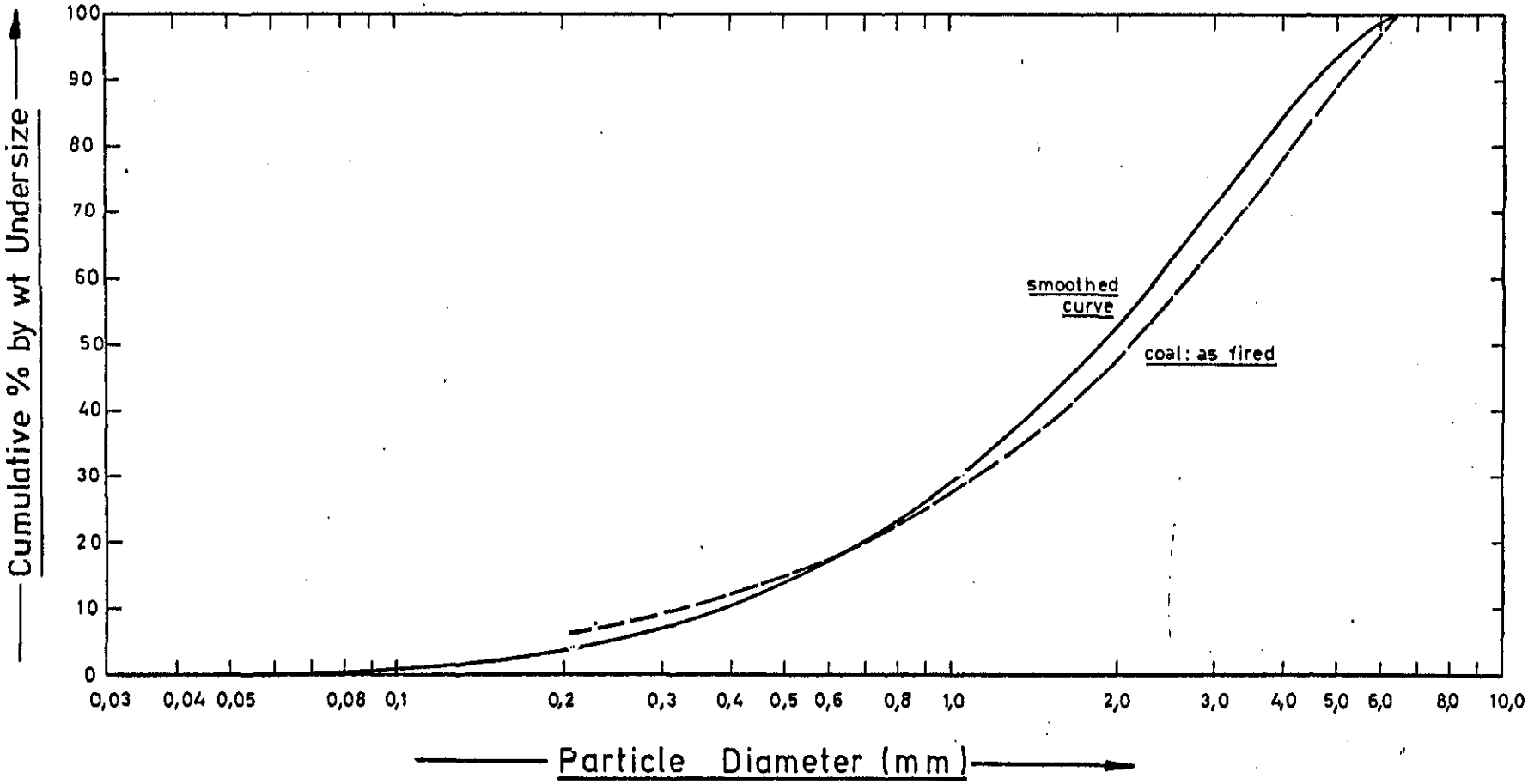

Figure C4 : Cumulative Size Distributions for the Coal Gradings of Figure C3

APPENDIX D

SAMPLING PROCEDURES

During the testing of the combustion of solid fuels, continuous analysis of some of the more important parameters is not possible. The evaluation of the calorific value of the fuel or the percentage carbon contained in the ash for instance are determined as mean values for an entire test run or for the particular test respectively. It is therefore imperative that representative values be found for these means. Although BS 1017 sets out the procedures to be adopted in obtaining representative samples, these procedures have not been strictly adhered to because of the relatively small quantities of fuel and ash used as compared to that generally found in practice.

D.1 Coal Sampling

As mentioned in Appendix C, two batches of coal were used for the tests. The first, designated as Batch A was used for Runs 6 and 7, comprised about 50 kg of coal. Coning and quartering of the sample is not recommended in the 1972 edition of BS 1017, but rather the use of specially designed separators. In view of the small quantity of coal, coning and quartering was employed as a means of rendering the sample down to about 6 kg. The coning and quartering was conducted in accordance with the procedure recommended in BS 1017 : 1942. Besides providing a small sample, the coning and quartering ensured that the coal was well mixed.

About 175 kg of coal was acquired for Runs 8, 9 and 10, and has been designated as Batch B. After air drying this coal, the fraction larger than 6,35 mm was removed. During the screening process, which was done manually, a small sample of coal was removed at discreet intervals. This resulted in a sample of about 18 kg, which was rendered into three

equal samples. A proximate coal analysis and calorific value determination was performed on the first sample, an ultimate analysis on the second, whilst the size grading of the coal was determined from the third sample. Details of the analyses are given in Appendix C.

D.2 Ash Sampling

The weight of ash collected in the cyclone varies from about 0,5 kg to 1,0 kg. The fraction of the collected product greater than 600 microns was removed before rendering the total quantity of ash collected into three equal samples. Each sample is obtained by taking a number of small amounts from the collected product and placing them into three containers labelled A, B and C in the following sequence:

ABC, BCA, CAB, ABC, ... etc.

A size grading was performed on the first sample, the percentage carbon in ash was determined from the second sample, whilst the third sample has been retained to verify any discrepancies.

APPENDIX E

GENERAL CALCULATIONS

In the assessment of the performance of the fluidized-bed combustion rig, a number of different calculations have had to be performed. A general outline of these calculational procedures is given in this Appendix.

E.1 Combustion Calculation

The familiar chemical reactions resulting in the formation of carbon dioxide, sulphur dioxide and water vapour are assumed to take place during the combustion of coal with the oxygen contained in the air. These reactions are quoted below:

$$C + O_2 \rightarrow CO_2$$

$$S + O_2 \rightarrow SO_2$$

$$H_2 + \frac{1}{2} O_2 \rightarrow H_2O$$

By making use of the ultimate analysis of the coal as given in Appendix C, the resulting flue gas components can be determined for the complete combustion of the coal in air for stoichiometric combustion as well as at different excess air levels. It is of value to obtain the flue gas components in order to determine the flue gas properties, as these differ from those of air even though the flue gas is made up mainly of nitrogen. Differences between the properties of air and the resulting exhaust gases are caused mainly by the presence of water vapour and carbon dioxide. Other quantities which are useful in any combustion calculation are the amounts of air required and resulting flue gases per kilogram of coal burnt at different excess air levels. The excess air factor is defined as the ratio of the volume of air supplied to the volume of air required for stoichiometric combustion. The results of two combustion

calculations performed for the combustion of the coal with an ultimate analysis given by Appendix C with air are produced in Table E.1. The combustion air is assumed to contain 10 grammes of moisture per kg of dry air. The first calculation has been chosen as that of stoichiometric combustion, whilst the second has been performed at an excess air factor of 3,0 which is similar to that prevailing for most of the tests.

Table E.1 : Results of Combustion Calculations of Douglas Duff with Air of Moisture Content, 10g/kg of Air

Excess Air level (-)	1,00	3,00
Gas Composition (Vol. %)		
Carbon Dioxide	17,62	6,04
Water Vapour	7,66	3,67
Oxygen	0,00	13,59
Sulphur Dioxide	0,07	0,02
Nitrogen	74,65	76,68
Gas per kg of Coal (kg)	9,711	27,42
Air per kg of Coal (kg)	8,912	26,74

E.2 Flue Gas Properties

The relevant thermodynamic properties of air have been extracted from Reference (84) for use in the theoretical model of Chapter 4. Calculations requiring the use of these properties in Chapter 3 however, use the flue gas properties determined by the method suggested by Brandt (85). This approach involves two corrections for the carbon dioxide and water vapour contents of the flue gas to the corresponding value of the property for nitrogen at the respective temperature. As the remaining flue gas components have only a minor effect on the respective properties, the result is very similar to that obtained by considering the effect of each gas component individually and then adding the separate effects by some mixing rule (86).

Figure E.1 is a nomograph to illustrate the determination of the mean specific heat at different temperatures, allowing for the water vapour and carbon dioxide concentration of the gas.

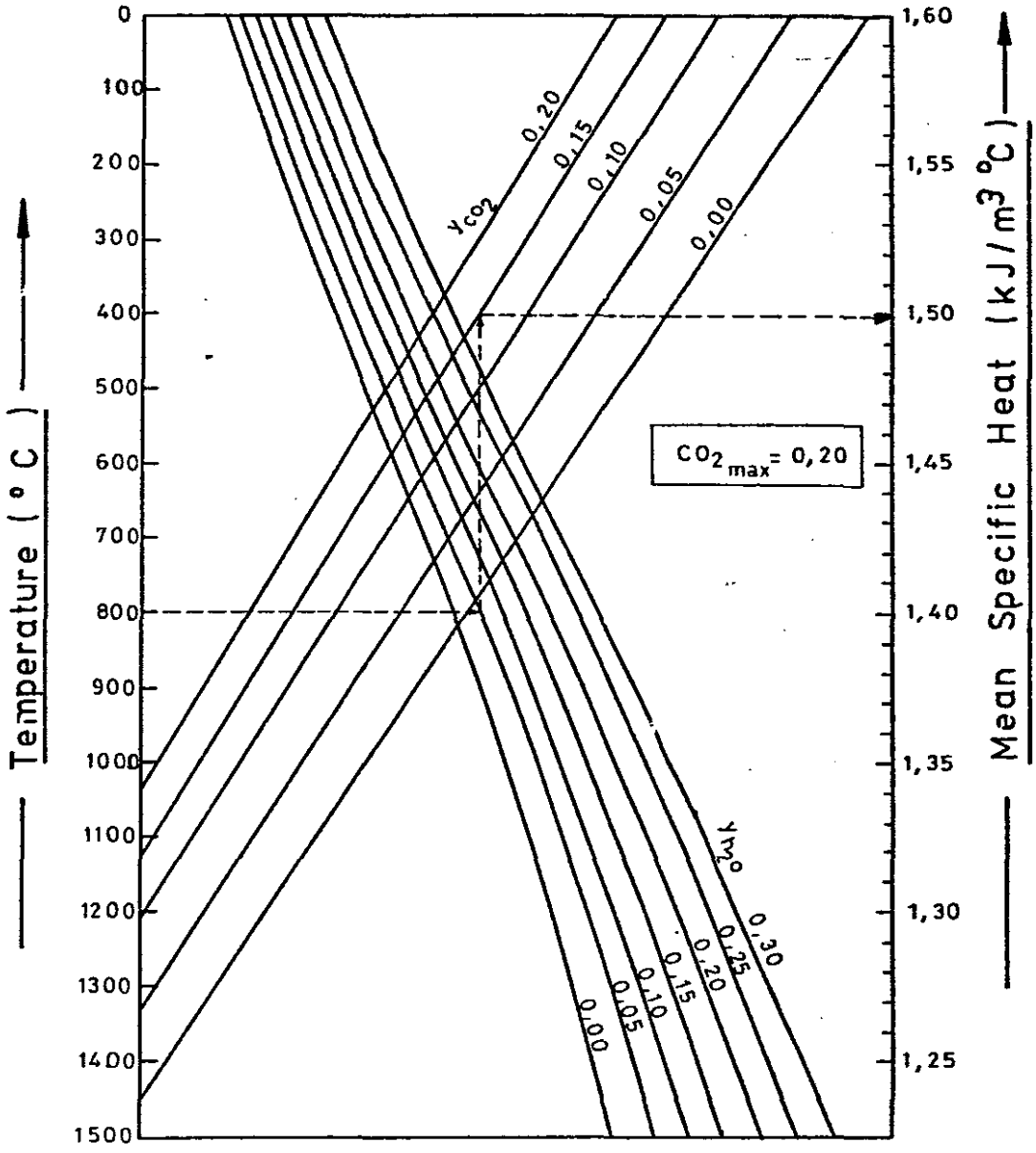

Figure E.1 : Mean Specific Heat of Flue Gas, referred to Normal Temperature and Pressure as a Function of the Volumetric Fractions of Carbon Dioxide and water Vapour, Brandt (85).

E.3 Overall Rig Calculations

In order to assess the performance of the fluidized-bed combustion rig the following heat balance is written

$$(\text{heat input}) = (\text{heat in off gases}) + (\text{heat loss through combustor walls}) \qquad (E.1)$$

Only the last term, the heat loss through the combustor walls needs further explanation. Although the rig is refractory lined and thermally insulated, some heat is lost through the walls and it is of value to estimate this heat loss to assess its effect on the overall heat balance.

The problem of determining this heat loss has been reduced to the simple heat transfer problem of heat passing from the inside to the outside of two concentric cylinders. The following values have been used:

Thermal conductivity of inner refractory lining	- 0,87 W/mC
Thermal conductivity of insulating lining	- 0,10 W/mC
Internal heat transfer coeff. (bed to wall)	- 300 W/m^{2}C
External heat transfer coeff. (wall to air)	- 5,5 W/m^{2}C

Using the above values, and assuming that the expanded fluidized bed is effective over a height of 300 mm, the product of the overall heat transfer coefficient and the area of heat transfer can be shown to be given by

$$U\,A = 0{,}473 \cdot 10^{-3} \qquad (kW/^{\circ}C) \qquad (E.2)$$

and the heat loss through the combustor walls is given as

$$Q_w = U \cdot A \cdot \Delta T \qquad (E.3)$$

or

$$Q_w = 0{,}473 \cdot 10^{-3} \cdot \Delta T \qquad (E.4)$$

It should be clear that the treatment of the heat loss through the combustor walls is a simplification of the real process. However, the heat loss as found by equation (E.4) would probably be in error by no more than about $\pm$ 25% of the true value. Further, at a bed temperature of 900°C and with the surrounding temperature of 20°C, the heat loss is found to be 0,46 kW, which is about 1% of the total heat liberated in the rig, thus justifying the above approach in the determination of the heat loss.

Equation (E.1) can be written as

$$M_f \cdot NCV = M_g \cdot c_p \cdot \Delta T + 0{,}473 \cdot 10^{-3} \cdot \Delta T \qquad (E.5)$$

$$\eta_c \cdot M_{fo} \cdot NCV = M_g \cdot c_p \cdot \Delta T + 0{,}473 \cdot 10^{-3} \cdot \Delta T \qquad (E.6)$$

APPENDIX F

STATISTICAL ANALYSIS

"Statistical methods are predicated on the single concept of variability. It is through this fundamental concept that a basis is determined for experimental design and analysis of data. In this sense, statistical methods are concerned with deriving maximum information from a given set of data (analysis), and conversely minimizing the amount of data (experimental design) to derive specific information." (70, Ch 2). The use of statistics in engineering and in general has been covered in a number of general and specific publications. This thesis has made reference to a number of publications and standard texts on the subject (70), (87), (88), (89), (90) and (91). The more fundamental concepts such as standard deviations, hypothesis testing, correlation coefficients, distribution functions, analysis of variance etc. are not discussed here and the reader is referred to any of the above texts for more details.

A major portion of this thesis is concerned with the determination of the factors influencing the combustion efficiency of the fluidized-bed combustion rig. A general description and definition of the terms and the approach employed in the multiple regression analysis is presented in this Appendix for ease of reference.

F.1 Multiple Regression

Multiple regression methods are used to relate a dependent variable (Y) to a number of independent variables $(X_1, X_2, \ldots X_m)$. Only linear multiple regression will be considered and a model of the following form is postulated:

$$Y = b_o + b_1 \cdot X_1 + b_2 \cdot X_2 + \ldots\ldots\ldots + b_m \cdot X_m \qquad (F.1)$$

The coefficients of the model $(b_0, b_1, \ldots .. b_m)$ are determined by the method of least squares. This involves minimising the squared differences between the observed value of the dependent variable i.e. Y_0 and that predicted by equation (F.1), i.e. Y_p .. Mathematically the solution is computed by taking the partial derivative with respect to each coefficient of the least squares equation

$$S = \Sigma (Y_0 - Y_p)^2 \qquad (F.2)$$

$$S = \Sigma \; Y_0 - (b_0 + b_1 \cdot X_1 + \ldots .. + b_m \cdot X_m) \qquad (F.3)$$

and setting the result of each partial differentiation to zero. This results in the following equations which may be solved simultaneously for $b_0, b_1, b_2, \ldots .. b_m$.

$$b_0 + b_1 \cdot \Sigma X_1 \quad + \ldots .... + b_m \cdot \Sigma X_m \quad = \Sigma Y_0$$

$$b_0 \cdot \Sigma X_1 + b_1 \cdot \Sigma (X_1)^2 + \ldots .... + b_m \cdot \Sigma (X_1 \cdot X_m) = \Sigma (X_1 \cdot Y_0) \qquad (F.4)$$

$$b_0 \cdot \Sigma X_m + b_1 \Sigma (X_1 \cdot X_m) + \ldots .... + b_m \Sigma (X_m)^2 = \Sigma (X_m \cdot Y_0)$$

However it is convenient to transform the above equations into the standard normal equations. The first step in this transformation results in the above equations being transformed to those given by the equations (F.5)

$$b_1 \cdot (s_{X1})^2 + b_2 \cdot s_{X1\ X2} + \ldots .... + b_m \cdot s_{X1\ Xm} = s_{X1\ Y0}$$

$$b_1 \cdot s_{X1\ X2} + b_2 \cdot (s_{X2})^2 + \ldots .... + b_m \cdot s_{X2\ Xm} = s_{X2\ Y0} \qquad (F.5)$$

$$b_1 \cdot s_{X1\ Xm} + b_2 \cdot s_{X2\ Xm} + \ldots .... + b_m \cdot (s_{Xm})^2 = s_{Xm\ Y0}$$

where $(s_{Xi})^2$ is the sample variance of X_i and $s_{Xi\ Xj}$ is the covariance between X_i and X_j . A bivariate correlation coefficient for X_i and X_j is defined as

$$r_{ij} = s_{Xi\ Xj} \; / \; \sqrt{(s_{Xi})^2 \cdot (s_{Xj})^2} \qquad (F.6)$$

and a standard partial correlation coefficient for variable X_j is defined as

$$B_j = \frac{b_j \cdot \sqrt{(s_{Xj})^2}}{\sqrt{(s_{YO})^2}} \qquad (F.7)$$

The Standard Normal Equations

By manipulation of the equations (F.5) the standard normal equations (F.8) are formed.

$$\begin{aligned} B_1 &+ B_2 \cdot r_{12} + \ldots\ldots\ldots + B_m \cdot r_{1m} = r_{Y1} \\ B_2 \cdot r_{12} &+ B_2 + \ldots\ldots\ldots + B_m \cdot r_{2m} = r_{Y2} \\ B_m \cdot r_{1m} &+ B_2 \cdot r_{2m} + \ldots\ldots\ldots + B_m = r_{Ym} \end{aligned} \qquad (F.8)$$

The bivariate correlation coefficients r, are easily evaluated, and by inverting the resulting matrix of these coefficients, the values for the standard partial correlation coefficients, B, may be determined. One of the advantages of using the standard partial regression coefficients, is that as these coefficients vary between -1 and 1, they may be directly compared. Further, the multiple correlation coefficient is easily determined by equation (F.9)

$$R^2 = \Sigma(B_i \cdot r_{Yi}) \qquad (F.9)$$

F.2 Tests on Coefficients

The Bivariate Correlation Coefficient

In order to determine whether a relationship exists between two variables the bivariate correlation coefficient is tested to determine whether it is significantly different from zero by the statistic

$$t = r \cdot \sqrt{\frac{n-2}{1-r^2}} \qquad (F.10)$$

where t is distributed as the Student's t distribution with $(n-2)$ degrees of freedom.

The Standard Partial Correlation Coefficient B

In any process a number of independent variables may be arbitrarily defined, and though one may be tempted to use a large number of these variables, the resulting equation will be unwieldy. Further, the contribution of some of the variables in predicting the independent variable may be small, such that these may be eliminated from the regression equation. In order to eliminate those independent variables which do not contribute significantly to the prediction, the values of B must be tested to determine whether they are different from zero. Should the interval estimate of the population standard partial regression coefficient B' include zero, then the hypothesis that B is zero is accepted. The interval estimate of B' is given as

$$B_j + t_{(\alpha/2)} \cdot A < B'_j < B_j + t_{(1-\alpha/2)} \cdot A \qquad (F.11)$$

where

$$A = \sqrt{(1-R^2) \cdot g_{ij} / (n - m - 1)} \qquad (F.12)$$

and g_{ij} *is a diagonal element on the inverted bivariate correlation coefficient matrix.*

The Multiple Correlation Coefficient R

Although a number of variables may be eliminated by the procedure given above, their combined effect may be significant. In order to determine whether the multiple correlation coefficient has been significantly lowered by the elimination of variables the multiple correlation coefficient after elimination of variables R' is compared with the original value R . As this is effectively a

test on the equality of two population variances the F -distribution is used. The appropriate statistic is given by equation (F.13).

$$F = \frac{[R^2 - (R')^2] \cdot (n - m - 1)}{(1 - R^2) \cdot (m - m')} \qquad (F.13)$$

where the superscript $(')$ refers to the variables after the variables have been eliminated
and F has $(n-m-1)$ and $(m-m')$ degrees of freedom.

APPENDIX G

PARTICLE SIZE ANALYSIS

Numerous methods are available for determining the sizes of particles contained in a particular sample (92, 93, 70 Ch 8). Particle shape is an important parameter in the determination of the particle diameter, for different shapes will result in different values being obtained by the different methods. The particle-size distribution resulting from the different methods will only be the same should the sample be composed of hard smooth spheres.

Cadle (92, pg 92) has placed the methods for determining particle sizes and particle size distributions into five general groups. However only three of these groupings are of interest in this thesis, viz the methods of size determination from microscopy, sieving and sedimentation. Table G.1 contains some representatives of these three groups, and has been extracted from a tabulation of Reference (92, pg 93).

Table G.1 : Particle Size Range for Various Methods of Particle Size Analysis

Class	Method	Approx. useful Size Range (microns)
Microscopy	Visible Light	0,2 - 100
	Ultraviolet Light	0,1 - 100
	Ultramicroscopy	0,01 - 0,2
	Electron microscopy	0,01 - 5
Sieving	Sieving	50 - 1000
Sedimentation and Elutriation	Sedimentation, gravitational	2 - 50
	Sedimentation, centrifugal	0,05 - 10
	Elutriation, liquid	5 - 50
	Elutriation, gas	5 - 50

The selection of a method for determining the particle size distribution of a given material should be made after considering the following factors (92, Ch 3) :

a) the particle size range,
b) the form in which one wants the results,
c) the application of the results, and
d) the accuracy required.

G.1 Optical Microscopy

Methods based on the optical microscope are often considered to be the most direct and fundamental of the methods. However they are quite tedious and are based on a particle size which is not easily defined. From Table G.1 it is seen that the range of greatest usefulness for these methods is from about 0,2 to 100 microns. "The two major problems in microscope methods of analysis are the collection of sufficient data to ensure adequate precision in the derived parameters, and the elimination of variables in the data due to operator performance. Statistical fluctuations in the occurrence of any given size profile (among the particle images) is a problem that becomes particularly acute if the size ratio of particles is more than 10 to 1" (70, pg 8-4). Cadle (92, pg 125) recommends that at least 200 particles be counted. If the particle size distribution is very wide, there may be a large number of small particles for each large one, the sample should be broken down into various size classes and studied separately.

G.2 Sieving

Sieving is one of the simplest methods of particle size analysis, resulting in a relatively inexpensive and accurate technique. Sieves with openings smaller than 50 microns are seldom used. However membranes with pore diameters less than 5 microns are commercially available for specialist

applications. Sieving has been conducted in accordance with BS 1796 : 1976 in this thesis. This standard recommends the use of hand sieving in preference to machine sieving, though both methods of sieving are acceptable.

G.3 Sedimentation

Unlike microscopy and sieving methods which compare particles on the basis of geometric similarity, sedimentation techniques compare particles on the basis of similar velocities of settling in a liquid or gas. A number of different sedimentation techniques are available, the pipette method making use of the equipment suggested by Andreasen (92, pg 212; 70, pg 8-5) has been used in this thesis. A precise description of the theory for use with this equipment is presented by Dallavalle (93, pg 74-76). In sedimentation methods, the Stokes diameter distribution of the material is deduced from a study of the concentration changes occurring within a settling suspension. The method is based on Stokes's law from which the particle diameter is deduced as

$$d = \sqrt{\frac{18 \cdot \mu \cdot u}{(\rho_s - \rho_g) \cdot g}} \qquad (G.1)$$

Equation (G.1) is theoretically only valid for a sphere. The difference between the volume of the irregular particle and the equivalent sphere does not represent an "error" but provides additional information on the shape of the particles. Although it is desirable to cover the range of a single distribution with a single method, this is not always possible. BS 1796 : 1976 gives the following approximate conversion factors:

Conversion of	Multiply by
Sieve size to Stokes diameter	0,94
Sieve size to projected diameter	1,4

The use of the Andreasen pipette as a means of determining the sizes of particles from 75 microns down to about 3 microns, is described by BS 3406 : Part 2 : 1963, as the fixed position incremental method. The principle of the method is described in the above standard and is quoted below:

> "The pipette sampling method involves the withdrawal of samples from the suspension during the sedimentation by means of a calibrated pipette at a series of known times after stirring, the tip of the pipette being at a known depth, h, below the surface. After time t, the samole contains only those particles with Stokes diameters less than that of particles settling at a rate h/t, since all the particles larger than this will have settled below the sampling point. The cumulative undersize distribution by weight of the powder is obtained directly by weighing the residue after removal of the suspending medium from the sample."

The density of the particle required in equation (G.1) is obtained by the SG bottle method described in BS 1377 : 1975.

D.4 Representation of Results .

"A number of equations have been proposed to correlate the quantity of a particulate material with its particle size to obtain a distribution relationship. In the literature it is often assumed that a powder must assume some distribution such as the Rosin Rammler .....". However, "there is no fundamental reason why a particular powder must obey one of these empirical laws; forcing it to do so will result in error. Furthermore it is difficult to tell whether the fit is good, because any cumulative size plot will give the appearance of a good fit" (70, Ch 8).

The results from the particle size analyses have been graphically illustrated as a cumulative percent by weight undersize (on normal co-ordinates) versus the particle diameter or linear dimension (on logarithmic co-ordinates) as recommended by BS 1796 : 1976. However in some instances the distribution has been plotted on Rosin-Rammler paper for ease of reference.

D.5 Coal Sampling

Because of the coarse grading of the coal, sieving has been employed as the means of size analysis. The following sieve nest was used

6,35 mm	600 microns
4,76 mm	420 microns
2,00 mm	211 microns
1,00 mm	

D.6 Ash Sampling

The size fraction greater than 600 microns was removed from each ash sample by sieving. The remaining ash was graded by means of sieving, using sieves with the following aperture sizes in the two sieve nests as indicated below:

600 microns	150 microns
420 "	106 "
211 "	75 "
	53 "

The ash fraction below 75 microns was analysed using an Andreasen pipette with distilled water as the dispersing medium. Two different methods of size analysis have therefore been employed to obtain an ash size grading from 600 to about 10 microns. However, an overlap in the two methods occurs between 75 and 53 microns. By comparing the results obtained by the two methods in this region, the Stokes diameter can be related to the corresponding sieve aperture.

APPENDIX H

TABULATION OF RESULTS

In order to facilitate the comparison of the findings of this thesis with other published information, the results have been presented in greater detail in this Appendix than in the main body of the thesis. Explanatory notes for each of the tables are contained below to explain various derived and measured quantities from the tables, in particular those quantities marked *).

Notes on Table H.1

Table H.1 contains accurate values for the more important parameters associated with each test. The coal flow has been determined from the combustion efficiency and the determination of the coal burnt from a relationship similar to that given by equation (E.5). The value thus obtained for the coal flow is more representative than that obtained from direct measurement as has been discussed previously.

Notes on Table H.2

Except for temperature and superficial gas velocity, the parameters of Table H.2 have been obtained from the static pressure tappings of the windbox and those situated along the combustor wall. The bed density, referred to in section 3.2.2, is represented by the static pressure difference between two static pressure tappings located within the bed. The distributor pressure drop has been obtained by measuring the difference in static pressure between the windbox and a probe located at the side of the combustor vessel within the refractory stone section, about 50 mm above the distributor plate, cf Section 2.2.7.c. Although the full pressure drop across the refractory stones

has not been monitored, the distributor pressure drop so obtained will be about 0,95 of the actual value.

Notes on Table H.3

Table H.3 has been formed to illustrate the magnitude of the bubble velocity which would be derived from the experimental evaluation of the dynamic bed height. Besides the superficial gas velocity and static bed height which are obtained from measurement, the following parameters have been derived:

a) Minimum fluidizing-velocity from equation (16)

b) Dynamic bed height from equation (17)

c) Fraction occupied by the bubbles from equation (J.6)

d) The bed expansion ratio is the ratio between the dynamic to static bed heights

e) The bubble velocity is easily determined, cf Reference (23), from the two-phase theory of fluidization by assuming that all the flow of gas in excess of that required to fluidize the bed flows through the bed in the form of bubbles. From a total gas balance on the bed:

$$\left\{\begin{matrix}\textit{total gas}\\ \textit{flow}\end{matrix}\right\} = \left\{\begin{matrix}\textit{gas in the}\\ \textit{bubble phase}\end{matrix}\right\} + \left\{\begin{matrix}\textit{gas in the par-}\\ \textit{ticulate phase}\end{matrix}\right\} \qquad (H.1)$$

$$\text{or} \qquad u_f = f \cdot u_{BS} + u_{mf} \cdot (1-f) \qquad (H.2)$$

from which the bubble velocity U_{BS} can be calculated.

The bubble diameter can easily be obtained from the relationships derived by Davidson and Harrison (12) and given by equations (J.8) and (J.9). However, the resulting

diameters range from two, to about 10 metres which are clearly wrong. These excessive diameters would indicate that the measurement of dynamic bed height is in error, resulting in a poor value for the fraction of bubbles in the bed. More realistic values, yielding bed expansion ratios of the order of two, would result in bubble diameters approaching that of the vessel. The accuracy of the static pressure probes is not sufficient to permit an accurate assessment of the dynamic bed height, whilst the problem is further complicated by the possible transition of the bed flow regime from that of bubbling to a slugging flow regime.

Notes on Table H.6

It has been assumed that the fraction collected by the cyclone of size in excess of 600 microns has been splashed from the vessel. The remaining ash has been graded resulting in the gradings as given in Table H.6. However, it will be noted that for Test 6, all of the sample is less than 420 microns. This has resulted as the bed material used for Test 6 is finer than that for the remaining tests, and as such the velocity for Test 6 was only 0,9 m/s. On grading this sample, almost all the material retained in the 420 micron sieve was made up of the silica sand forming the bed material, and this quantity has therefore been included with the splashed material.

Notes on Table H.7

For those tests given in Table H.7, the fraction of the particles of size less than 75 microns was analysed by the incremental sedimentation technique making use of an Andreasen Pipette. The method is briefly described in Appendix G. Although BS 1796 : 1976 gives the sieve size from the Stokes diameter by multiplying this latter diameter by 1,06, this has not been used. Instead, a multiplying factor has been obtained from drawing the smoothed curve

obtained by sieving down to 53 microns and comparing it with the result obtained from the sedimentation technique. This method is also mentioned in BS 1796 : 1976, and results in multiplying factors of:

1,06	for	Test 7A
0,90	for	Test 7B
0,88	for	Test 8A
0,84	for	Test 8C
0,88	for	Test 9A
1,04	for	Test 9B
0,90	for	Test 9C
1,07	for	Test 9D

Notes on Table H.8

In Table H.8, the various entrainment rates have been divided into the different flow components, ash, carbon and sand flow. The coal feed rate is the same as that for Table H.1, being derived from the temperature and the combustion efficiency.

Measured entrainment rates have been obtained from weighing the product collected by the cyclone and separating the sand from the ash and carbon. Cyclone efficiencies of 100% and 75% are applied to the sand, and carbon and ash flows respectively to obtain the measured entrainment rates from the collected flow rates. The carbon and ash flows are separated from each other by considering the percentage carbon in ash.

The deduced entrainment rates are determined by assuming that all the ash is entrained from the coal feed. This deduced ash flow rate is then compared with the measured ash flow rates and is used to obtain the remaining deduced flow rates.

TABLE H.1 : SUMMARY OF TEST CONDITIONS

Test	Duration	Coal Flow	Air Flow	Gas Flow	Excess Air Factor	Bed Temperature				Velocity	Comb. Eff.
						Mean	Std. Dev.	Max.	Min.		
	Mins.	kg/h	kg/h	kg/h	-	°C	°C	°C	°C	m/s	%
6	90	2,89	74,4	76,6	3,26	798,4	8,5	815	785	0,899	88,6
7A	45	3,48	90,1	92,7	3,29	804,8	4,4	815	794	1,095	88,3
7B	45	3,83	82,0	84,7	2,88	903,2	6,4	922	892	1,071	88,4
7C	46	3,66	94,7	97,7	3,55	753,5	6,3	764	737	1,095	81,8
8A	35	4,34	105,9	109,0	3,30	805,3	5,8	816	791	1,288	83,0
8B	35	4,88	119,1	122,5	3,28	807,5	4,5	820	799	1,454	84,3
8C	32	4,79	109,5	113,1	2,89	904,1	5,0	913	897	1,462	88,9
8D	35	5,17	126,2	129,6	3,58	751,7	8,5	770	738	1,458	76,6
8E	32	4,49	109,5	112,4	3,56	752,9	6,5	772	744	1,267	76,9
8F	35	4,27	96,7	99,9	2,89	901,0	4,7	907	883	1,288	87,8
8G	32	4,47	96,7	100,1	2,71	955,1	5,1	965	947	1,351	89,7
8H	18	7,12	143,7	146,8	4,36	632,4	13,4	641	611	1,460	52,0
9A	30	5,67	122,6	126,1	3,32	801,7	16,6	635	774	1,483	73,1
9B	30	3,77	89,4	92,0	3,31	800,3	8,5	810	771	1,084	80,2
9C	30	5,30	109,4	113,1	2,91	900,2	11,3	923	880	1,457	79,8
9D	40	3,62	81,8	84,5	2,89	899,8	13,5	925	878	1,088	87,7
9E	35	4,31	91,5	94,7	2,71	954,1	9,4	973	937	1,277	88,0
10A	30	4,98	126,2	129,6	3,57	752,4	13,2	791	930	1,459	78,6
10B	40	4,29	101,3	104,4	3,09	851,0	12,0	874	822	1,289	85,6
10C	40	3,72	83,9	96,4	3,56	752,1	11,8	782	730	1,085	79,6
10D	35	4,74	117,1	120,0	3,87	700,7	19,3	746	671	1,283	71,7
10E	40	4,73	97,7	101,4	2,54	1010,6	17,5	1048	988	1,429	91,4

TABLE H.2 : Mean Bed Pressure Levels and associated Parameters

Test	Temperature °C	Superficial Gas Velocity m/s	Windbox Pressure mm Wg	*) Bed Density mm Wg	*) Distributor Pressure Drop mm Wg	Bed Pressure Drop mm Wg	Bed Height Static mm	Bed Height Dynamic mm
6	798,4	0,899	395	170	48	347	205	266
7A	804,8	1,095	440	190	49	391	225	269
7B	903,2	1,071	430	197	40	390	219	257
7C	753,5	1,095	434	201	59	375	213	240
8A	805,3	1,288	465	191	69	396	237	271
8B	807,5	1,454	477	184	93	384	229	273
8C	904,1	1,468	468	177	102	366	228	270
8D	751,7	1,458	464	169	110	354	224	274
8E	752,9	1,267	403	160	74	329	219	268
8F	901,0	1,288	429	175	64	365	225	273
8G	955,1	1,351	430	175	58	372	219	279
8H	632,4	1,460	495	175	123	372	207	279
9A	801,7	1,489	345	168	77	268	161	199
9B	800,3	1,084	227	112	38	189	158	213
9C	900,2	1,457	338	158	78	260	155	207
9D	899,8	1,088	241	134	30	211	151	196
9E	954,1	1,277	292	162	45	247	148	189
10A	752,4	1,459	327	157	78	249	159	198
10B	851,0	1,289	283	154	52	231	156	185
10C	752,1	1,085	224	125	29	195	154	194
10D	700,7	1,283	293	146	66	227	151	193
10E	1010,6	1,429	311	174	57	254	148	179

TABLE H.3 : Tabulation of Values associated with the Experimental Determination of the Bubble Velocity.

Test	Velocities		Bed Heights		Fraction of Bed occupied by Bubbles	Bed Expansion Ratio	Bubble Velocity
	Minimum Fluidizing U_{mf} m/s	Superficial Gas U_f m/s	Static mm	Dynamic mm			m/s
6	0,171	0,899	205	266	0,229	1,30	3,34
7A	0,231	1,095	225	269	0,164	1,20	5,51
7B	0,219	1,071	219	257	0,148	1,17	5,98
7C	0,238	1,095	213	240	0,113	1,13	7,85
8A	0,231	1,288	237	271	0,126	1,14	8,65
8B	0,231	1,454	229	273	0,161	1,19	7,82
8C	0,219	1,468	228	270	0,156	1,18	8,21
8D	0,238	1,458	224	274	0,183	1,22	6,92
8E	0,238	1,267	219	268	0,183	1,22	5,87
8F	0,219	1,288	225	273	0,176	1,21	6,30
8G	0,214	1,351	219	279	0,215	1,27	5,50
8H	0,255	1,460	207	279	0,265	1,35	4,80
9A	0,231	1,489	161	199	0,199	1,24	6,55
9B	0,231	1,084	158	213	0,258	1,35	3,54
9C	0,219	1,457	155	207	0,251	1,34	5,15
9D	0,219	1,088	151	196	0,230	1,30	4,01
9E	0,214	1,277	148	189	0,217	1,28	5,11
10A	0,238	1,459	159	198	0,197	1,25	6,44
10B	0,225	1,289	156	185	0,157	1,19	7,01
10C	0,238	1,085	154	194	0,206	1,26	4,36
10D	0,245	1,283	151	193	0,218	1,28	5,02
10E	0,209	1,429	148	179	0,173	1,21	7,25

TABLE H.4 : Input Data for Initial Regression Analysis with six Independent Variables

Test	Independent Variables						Dependent Variable
	Temperature	Superficial Gas Velocity	Static Bed Height	Bed to Distributor Pressure Drop Ratio	Vigorousness of Fluidization $(U_{mf}-U_f)/U_{mf}$	Splashing Rate	Efficiency
	°C (X_1)	m/s (X_2)	m (X_3)	- (X_4)	- (X_5)	kg/h (X_6)	% (Y)
6	798,4	0,8991	0,205	7,23	4,26	0,053	88,6
7A	804,8	1,0950	0,225	7,98	3,74	0,094	88,3
7C	753,5	1,0947	0,213	6,36	3,60	0,050	81,8
8A	805,3	1,2875	0,237	5,74	4,57	0,286	83,0
8B	807,5	1,4544	0,229	4,13	5,30	0,519	84,3
8C	904,1	1,4623	0,228	3,59	5,68	0,286	88,9
8D	751,7	1,4581	0,224	3,22	5,13	0,225	76,6
8E	752,9	1,2668	0,219	4,45	4,32	0,047	76,9
8F	901,0	1,2878	0,225	5,70	4,88	0,057	87,8
8G	955,1	1,3501	0,219	6,41	5,31	0,099	89,7
9A	801,7	1,4886	0,161	3,48	5,44	0,020	73,1
9B	800,3	1,0841	0,158	4,97	3,69	0,006	80,2
9C	900,2	1,4572	0,155	3,33	5,65	0,010	79,8
9D	899,8	1,0883	0,151	7,03	3,97	0,002	87,7
9E	954,1	1,2765	0,148	5,49	4,97	0,009	88,0
10B	851,0	1,2890	0,156	4,44	4,73	0,005	85,6
10C	752,1	1,0885	0,154	6,72	3,57	0,005	79,6
10D	700,7	1,2831	0,151	3,44	4,24	0,005	71,7
10E	1010,6	1,4290	0,148	4,46	5,84	0,012	91,4

TABLE H.5 : Some selected smoothed curves of the size gradings of ash on a cumulative percent-by weight undersize

	CUMULATIVE % BY WEIGHT UNDERSIZE (mm)								
	0,420	0,211	0,150	0,106	0,075	0,053	0,032	0,016	0,008
Test 7B									
Inlet to cyclone	99,3	91,3	82,5	70,0	55,5	43,0	29,0	15,0	8,5
Collected by cyclone	99,1	88,3	76,4	59,9	41,7	27,7	14,4	5,0	2,3
Leaving cyclone				99,2	95,3	87,2	71,2	44,0	26,5
Test 8A									
Inlet to cyclone	98,4	85,8	73,5	60,0	46,0	34,8	21,0	10,3	5,5
Collected by cyclone	98,0	82,0	66,5	49,6	33,2	21,4	9,1	2,5	0,8
Leaving cyclone				99,0	94,3	85,2	65,7	39,5	23,3
Test 9A									
Inlet to cyclone	97,7	84,2	74,0	60,0	47,0	36,0	20,0	11,8	5,3
Collected by cyclone	97,1	79,9	66,9	49,3	33,9	22,3	8,3	3,3	0,8
Leaving cyclone				99,1	94,9	86,0	62,8	42,8	21,9
Test 9C									
Inlet to cyclone	99,2	87,5	75,0	60,0	45,0	32,0	19,0	8,6	4,0
Collected by cyclone	99,0	84,5	69,1	50,7	33,5	20,2	8,8	2,4	0,6
Leaving cyclone				99,0	93,2	81,8	62,0	34,9	18,2

TABLE H.6 : Size Gradings of Ash on a Cumulative Percent by Weight Undersize after the fraction greater than 600 microns has been removed.

Test	Cumulative Percent by Weight Undersize (Microns)					
	420	211	150	106	75	53
6	100,0 *)	93,3	85,5	72,3	61,8	48,3
7A	98,9	86,8	72,9	59,3	49,8	37,2
7B	98,7	88,0	75,8	61,0	51,3	37,2
7C	98,7	85,3	67,2	48,9	40,7	27,4
8A	96,7	80,3	66,1	53,2	44,1	31,6
8B	96,0	78,6	66,7	53,5	44,1	33,0
8C	96,8	80,9	68,9	55,0	45,8	33,5
8D	95,8	76,9	64,3	50,0	40,3	28,9
8E	97,4	79,2	66,8	53,2	43,8	36,0
8F	97,7	83,2	72,0	56,1	46,6	33,2
8G	97,6	84,6	73,6	60,4	50,6	38,7
8H	93,5	68,0	52,6	38,9	30,1	19,6
9A	96,0	73,9	65,9	53,0	44,1	32,1
9B	99,2	83,4	72,9	57,9	43,2	26,8
9C	98,2	81,9	67,2	52,8	42,6	29,1
9D	99,1	89,2	79,0	58,5	43,0	23,1
9E	98,1	83,7	71,1	57,2	48,6	34,6
10A	96,1	77,4	68,0	55,0	45,6	31,7
10B	98,8	84,3	71,5	58,5	49,1	36,6
10C	98,7	88,1	72,8	56,2	45,2	32,9
10D	97,6	76,2	60,8	46,7	37,8	26,8
10E	98,3	85,6	74,0	61,3	52,1	40,1

TABLE H.7 : Particle Size Analysis for the Ash Fraction less than 75 microns, by means of an Andreasen Pipette using Distilled Water as the Suspending Medium

Test Number 7A						
Stokes Diameter (microns)	53,2	26,0	18,2	12,8	8,9	6,2
Corresponding Sieve Diameter (microns)	56,4	27,6	19,3	13,6	9,4	6,6
Cum. % by weight Undersize) Sample of 75 microns Top Size	82,6	5,4	4,2	4,0	3,5	3,4
Cum. % by weight Undersize) Sample of 600 microns Top Size	41,1	2,7	2,1	2,0	1,7	1,7
Test Number 7B						
Stokes Diameter (microns)	52,9	35,5	25,6	17,9	12,5	8,8
Corresponding Sieve Diameter (microns)	47,6	32,0	23,0	16,1	11,3	7,9
Cum. % by weight Undersize) Sample of 75 microns Top Size	66,8	10,2	7,2	5,7	5,5	4,7
Cum. % by weight Undersize) Sample of 600 microns Top Size	34,3	5,2	3,7	2,9	2,8	2,4
Test Number 8A						
Stokes Diameter (microns)	53,0	35,3	25,5	17,3	8,7	
Corresponding Sieve Diameter (microns)	46,6	31,1	22,4	15,2	7,7	
Cum. % by weight Undersize) Sample of 75 microns Top Size	49,0	6,8	4,7	3,6	3,2	
Cum. % by weight Undersize) Sample of 600 microns Top Size	21,6	3,0	2,1	1,6	1,4	
Test Number 8C						
Stokes Diameter (microns)	52,9	31,7	25,6	17,9	11,6	8,8
Corresponding Sieve Diameter (microns)	44,4	26,6	21,5	15,0	9,7	7,4
Cum. % by weight Undersize) Sample of 75 microns Top Size	44,7	7,8	6,8	5,7	4,9	4,5
Cum. % by weight Undersize) Sample of 600 microns Top Size	20,5	3,6	3,1	2,6	2,2	2,1

Test Number 9A						
Stokes Diameter (microns)	53,6	32,1	26,0	18,2	12,5	8,9
Corresponding Sieve Diameter (microns)	47,2	28,2	22,9	16,0	10,7	7,8
Cum. % by weight) Sample of 75 microns Top Size	37,8	5,9	4,0	3,9	3,2	2,8
Undersize) Sample of 600 microns Top Size	16,7	2,6	1,8	1,7	1,4	1,2
Test Number 9B						
Stokes Diameter (microns)	52,6	35,2	25,5	16,7	12,5	8,4
Corresponding Sieve Diameter (microns)	54,7	36,6	26,5	17,4	13,0	8,7
Cum. % by weight) Sample of 75 microns Top Size	68,3	7,9	4,8	3,5	3,1	3,1
Undersize) Sample of 600 microns Top Size	29,5	3,5	2,1	1,5	1,3	1,3
Test Number 9C						
Stokes Diameter (microns)	66,5	35,6	25,7	18,0	11,7	8,8
Corresponding Sieve Diameter (microns)	59,9	32,0	23,1	16,2	10,5	7,9
Cum. % by weight) Sample of 75 microns Top Size	84,5	8,8	4,5	3,5	2,9	2,6
Undersize) Sample of 600 microns Top Size	36,0	3,7	1,9	1,5	1,2	1,1
Test Number 9D						
Stokes Diameter (microns)	52,7	31,6	25,5	17,9	12,5	8,7
Corresponding Sieve Diameter (microns)	56,4	33,8	27,3	19,2	13,4	9,3
Cum. % by weight) Sample of 75 microns Top Size	72,0	6,7	5,5	4,0	3,3	3,1
Undersize) Sample of 600 microns Top Size	31,0	2,9	2,4	1,7	1,4	1,3

TABLE H.8 : Entrainment Rates and Associated Data for the Fluidized-Bed Combustion Rig

Test	Coal Feed Rate	% Carbon in Ash	*) Measured Entrainment Rates				*) Deduced Entrainment Rates				% Sand of Total Entrain. Flow
			Ash & Carbon Flow	Ash Flow	Carbon Flow	Sand Flow	Ash & Carbon Flow	Ash Flow	Carbon Flow	Sand Flow	
	kg/h	%	kg/h	kg/h	kg/h	kg/h	kg/h	kg/h	kg/h	kg/h	%
6	2,89	36,95	0,521	0,328	0,193	0,053	0,702	0,442	0,260	0,071	9,2
7A	3,48	37,54	0,987	0,616	0,371	0,094	0,852	0,532	0,320	0,081	8,7
7B	3,83	46,03	0,876	0,473	0,403	0,056	1,083	0,585	0,498	0,069	6,0
7C	3,66	48,27	1,023	0,529	0,494	0,050	1,081	0,559	0,522	0,053	4,7
8A	4,34	46,54	1,069	0,571	0,498	0,286	1,241	0,663	0,578	0,332	21,1
8B	4,83	44,62	1,279	0,708	0,571	0,519	1,333	0,738	0,595	0,541	28,9
8C	4,79	36,16	1,319	0,842	0,477	0,286	1,147	0,732	0,415	0,249	17,8
8D	5,17	54,52	1,446	0,658	0,788	0,225	1,736	0,790	0,946	0,270	13,5
8E	4,49	54,17	0,972	0,445	0,527	0,047	1,498	0,686	0,812	0,072	4,6
8F	4,27	38,48	0,984	0,605	0,379	0,057	1,060	0,652	0,408	0,061	5,5
8G	4,47	34,48	0,978	0,641	0,337	0,099	1,042	0,683	0,359	0,105	9,2
8H	7,12	71,09	2,810	0,812	1,998	0,312	3,765	1,088	2,677	0,418	10,0
9A	5,67	57,98	1,253	0,527	0,726	0,020	2,059	0,866	1,193	0,033	1,6
9B	3,77	50,35	0,552	0,274	0,278	0,006	1,160	0,576	0,584	0,013	1,1
9C	5,30	50,88	1,240	0,609	0,631	0,010	1,649	0,810	0,839	0,013	0,8
9D	3,62	38,61	0,537	0,330	0,207	0,002	0,900	0,553	0,347	0,003	0,4
9E	4,31	38,04	0,720	0,446	0,274	0,009	1,064	0,659	0,405	0,013	1,2
10A	4,98	51,05	1,049	0,513	0,536	0,014	1,556	0,761	0,795	0,021	1,3
10B	4,29	42,52	0,754	0,433	0,321	0,005	1,142	0,656	0,486	0,008	0,6
10C	3,72	51,10	1,074	0,525	0,549	0,005	1,162	0,568	0,594	0,005	0,5
10D	4,74	59,19	1,410	0,575	0,835	0,005	1,775	0,724	1,051	0,006	0,4
10E	4,73	30,57	0,963	0,669	0,294	0,012	1,041	0,723	0,318	0,013	1,3

APPENDIX I

NUMERICAL ANALYSIS

The theoretical model of Chapter 4 has been programmed for solution on the UNIVAC computer at the university. This has necessitated the use of some numerical techniques, in particular for interpolation, integration and iteration. All of the methods adopted have been obtained from standard texts on numerical analysis and are briefly described in this Appendix for completeness.

I.1 Interpolation

Much of the input data have to be supplied as discrete points of a continuous curve, eg the size distributions of the coal feed or the bed material. Intermediate points are determined by interpolation. Scheid (94, pg 79) presents the characteristics and differences of the various interpolation formulae. It is clear, however, that the nature of the size distribution curves enables them to be best described by size intervals which increase in size as some geometric progression. In other words, only unequal size intervals are considered. Therefore a Lagrangian type or a finite difference type of interpolation procedure can be employed. The latter has been used in preference to Lagrangian interpolation as the Lagrangian methods do not provide an easy estimate of the accuracy of the interpolation. Further, Lagrangian interpolation requires that the degree of the polynomial be chosen at the outset, and as the size distribution curves may best be described by logarithmic co-ordinates of the linear dimension, the accuracy of a Lagrangian type will be improved by specifying polynomial of different degrees at different sections of the curves. Therefore an iterative type of interpolation has been employed, Aitken's method of linear cross means (95, pg 212),

(96, pg 66) which is equivalent to Newton's formula with divided differences. Aitken's method is very efficient and suitable for digital computers. In order to improve the efficiency of the calculation the abscissa nearest the argument of the interpolant $\bar{x}$ is designated by x_0, the next nearest by x_1, and so on. A square matrix of order 2 is generated of which the diagonal elements are equal to the interpolated value of $\bar{x}$. By increasing the order of the matrix the interpolated values are found to converge, the calculation being terminated once the required accuracy has been obtained. The method as described by Khabaza (95) for using Aitken's interpolation procedure has been adopted.

I.2 Integration

Numerical integration of complex functions is well known. In order to use a simple integration formula, the function is assumed to be divided into equal intervals. A more efficient approach would have been to employ a formula with unequal intervals. However satisfactory results have been obtained by dividing the function into intervals of 75 microns. The Gregory formula, derived from finite differences has been used. The following expression of Gregory's formula of numerical integration has been obtained from Wylie (97, pg 104).

$$\int_{x_0}^{x_n} f(x)\,dx = h\,(f_0/2 + f_1 + \ldots\ldots + f_n/2) - \frac{h}{12}\cdot(\Delta f_{n-1} - \Delta f_0) - \frac{h}{24}\cdot(\Delta^2 f_{n-2} + \Delta^2 f_0) - \frac{19\cdot h}{720}\cdot(\Delta^3 f_{n-3} - \Delta^3 f_0) \ldots\ldots \qquad (I.1)$$

where f_i is the value of the function at x_i and where the term Δ^j refers to the j th difference of the function. These differences can be written as

$$\Delta f_i = f_{i+1} - f_i$$

$$\Delta^2 f_i = \Delta f_{i+1} - \Delta f_i \qquad \text{and so on.}$$

As the contribution to the integration of the higher difference orders decreases as the order increases, equation (I.1) has been terminated after fourth difference in the solution of integrals contained in the theoretical model.

I.3 Iteration

In order to solve the equations of either the combustion or entrainment models, an iterative procedure has to be adopted. The technique of successive approximations (82, pg 125), though quite simple has been found to be adequate in that a solution to the equations has been found to the required accuracy within four to five iterations. The method is described as follows:

Assume that given a function of x, F(x), a value of x is to be found for which

$$F(x) = 0 \qquad (I.2)$$

The method of successive approximations can be described by two main steps:

a) Finding an approximate root

b) Refining the approximation to some prescribed degree of accuracy.

Equation (I.2) is rewritten as

$$x = f(x) \qquad (I.3)$$

A number of equations of the form of equation (I.3) can be written from equation (I.2). It is of importance that the absolute value of the derivative of the function of x, f(x), so formed has a value less than unity to ensure that the resulting approximations of x from f(x) converge to a solution (82).

Let x_0 be the initial approximation to the solution of equation (I.2), then the next approximation becomes

$$x_1 = f(x_0)$$

and

$$x_2 = f(x_1)$$

and so on.

The nth approximation or nth iterate is therefore written as

$$x_n = f(x_{n-1}) \qquad (I.4)$$

The procedure is terminated when the values obtained for x_n and x_{n-1} are sufficiently close to each other.

APPENDIX J

SOME CONSEQUENCES OF THE TWO-PHASE THEORY OF FLUIDIZATION

Davidson and Harrison (12, pg 19) have proposed the two-phase theory of fluidization as a means of describing aggregative fluidization. The model is set up by considering a bed as a two-phase system, consisting of a particulate phase in which the flow rate is equal to the flow rate at incipient fluidization i.e. the voidage in this phase remains essentially the same as that at incipient fluidization; and a bubble phase carrying the flow in excess of that required to fluidize the bed. This two-phase model was developed from work on systems having fluidizing velocities less than about ten times that at incipient fluidization.

In much of the work associated with fluidization, a knowledge of the bubble diameter is necessary. A theoretical prediction is extremely difficult and has led to empirical solutions which at best relate to specific ranges of particle diameter, minimum fluidizing velocities. the velocity in excess of this minimum, etc. It is therefore of value to be able to measure or determine the bubble diameter by experiment. However, even the experimental determination is extremely difficult due to the variation in bubble diameter with bed height, and the fact that the disturbance caused by a bubble bursting at the surface may be some 50% larger than the bubble causing it (98). Further, an assessment has to be made of the initial bubble size which is dependent on the type of distributor.

Based on the two-phase theory of fluidization, an empirical formula for the bubble diameter has been extracted from the literature for use in this thesis. The experimental approach into the assessment of bubble diameter based on measured bed expansion is also discussed in this appendix.

J.1 Bubble Diameter from Published Data

Mori and Wen (99) have examined the bubble size and bubble growth rate in the light of bed diameter and in the design of distributor plates. They (99) have summarized the findings of a number of authors and conclude that the correlations of these authors are not useful in predicting the change in the bubble diameter when the bed diameter changed. They (99) derive a maximum possible bubble diameter as a result of coalescence based on the vessel diameter and the amount by which the fluidizing velocity exceeds the minimum fluidizing velocity, i.e. the quantity $(U_f - U_{mf})$. A relationship was derived from which the bubble diameter could be determined, and is given below:

$$\frac{d_{BM} - d_B}{d_{BM} - d_{BO}} = exp\ (-0,3\ H/D_t) \qquad (J.1)$$

where

$$d_{BO} = 0,347 \cdot \left[\frac{A_t}{N}(u_f - u_{mf})\right]^{0,4} \qquad (J.2)$$

and

$$d_{BM} = 0,652 \cdot \left[A_t \cdot (u_f - u_{mf})\right]^{0,4} \qquad (J.3)$$

where the equations (J.1), (J.2) and (J.3) are found to be fairly accurate over the following variable ranges.

$$0,05 < u_{mf} < 0,20\ m/s$$

$$0,06 < d_p < 0,45\ mm$$

$$u_f - u_{mf} < 0,48\ m/s$$

$$D_t < 1,30\ m$$

In a publication not referred to by the above authors, Geldart (100) has shown the fluidization behaviour to be independent of mean particle size and particle size distribution. In particular, he has found the mean bubble size to be dependent only upon, the gas distributor, the height above the distributor and the excess gas velocity $(U_f - U_{mf})$. An equation has been derived by making use of results

obtained from a 300 mm diameter bed. This equation has been found to give good agreement with published data on bubble sizes and is given below:

$$d_B = 1{,}43 \cdot \left(\frac{u_f - u_{mf}}{N}\right)^{0{,}4} \cdot \frac{1}{g^{0{,}2}} + 2{,}05 \cdot H \cdot (u_f - u_{mf})^{0{,}94} \qquad (J.4)$$

This equation has been derived for perforated plate type distributors, and may easily be applied to porous plate type distributors by assuming that they behave as though they have 1000 holes/m^2 of bed cross section (N = 1000 holes/m^2). One of the major restrictions of the above equation is that it has been derived by excluding any data which may have been obtained from slug-flow in accordance with Stewart's criterion, cf Section J.3. As a result, equation (J.4) has been derived with excess gas velocities, $U_f - U_{mf}$, of the order of 0,1 m/s and less. The equation has also been restricted to the following particle properties:

$$0{,}04 < d_p < 0{,}50 \text{ mm}$$

$$1400 < \rho_p < 4000 \text{ kg/m}^3$$

It is evident that work into the mechanism of fluidization has been limited to low velocities and small particle diameters. These low values will tend to produce more uniform fluidization, in particular when the prime objective may be to evaluate the two-phase system of fluidization. In this thesis, a bed material with a mean particle diameter of 0,795 mm was used, whilst a coal feed with a top size of 6,35 mm was introduced into the bed. The excess fluidizing velocity ranged from about 0,7 m/s to 1,3 m/s. These values are clearly outside the ranges for which equations (J.1) to (J.4) are valid. However, they do represent realistic values under which the combustion of coal in fluidized beds can be achieved.

Equation (J.4) has been chosen for use in the theoretical model in order to determine the bubble diameter.

J.2 Experimental Determination of the Bubble Diameter

The most usual method of determining the bubble diameter is by photographing the bubbles as they burst at the surface of the bed and by making a correction for the actual bubble size which may be appreciably smaller than that photographed (98). Lewis and Partridge (101) have reported on an X-Ray technique, whilst two dimensional methods have also been used. However, by considering the two-phase theory of fluidization, and as all the gas in excess of that required for fluidization passes through the bed as bubbles, the bed expansion can be related to the bubble diameter. Geldart (102) derives the following expression relating the static and dynamic bed heights to the rate of rise of a swarm of bubble U_{BS}

$$\frac{H_f - H_{mf}}{H_f} = \frac{u_f - u_{mf}}{u_{BS}} \qquad (J.5)$$

But the fraction of bubbles f in the bed is also given by

$$f = \frac{H_f - H_{mf}}{H_f} \qquad (J.6)$$

Geldart (102) further reports, that two equations relating the expansion ratio H_f/H_{mf} to the mean bubble diameter can be derived. These two equations differ in the way in which the bubble velocity, or the natural rising velocity of the bubbles, U_B, is related to the absolute velocity of rise of a bubble in a swarm U_{BS}. The first assumes that providing the bubbles do not interfere with one another,

$$u_{BS} = u_B \qquad (J.7)$$

whilst the second, proposed by Davidson and Harrison (12, pg 100), assumes that the absolute velocity of rise of a bubble is assumed to be the sum of the natural rising velocity U_B, plus the upward velocity of the particulate

phase between the bubbles, $U_f - U_{mf}$. This is given by

$$u_{BS} = (u_f - u_{mf}) + u_B \qquad (J.8)$$

where

$$u_B = 0{,}711\ (g \cdot D_B)^{0{,}5} \qquad (J.9)$$

By adopting this latter approach, and by assuming that

$$u_B \simeq (g \cdot D_B / 2)^{0{,}5} \qquad (J.10)$$

Geldart (J.5) derives the following expression for the mean bubble diameter in terms of the bed expansion ratio $R = H_f/H_{mf}$,

$$D_B = \frac{2}{g} \left(\frac{u_f - u_{mf}}{R - 1} \right)^2 \qquad (J.11)$$

A similar relationship can be derived by making use of the assumption of equation (J.7). However, as it is not possible to choose between the equations (J.7) and (J.8) on theoretical grounds (102), the Harrison and Davidson relation of equation (J.8) has been chosen. In fact the diameters predicted by equation (J.11) by this relation are always less by a factor R^2 than that predicted by equation (J.7).

In order to determine the bubble diameter from experimental results, the excess velocity $U_f - U_{mf}$ and the bed expansion ratio are substituted into equation (J.11). It should be noted that Geldart (102) has only used excess gas velocities of $U_f - U_{mf}$ up to 0,07 m/s resulting in the highest value for the bed expansion ratio R, being observed as 1,16. As the values for excess gas velocities and hence also for the bed expansion ratio are much greater for this thesis, the use of equation (J.11) is restricted to qualitative assessments of bubble diameter, and to obtaining the relative effect when changing from one velocity to another.

J.3 Criterion for Slugging Flow

The criterion for determining the transition from bubbling flow to slugging flow in fluidized beds has been suggested by Stewart (103). Geldart (100,102) has used this criterion which is given below for eliminating experimental work where slugging may have been suspected in order to determine bubble diameters. Stewart (103) proposes that slug flow will occur in a tube of diameter D_t if

$$(u_f - u_{mf}) \;/\; 0{,}35 \;/\; (D_t\, g)^{0{,}5} \;<\; 0{,}2 \qquad (J.12)$$

For a 300 mm diameter tube, as has been used in this thesis, and assuming a minimum fluidizing velocity of 0,3 m/s, a fluidizing velocity of 0,42 m/s should not be exceeded in order to ensure bubbling flow conditions.

However, it is evident that bed height must have an effect on the bubble size, as for shallow beds particularly where the bed height is less than the bed diameter, coalescence may not have taken place to the extent that fully developed slug flow is possible before the bubble erupts at the surface.

APPENDIX K

CYCLONE PERFORMANCE

The dust is separated from the flue gases by means of a cyclone situated on the suction side of the boiler induced draft fan. The cyclone has been designed having the standard dimensions of a medium efficiency type cyclone.

From the data presented in Reference (70, Ch 20) the pressure drop across the cyclone is determined as being equivalent to 6,5 inlet velocity heads. The pressure drop across the cyclone is measured as being equal to 39 mm W.g.

By equating the values an equation results having temperature and mass flow rates as the unknowns. A second relationship is generated based on a mass balance of flue gas from the combustor and cooling air absorbed from the surroundings. To simplify the calculation, the flue gas is assumed to be emitted from the combustor at a flow rate of 100 kg/h and 800°C for all of the tests considered. By solving these two equations simultaneously, the following is determined for the cyclone:

Temperature at cyclone inlet = 70°C
Velocity at cyclone inlet = 10,7 m/s

From this the correction factor for the cyclone efficiency to particle size as given by Nonhebel (78) is determined as 2,06.

Figure K.1 is drawn and this has been used for all of the tests to relate the quantity of ash collected with the incoming dust burden.

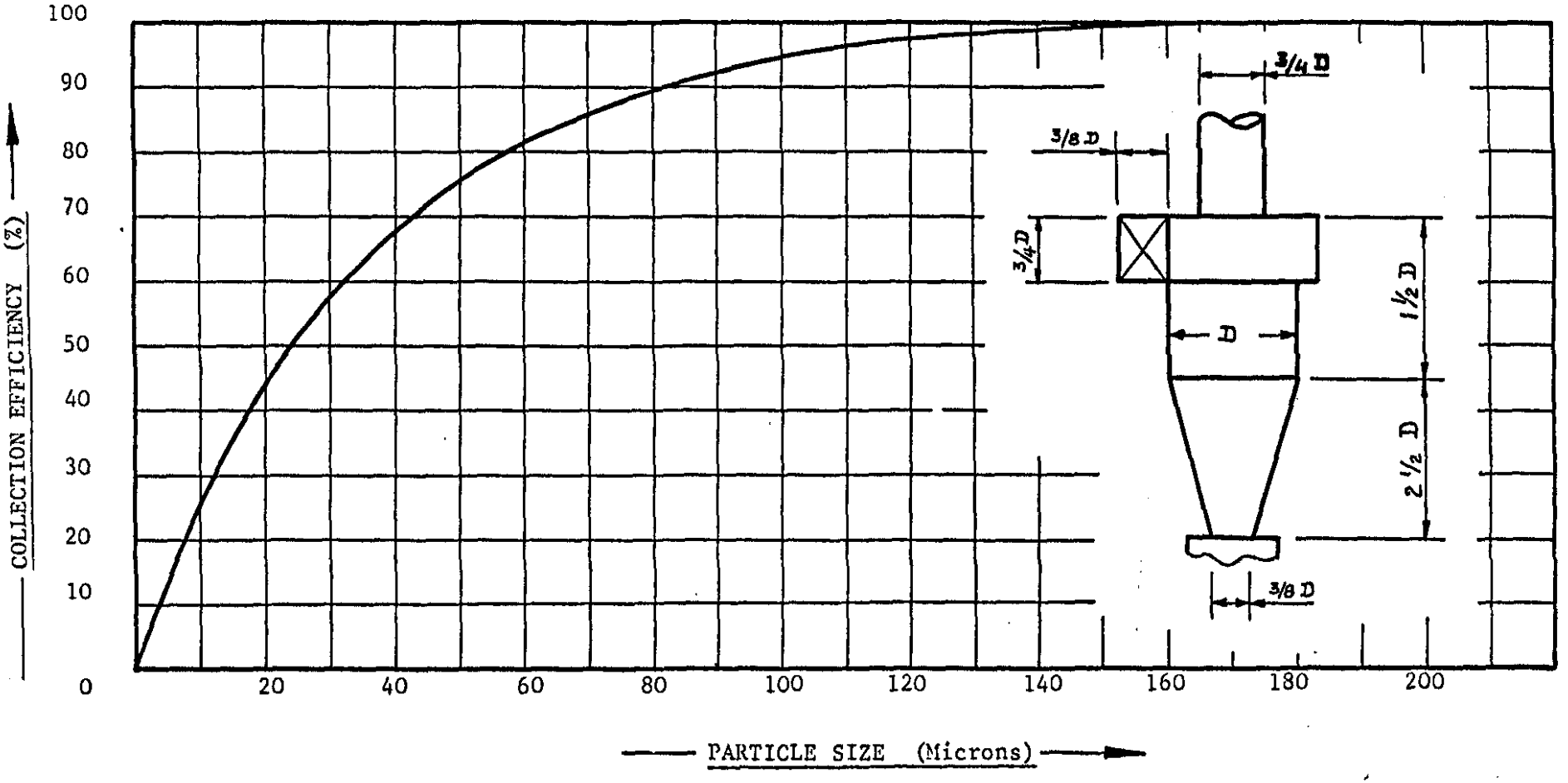

FIGURE K1 ; Corrected Cyclone Efficiency Curve for a Gas Inlet Velocity of 10,7 m/s and Temperature of 70°C

APPENDIX L

COMPLETE TABLE OF CONTENTS